Aus dem Department für Augenheilkunde Tübingen
Universitäts-Augenklinik

Retinal Gene Therapy: Bridging the Gap

Inaugural-Dissertation
zur Erlangung des Doktorgrades
der Medizin

der Medizinischen Fakultät
der Eberhard Karls Universität
zu Tübingen

vorgelegt von

Seitz, Immanuel Philipp

2022

Dekan: Professor Dr. B. Pichler

1. Berichterstatter: Professor Dr. M. D. Fischer
2. Berichterstatter: Professor Dr. K. Januschowski
3. Berichterstatter: Professor Dr. Dr. D. Barthelmes

Tag der Disputation: 26.01.2022

Dedication:

To my grandmother Hanneliese, who was denied a career in academia by a twist of fate, and instead dedicated her life to enabling her children and grandchildren to live the life she couldn't.

TABLE OF CONTENTS

List of Abbreviations

RGC: Retinal Ganglion Cell

LGN: Lateral Geniculate Nucleus

RPE: Retinal Pigment Epithelium

ILM: Inner Limiting Membrane

NFL: Nerve Fibre Layer

GCL: Ganglion Cell Layer

IPL: Inner Plexiform Layer

INL: Inner Nuclear Layer

OPL: Outer Plexiform Layer

ONL: Outer Nuclear Layer

OLM: External Limiting Membrane

BM: Bruch's Membrane

OS: Outer Segment

IS: Inner Segment

CC: Connecting Cilium

PR: Photoreceptor

GC: Guanylate Cyclase

cGMP: Cyclic Guanosine Monophosphate

GDP: Guanosine Diphosphate

GTP: Guanosine Triphosphate

CNG: Cyclic nucleotide-gated cation channel

RHO: Rhodopsin

TD: Transducin

PDE6: Phosphodiesterase 6

CCT: Cambridge Colour Test

CMYK: Cyan Magenta Yellow Key

RBG: Red Blue Green

CIE: Commission Internationale de l'éclairage

REP1: Rab Escort Protein 1

REP2: Rab Escort Protein 2

ACHM: Achromatopsia

AAV: Adeno-Associated-Virus

GT: Gene Therapy

DNA: Desoxyribonucleic Acid

CAR-T: Chimeric Antigen Receptor T-cell

CRISPR: Clustered Regularly Interspaced Short Palindromic Repeats

TALEN: Transcription Activator-like Effector Nuclease

IRD: Inherited Retinal Disorder

FDA: U.S. Food and Drug Administration

CRS: Cytokine Release Syndrome

SCID-X1: Severe Combined Immunodeficiency

ALL: Acute Lymphoblastic Leukaemia

LCA: Leber's Congenital Amaurosis

RV: Retrovirus

LV: Lentivirus

Ad: Adenovirus

mRNA: Messenger Ribonucleic Acid

ATP: Adenosine Triphosphate

wtAAV: Wild-Type Adeno-Associated-Virus

rAAV: Recombinant Adeno-Associated-Virus

ITR: Inverted Terminal Repeats

cds: Coding Genome Sequence

kb: Kilobases

IVT: Intravitreal Injection

SR: Subretinal Injection

vg: Vector genome copies

INTRODUCTION

1.1. The Retina

1.1.1. General

From the antiquities, up until the dawn of the sixteenth century most scholars interested in vision regarded the lens as the eye's central photoreceptive element. Only in 1583 Swiss physician Felix Platter (1536-1614) insisted, that the retina was to be recognized as the pars primaria visionis, the "primary component of vision", and relegated the lens to the role of a mere perspicillum, a *"looking glass" (1)*. The retina is a sheet of central neurons, a protuberance of the diencephalon, and the innermost lining of the back of the eye. The retina's core function is to convert incoming light rays (photons), precisely refracted by the cornea and lens, into electrical impulses and pre-process them for upstream visual integration.

1.1.2. Funduscopic landmarks

Upon fundoscopic inspection (Fig.1), the retina shows two landmarks towards its centre. One is the optic disc, the macroscopic origin of the optic nerve, where nerve fibres converge and leave the eye. Embedded in and branching from it are the central retinal artery and vein. The second landmark is the fovea centralis (*from latin: fovea - "small* pit"), which lies 4mm temporally of the optic disc. The fovea is a shallow depression in the retinal contour, which is densely packed with cone photoreceptors, where the inner retina is retracted towards the sides to minimize optical obstruction. It is the only retinal locus capable of resolving a spatial pattern separated by a visual angle of less than one minute of arc (Snellen visual acuity of <20/20). The region surrounding the fovea centralis is referred to as macula lutea, named after its yellowish appearance, and just as the fovea, it contains a high density of cone photoreceptors. As such, macula and fovea are essential for human vision despite their very limited spatial extent. Their importance

is highlighted by the time and effort humans spend to continuously move their eyes and heads around, to keep visual points of interest projected exactly onto the macula at most times. An excessive effort compared to non-maculated animals. Behind the retina lies the uvea, which is comprised of blood vessels and connecting tissue, and the sclera, a firm connective tissue, colloquially known as the "white of the eye".

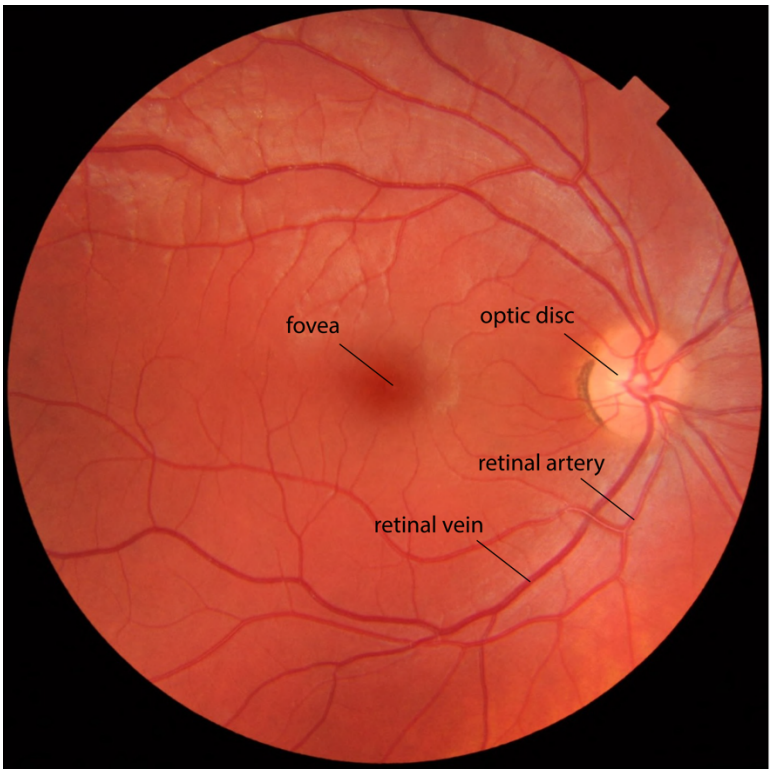

Figure 1: Fundus photograph of a healthy right eye. In the fovea, the locus of highest visual acuity, cones are tightly packed, and the rest of the retina is retracted to the sides. This is marked by a characteristic "foveal reflex" on fundoscopy. Retinal nerve fibres converge into the optic nerve and leave the eye at the optic disc. The optic disc does not contain photoreceptors and is responsible for the physiological "blind spot". *source: Modified from Häggström*(2)*, used with permission.*

1.1.3. Circulation

As mentioned, the retina sits on top of a network of uveal blood vessels, called the choroid, which is supplied by ciliary arteries, and nourishes the outer retinal layers (i.e. photoreceptors and retinal pigment epithelium). The inner retinal layers cannot be

supplied by diffusion of oxygen from the choroid and are supplied separately by branches of the central retinal artery, which is in turn a branch of the ophthalmic artery. Fine arterioles and capillary branches of the retinal artery permeate most of the inner retina, with exception of the avascular, visually unobstructed fovea. Photoreceptors and retinal pigment epithelium have among the highest metabolic activity of all cells in the human body. Correspondingly, choroidal blood flow per gram tissue, is the highest in the body at around 800µL per minute, 4 times higher than in the renal cortex (3). Venous outflow of the inner retina happens through the central retinal vein, while the choroid is drained via a set of so-called vortex veins.

Yet, circulation in the eye is not limited to blood flow. Another important part of ocular circulation is the aqueous humour. It is produced by the ciliary body epithelium, nourishes the anterior segment, especially lens and cornea, and leaves the eye via the trabecular meshwork and Schlemm's canal, or by transscleral diffusion. While this aspect of ocular anatomy and physiology is less important to retinal considerations, it is important to keep in mind that the cavity of the eye is connected to systemic circulation.

1.1.4. Visual Pathway

Vision is a combined achievement of the optical eye (cornea and lens) and the central nervous system (retina, optic nerve, and visual cortex). The retina contains the first (photoreceptor), second (bipolar cell) and third (ganglion cell) neurons of the visual pathway. There are approximately 90 million rod and 4.5 million cone photoreceptors in the human retina, which relay onto around 1 million retinal ganglion cells (RGC) via bipolar cells. Of note, the number of photoreceptors that synapse to one ganglion cell define the size of its receptive field. In the fovea, receptive field size is minimized to increase visual acuity. As a result, the ratio of photoreceptors to receptive ganglion cells between fovea and peripheral retina varies by a factor of more than 1000x (4). In the nerve fibre layer, the ganglion cells' axons converge to form the optic nerve, which leaves the orbit and meets the contralateral optic nerve at the optic chiasm. Here, the fibres arriving from the nasal retina cross over to the other side, to join temporal fibres of the contralateral eye. These post-chiasmal bundles of RGC axons terminate at the lateral

geniculate nucleus (LGN), where signals are transmitted over to the 4th neuron. Finally, the LGN projects to the occipital visual cortex, where retinal signals are integrated, interpreted, and relayed for further use to other parts of the brain. Interestingly, the vast over-representation of the foveal region, which is already present at the ganglion cell receptive field level, carries over to the visual cortex (5). While sources differ on the exact figures, the fovea, which covers roughly 0.02% of the retinal area, occupies up to 40% of the visual cortex (6), a situation comparable to the cortical magnification of the hands and fingers in the sensory and motoric cortices.

1.1.5. Retinal architecture

In the 1870s, almost three centuries after Platter, German anatomist Max Schultze, spurred by improvements in tissue fixation and the advent of microscopy, created some of the first accurate depictions of the layered retinal architecture (Fig.2).

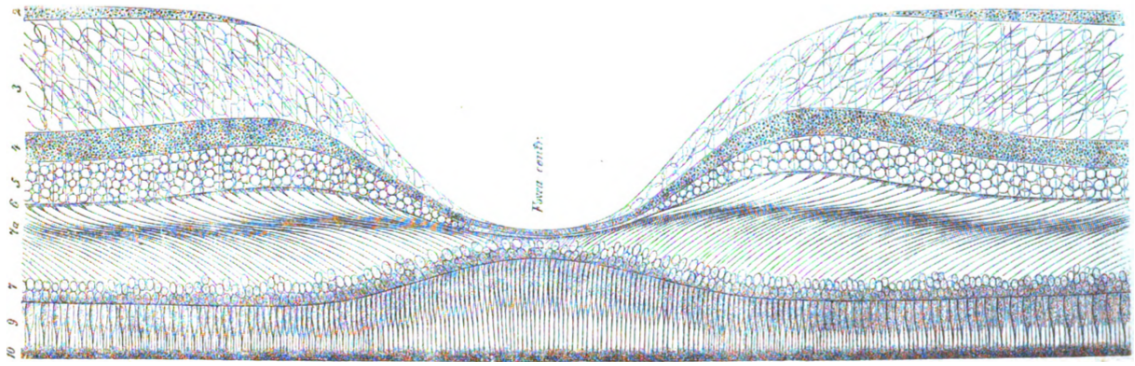

Figure 2: Digitized drawing of a retinal section (400x magnification) by Max Schultze, published in 1873, illustrating the retina's ten-layered architecture, including the fovea: 1. Inner Limiting membrane (not shown) 2. Nerve Fibre Layer 3. Ganglion Cell Layer 4. Inner Plexiform Layer 5. Inner Nuclear Layer 6. Outer Plexiform Layer 7. Outer Nuclear Layer 8. External Limiting Membrane (not labelled) 9. Photoreceptors 10. Retinal Pigment Epithelium. Taken from the Manual of Human and Comparative Histology 1873 by Salomon Stricker, artwork published as *gemeinfrei* under German §64 UrhG.

Among the first to elucidate the cellular contents of these retinal layers was Spanish neuropathologist Ramon y Cajal, who created detailed, semi-schematic drawings of Golgi-stained retinal sections, the most famous of which were published in 1911. The neural retina is built from nine layers of central neurons and specialized glia cells (Müller glia). It is completed by an outermost tenth layer of a specialized epithelium, the retinal pigment epithelium (RPE).

Fig.3 gives a schematic overview of retinal architecture. Following the path of light, the first, innermost layer of the retina is the inner limiting membrane (ILM), a slim stratum of Müller cells' appendages, that interfaces neuroretina and the vitreous cavity. As will be discussed later, the ILM can block retinal uptake of certain substances from the vitreous cavity. Below it lies the nerve fibre layer (NFL). Its namesake nerve fibres are the axons of retinal ganglion cells, that converge to form the optic nerve. A thinning of the NFL, as an expression of Ganglion cell loss, is a typical finding in glaucoma. In accordance, the third layer is the ganglion cell layer (GCL), which houses the ganglion cells' somata. They are the main hub of retinal signal pre-processing. As such, ganglion cells receive a plethora of synaptic connections from bipolar and amacrine cells, whose cell bodies populate the inner nuclear layer (INL). The mass of these axonal and synaptic appendages between GCL and INL forms the inner plexiform layer (IPL). Apart from bipolar and amacrine cells, the INL also contains the somata of two more cell types. First off, the aforementioned Müller cells, glia cells, and secondly horizontal cells, inhibitory interneurons, whose interplay with bipolar and ganglion cells gives rise to key mechanisms of retinal signal pre-processing (i.e. centre-surround receptive fields, cone-mediated rod-inhibition etc.). Beyond the INL, with all its regulatory neurons, lies another stratum of axons and synaptic ribbons, which interfaces to the photoreceptors, and is called outer plexiform layer (OPL). Below it lies the final granulated layer of the retina, the outer nuclear layer (ONL). It contains the photoreceptor somata and is the subject of degeneration in a plethora of retinal diseases. Its basal boundary is the outer limiting membrane (OLM), again formed by appendages of Müller glia. Apically, photoreceptor cells contact the retinal pigment epithelium (RPE), which they are metabolically coupled to. Completing the retina, the RPE is anchored onto a basement membrane called Bruch's membrane (BM), which interfaces RPE and the underlying choroid.

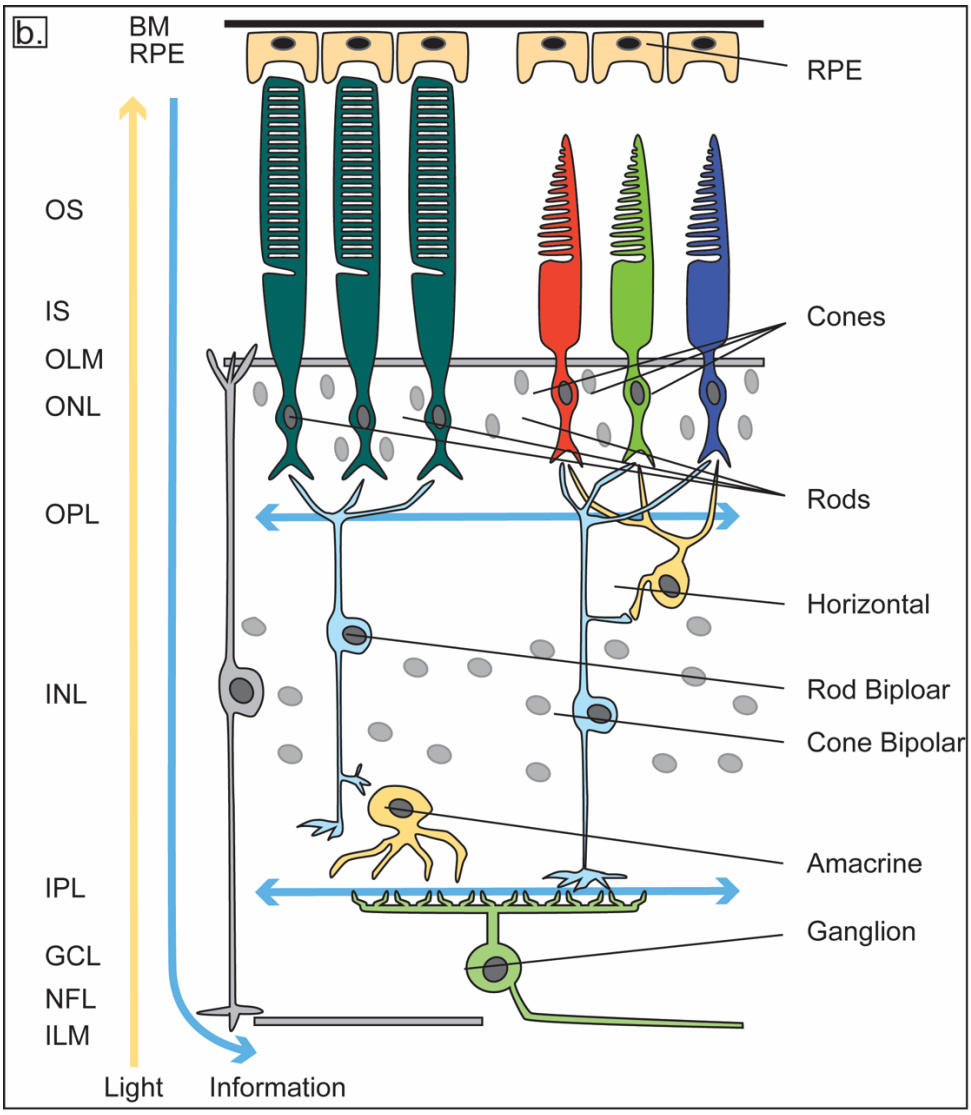

Figure 3 Schematic of the retinal architecture: ILM: Inner limiting membrane, NFL: Nerve fibre layer, GCL: Ganglion cell layer, IPL: Inner plexiform layer, INL: Inner nuclear layer, OPL: Outer plexiform layer, ONL: Outer nuclear layer, OLM: Outer limiting membrane, IS: Inner segment, OS: Outer segment, RPE: Retinal pigment epithelium, BM: Bruch`s membrane. Müller cell depicted in grey. Note the inverted flow of light and information. Own work.

Structural abnormalities in one or more retinal layers are a common symptom of most retinal disease, and can be readily visualized by optical coherence tomography. The types of retinal disease relevant to this manuscript illustrate the large spectrum and complexity of retinal disruption, ranging from barely detectable structural changes in Achromatopsia to drastic, near-complete atrophy in Choroideremia, that spares only the inner retina.

1.1.6. Photoreceptors

Photoreceptor cells (PR) are the sensory neurons of the retina, responsible for the conversion of photons into electrical stimuli (phototransduction). Fig.4a illustrates their highly polarized morphology. This unusual morphology is a consequence of the need for a high-turnover "reaction chamber" that can house the phototransduction cascade: the outer segment (OS). The OS is stacked with membrane discs that contain visual pigment. These discs are constantly replenished from the base and shed apically towards the RPE. In cones, the process involves parallel infoldings of the cell membrane, while in rods, these infoldings close to form double membrane discs. Outer segments are in constant flux, and are fully replaced every 9-13 days (7). Fig 4b. illustrates how depleted visual pigment is shed alongside other OS components, and taken up by the RPE to be replenished and relayed back into the photoreceptor. The OS is complemented by an inner segment (IS). The IS houses the metabolic machinery of the photoreceptor (mitochondria and endoplasmatic reticulum) and helps satisfy the constant energy demand and protein turnover of the OS. IS and OS are connected via the connecting cilium (CC), a specialized, non-motile cilium. The CC is coupled to the photoreceptor's cytoskeleton and acts as a hub for coordinated, bidirectional, inter-segment transport. Its basal body is embedded into a network of fibres which mark the transition zone, an aptly named structure, that serves as a diffusion barrier between OS and IS.

Photoreceptors can be classified as either rod or cone photoreceptors. Rods are able to reliably detect singular photons and are therefore optimized for scotopic (dark) conditions. The light sensitivity of the rod system is around 100 times higher compared to cones, but this comes at the cost of lower spatial and temporal resolution, as well as monochromatic vision. In contrast, the cone system excels under photopic (bright) conditions, providing low latency, trichromatic and high acuity vision. While most cones are tightly packed in the avascular fovea centralis, rods primarily populate the parafoveal region, as well as the periphery (Fig.4a).

Both photoreceptor types are integral to vision. The disorders discussed in this manuscript highlight the clinical importance of discerning rod and cone photoreceptors. A patient affected by cone-specific Achromatopsia might not be able to see colour, drive, or read, due to diminished visual acuity, but will orient him-/herself just fine, even in unknown

territory or in the dark, due to intact peripheral and scotopic vision. Contrast this to a patient affected by (initially) rod-centric disease like Choroideremia, who will (for a long time) have no trouble reading even fine print, but will be susceptible to falling, colliding with peripheral objects and being unable to see in darker conditions due to rapid decline of peripheral vision.

1.1.7. Retinal Pigment Epithelium

The outermost and only non-neuronal layer of the retina is the retinal pigment epithelium. It is anchored on Bruch's membrane, which covers the underlining choroid. Individual RPE cells are hexagonal in shape, form a monolayer, and are linked by tight junctions. Through these tight junctions the RPE establishes a sealed diffusion barrier, the outer blood-retina barrier. Complementing this, the inner retinal capillary network is lined with continuous, non-fenestrated epithelium (inner blood-retina barrier), which further limits diffusion of macromolecules.

Despite their proximity, photoreceptors and RPE are not connected through a strong mechanical interface. This creates a potential subretinal space, which is constantly and actively drained by the RPE. Any violation of the barriers forming this subretinal space (retinal hole/tear, RPE or tight junction leakage, exudative processes) can result in accumulation of fluid in the subretinal space, leading to retinal detachment. Vice versa, given intact or restored barriers, the RPE can resorb subretinal fluid. The latter is essential not only for standard procedures like retinal detachment repair, but also for subretinal gene therapy.

Yet, the most prominent function of the RPE is phagocytosis of outer segment debris. Through this, it maintains the regenerative part of the visual cycle through the isomerization of *all-trans retinal,* a biochemical end-product of the phototransduction, to *11-cis-retinal*, which is then taken up again by the photoceptors for the next round of phototransduction (Fig 4b.).

1.1.8. The Visual Cycle

As established, phototransduction takes place in the outer segments, which are metabolically coupled to both the RPE and the inner segments. To achieve phototransduction, photoreceptors carry a class of specialised G-coupled receptors called opsins[*1]. Opsins are made light sensitive by the chromophore 11-*cis*-retinal, which can absorb incoming photons ("quantum catch") and undergo conformational change as a result ("photoisomerization"). Fig.4c gives a schematic overview of the phototransduction cascade. Curiously, PR depolarize in the dark, creating a "dark current" that inhibits upstream signalling to the cortex via glutamate release, which here acts as an inhibitory neurotransmitter. Incoming light hyperpolarizes the photoreceptor, which decreases glutamate release and facilitates upstream signalling via disinhibition of interneurons. An unimpeded visual cycle is essential not only to visual function, but in itself trophic to the photoreceptor.

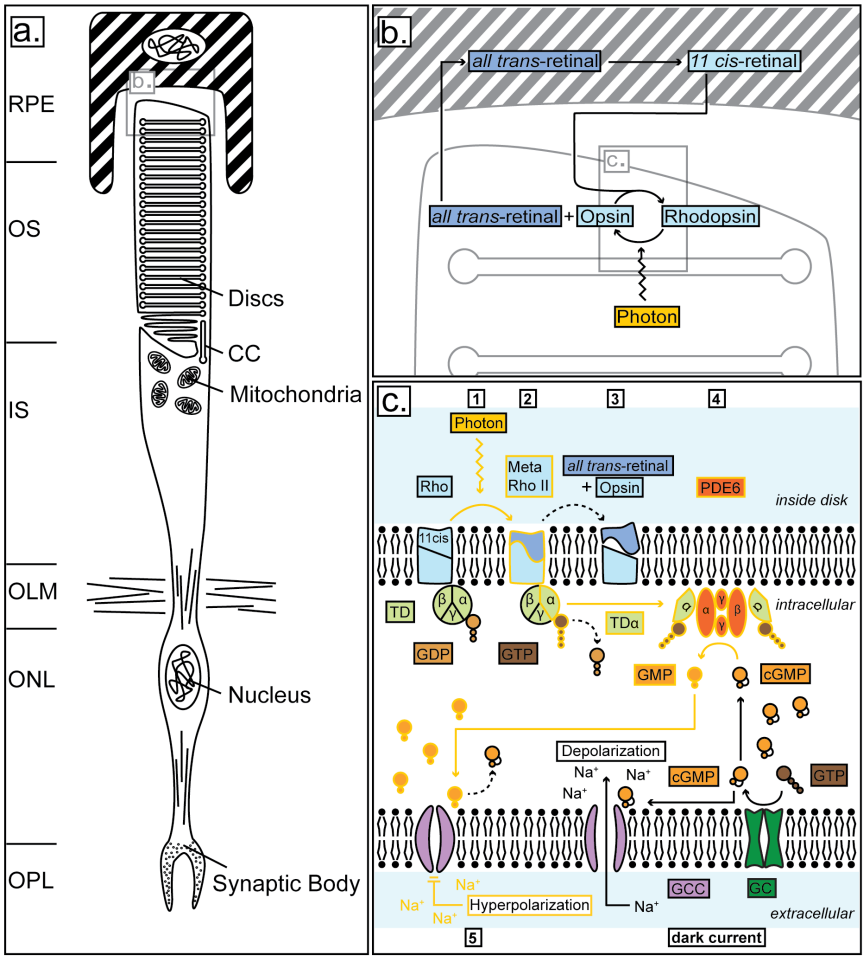

Figure 4: a. Rod photoreceptor and RPE anatomy. b. Illustration of metabolic coupling between rod photoreceptor and RPE cell, consisting of the retinoid cycle and phototransduction. c. Schematic overview of the phototransduction cascade: Dark current (black arrows): Basal guanylate cyclase (GC) activity leads to high levels of cGMP, and open cGMP-gated cation channels (CNG) which results in depolarisation of the cell membrane. Phototransduction - Step 1: Rhodopsin (Rho; 11-cis retinal + Opsin) quantum catch. Step 2: Photoisomerization of Rho to Metarhodopsin II (11-cis to all-trans retinal), and subsequent activation of alpha-transducin (TD). Step 3: Spontaneous decay of MetaRhoII, and liberation of free alpha-transducin (TDa). Step 4: Phosphodiesterase-6 (PDE6) activation, resulting in a decrease of cGMP levels. Step 5: Closure of cGMP gated cation channels, reduced cation influx, hyperpolarization of the photoreceptor cell membrane, and reduced glutamate release (not shown) from synapse in the outer plexiform layer (OPL); *source: own work*

1.2. Specific Retinal Physiology - Colour Vision

1.2.1. Emergence and Organisation

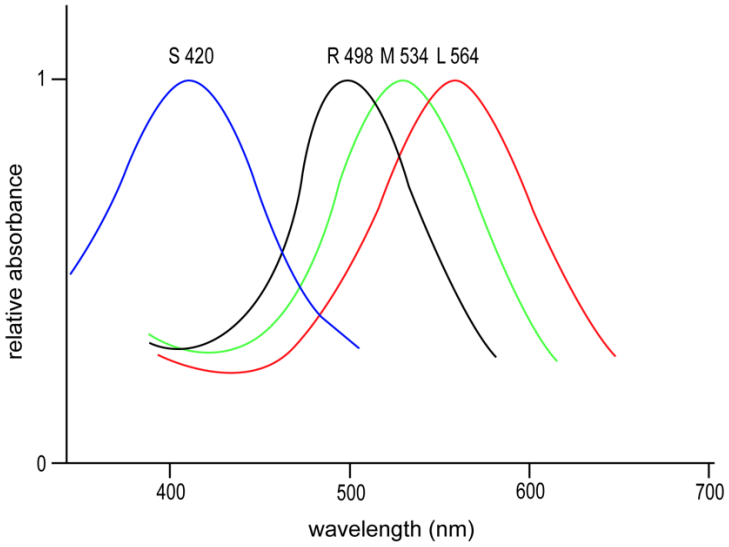

Figure 5: Normalized wavelength absorbance of S, M and L cones, after data from Bowmaker and Dartnall(8): R denotes rhodopsin, the visual pigment of rods, which is not relevant to colour vision; *source: own work*

The fundamentals of light perception have already been discussed in Chapter 1.1.3. Cones can be divided into three spectral classes, each with their own wavelength-specific opsins, which constitute the foundation of colour vision.

Paramount to the emergence of colour vision, the photon wavelength at which quantum capture is most likely to occur is determined by the subtype of opsin. Human cone photoreceptors usually contain either of the following subtypes of opsin: short- (S), medium- (M) or long (L)- wavelength. Fig 5 illustrates normalized photon absorbance by wavelength for these three opsins. The two other classes of human opsins, rhodopsin (rod opsin) and melanopsin (circadian rhythm), are not relevant to colour vision.

Due to the spectral classes, cone signals are colour-coded. This signal is integrated further by two phylogenetically distinct pathways: The first pathway, presumed to be older,

compares the amount of quantum catches between S-cones and M- and L-cones, giving rise to tritan (blue) discrimination. The second pathway is presumably newer, as it does not exist in American new world apes, and is therefore regarded as phylogenetically recent (9). It foregoes S-cone input and instead compares quantum catches between M- and L-cones, which gives rise to protan (red) and deutan (green) discrimination. In line with this, M- and L-opsins are phylogenetically closer to each other, than to the S-opsin. The separated status of S-cones also extends to their anatomical distribution in the retina, as S-cones are much less prevalent in the fovea than M- and L-cones (Fig.6). It has also been proposed that the blue-cone pathway is more vulnerable to injury than the M/L-pathway (10).

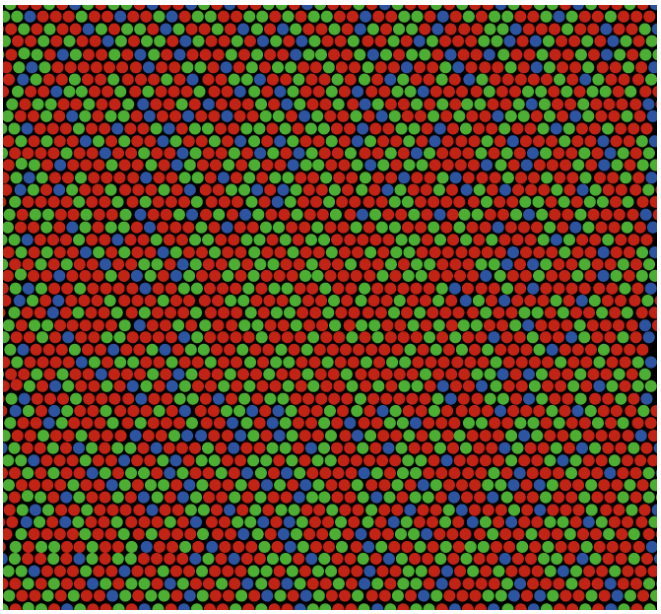

Figure 6: Illustration of anatomical spectral class distribution pattern in the foveal and parafoveal region, with foveal absence of S-cones; *source: own work.*

[*1] In German literature the word “opsin” often refers only to the protein component of the visual pigment. In English literature “opsin” is used for the whole visual pigment, including the chromophore.

1.2.2. Clinical Colorimetry

Apart from visual acuity, colour vision is another functional endpoint of cone function with immediate relevance to the patient. Different systems are used to test colour vision in clinical practice, such as the anomaloscope and the well-known Ishihara plates, which are designed to detect common colour vision disorders, but are not useful when aiming to quantify colour vision deficits. The most common colour vision tests used in specialized centres and research are the Farnsworth Munsell Panel D15, Roth 28 and Panel D100 colour test. They are based on a sequence of small, coloured discs, which are rearranged by the patient based on perceived chromaticity. Given the pile of small discs that need to be perceived at once for comparison, the main limitation of these tests is the large amount of visual search required to complete the test, a daunting task for patients with severe visual field restrictions. Also, while colour confusion along different axes can be semi-quantified, the total colour confusion score is irrespective of axes and therefore formal quantification of the colour discrimination remains incomplete. One newer test that aims to overcome these problems is the Cambridge Colour Vision Test (CCT). Here, a coloured Landolt-style C, with a gap of 1 deg is presented to the subject on a computer screen, and the subject has to repeatedly locate the orientation of the gap (top, bottom, left or right). After each cue, the colours of the background and the stimulus are varied in an interleaved stairway pattern to narrow in on the perceptual threshold of the subject. To prevent the use of brightness cues in solving the test, both the stimulus and the background are composed of a mosaic of spheres with different brightness. Chapter 2.3 reports results generated with the CCT. To further illustrate the CCT methodology and its interpretation, the following section gives a brief introduction to clinical colorimetry, with a focus on colour spaces and the chromaticity diagram.

Historically, the first attempts to standardize and quantify human perception of colour were undertaken independently by Guild (11) and Wright (12) in the nineteen-twenties, through colour matching experiments. Their basic premise was that every incoming wavelength of visible light (= any specific colour) can be matched by subjects through mixing of three primaries: red (r), blue (b) and green (g). As will be discussed later, this turned out to not be completely true, but it still laid the foundation for clinical colorimetry. The results of these colour matching experiments meant, that from now on each

wavelength of visible light could alternatively be expressed as a tristimulus value, which denotes the amount of each rgb primary required to match any colour (a common representation of this is the colour matching function). If you plot all of these tristimulus values, you need three axes, and therefore generate a colour space. Many different such colour spaces, also called gamuts, are used to describe and quantify colour palettes in various industrial and design settings (i.e. colours produced by computer displays (RGB) or by printers (CMYK)). Note, that these industrial gamuts are different from the tristimulus colour space generated by the method mentioned above. Firstly, industrial gamuts by definition have to fit inside the latter (i.e. encompass fewer colours), as displaying or printing colours that cannot be seen, would be fairly inefficient. But more importantly, the tristimulus colour space does not describe physical colours at all, but perception of colour, which varies tremendously under changing conditions. One crucial condition is illumination, also referred to as temperature, which needs to be specified by a white-point whenever you are quantifying colour perception, especially in a clinical setting. Digital cameras also account for this through an in-built white-balance, which helps mimic human colour perception in their imagery, independent of illumination. Another is the field of view, due to the uneven anatomical distribution of the different cone spectral classes (the 1931 'standard observer' was defined with 2 deg visual field). Lastly, perception of 'brightness' of a stimulus in humans is inherently linked to the perceived colour of a stimulus. Greens of the same power are perceived brighter (greater perceived luminosity) than reds and blues. In fact, the perceived luminosity for all given wavelengths (=luminosity function) in humans aligns closely to the spectral sensitivity of the "green" M-cone.

A commonly used 2D-representation of colour spaces is the chromaticity diagram. In colour science, a colour is defined by two variables: Chromaticity (= hue and saturation) and Luminosity (= brightness). For example, white and grey are of the same chromaticity, but of different luminosities. In the same way, reducing the luminosity of a given orange might result in a brown, without changing chromaticity. The first chromaticity diagram was designed by the Commission internationale de l'éclairage (CIE) in 1931. It projects the CIE 1931 XYZ colour space onto a two-dimensional x'y'-plane. In order to make this feasible, several mathematical changes had to be made to the original tristimulus RGB colour space. In the CIE XYZ colour space X, Y and Z do not correspond to R, G and B.

Rather, their chosen primaries x, y and z were defined arbitrarily to avoid otherwise necessary negative values:

Despite the possibility of close proximation, all fully saturated i.e. “spectral” colours, which lie along the curved edge of the chromaticity diagram (referred to as “spectral locus”) cannot be colour-matched by additive mixing of the r,g,b primaries. For example, many cyan hues can be matched by mixture of b and g, without any r. Yet, no mixture of b and g can create fully saturated cyan. This could only be achieved by adding ‘negative’ red, which was not intended. As a result, the new, deliberately chosen, primaries x,y and z are imaginary colours, which do not correspond to physical colours, that could be perceived in reality. Yet, by mixing these new primaries you can now encompass all real colours, including the spectral colours. In addition, based on the abovementioned similarity of green-intensity and perceived luminosity of a colour, the CIE XYZ colour space was deliberately defined with Y also serving as a measure of luminosity.

Using the XYZ colour space, with its imaginary primaries, the tristimulus values are finally represented in a two-dimensional x’y’-diagram, by normalization of the tristimulus values through the following operation:

$$x = \frac{X}{X+Y+Z};\ y = \frac{Y}{X+Y+Z};\ z = \frac{Z}{X+Y+Z};\ x + y + z = 1;$$

x here is roughly equal to the relative red-green content of a colour and y is roughly equal to the relative blue-yellow content of a colour. As the name implies, the resulting diagram contains only chromaticity (i.e. no dark/light shades, no brown/grey in the examples above etc.). Yet, given any chromaticity value, as well as a luminosity Y, you can still extrapolate all corresponding XYZ, RGB, or any other tristimulus values. This makes the XYZ colour space, and the x’y’ chromaticity diagram a *lingua franca* of colour vision research and practical applications in the field.

The work in this dissertation is based on measurements using a modified version of the original 1931 chromaticity diagram, the 1976 CIE u’v’ chromaticity diagram. It was created in an attempt to normalize the distance between individual colours. In the original 1931 CIE x’y’ diagram, if you take two colours of origin, you can create all colours along a line between them, by mixing these two colours together. Yet, if you mix the colours 1:1, the mixed colour will not be in the middle of that line in the diagram, as the distances

between colours are distorted, compared to how they are perceived. Therefore, multiple iterations of the chromaticity diagram have been developed in an effort to create a chromaticity diagram in which any two colours are equidistant in geometry and perception.

In practice, the CCT tests multiple colour confusion axes in the 1976 CIE L*u*v* colour space (eight vectors in case of Chapter 2.3). For each axis, the CCT records the perceptual threshold, measured as the smallest difference between colours (i.e. the smallest distance in the u'v' diagram), that can be reliably detected by a subject. Worse discrimination results in larger distances. In a last step, the individual axes' threshold results are curve fitted using least-square ellipses, and plotted in the u'v' chromaticity diagram. As a result, the ellipses' long axes align with the combined axes of greatest confusion. Homogenous detection thresholds across the spectrum, as in normal colour vision, or global colour-vision defects, will result in more circular ellipses, while colour-discriminate defects will result in elongated ellipses. Another value that can be measured is total achromatic area, which gives an estimate of the overall magnitude of colour confusion. Figure 7 illustrates the u'v' chromaticity diagram and CCT measurements.

With the 1976 CIE L*u*v* as a basis for displaying and quantifying stimuli, the CCT is a powerful tool to examine human colour vision. It allows to freely adjust the tested confusion axes, and its results can be precisely quantified. In addition, the use of a monitor allows for variable stimuli size adapted to low vision, and requires almost no visual search from the patient, especially compared to tests like the Farnsworth Panel D100. This makes it attractive for patients with heavily constricted visual fields and diffuse colour vision defects (i.e. Choroideremia patients).

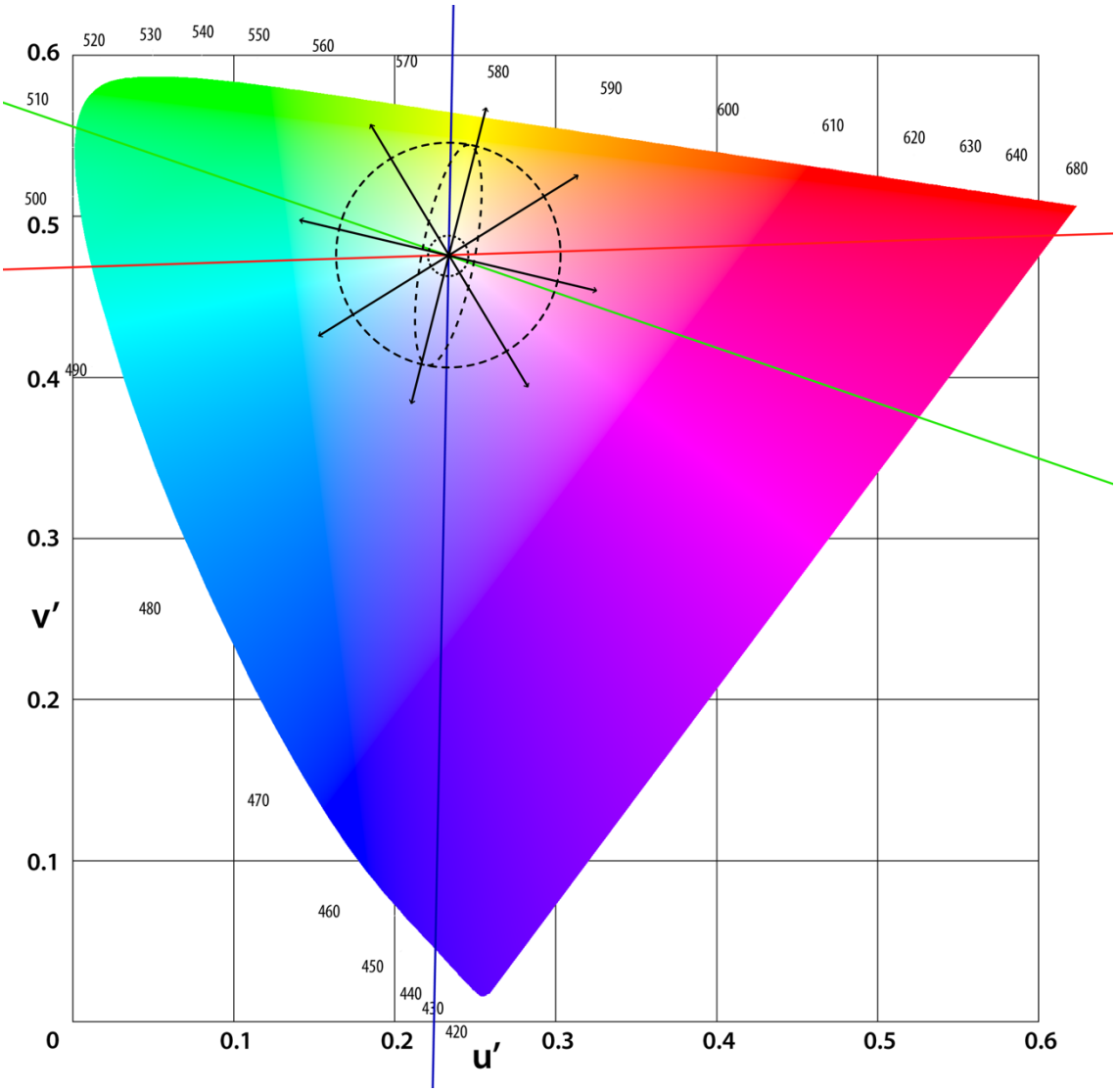

Figure 7: Illustration of the 1976 u′,v′ chromaticity diagram and CCT ellipse colorimetry: Colour discrimination thresholds are tested along a number of vectors (black arrows). A patient's results along all vectors are then curve fitted using least-squares ellipses (dashed lines, 3 sample ellipses shown). From these ellipses, sensitivity thresholds can be derived along any confusion axis, traditionally protan, deutan and tritan (red, green and blue lines). The three depicted ellipses illustrate normal colour vision, tritanopia, and a global colour vision defect. Note, that the displayed test vectors, and colour confusion axes were altered slightly to improve readability of the illustration. They do not reflect the exact coordinates used in testing. ***source: u'v' diagram - artwork released by the author into public domain; CCT-specific annotations - own work.***

1.3. Inherited Retinal Disorders

1.3.1. Choroideremia

Choroideremia is a X-linked, monogenetic, inherited retinal degeneration, with a prevalence of 1:50,000-1:100,000. It usually manifests in the first to second decade of life. Patients suffer from night blindness, followed by a concentric loss of visual fields. Visual acuity is usually preserved until late disease, yet, most patients are legally blind by their fifth or sixth decade of life. Structural equivalent of these symptoms is a comprehensive atrophy of photoreceptors, retinal pigment epithelium and choroid, which spares only the inner retina. This leads to a characteristic, bright, sclera-dominated funduscopic appearance. Atrophic zones usually develop in the mid-periphery and then extend both centrifugally and centripetally. Later stages typically feature a central island of residual outer retina (Fig.8). Choroideremia is caused by mutations in the *CHM* gene, which encodes Rab Escort Protein 1 (REP-1). REP-1 is involved in vesicular transport, and its loss entails an accumulation of outer segments in the retinal pigment epithelium (13,14). In non-ocular tissues its homologue retrogene REP-2 is able to compensate for REP-1 deficiency, mostly preventing a syndromic phenotype (15,16). REP-1's compact open reading frame of around 2kb and its low genetic heterogeneity (almost all cases are due to *null* mutations (17,18)) have made Choroideremia one of the prime targets for AAV-based gene addition therapy, which will be discussed further in the next section. After multiple Phase I/II trials have demonstrated a favourable safety profile, a multicentre phase III trial with over 160 participants is currently ongoing (19). This dissertation contains work surrounding one of the pivotal phase II gene therapy trials (THOR), which was conducted at Tübingen University from 2016 to 2018 (20).

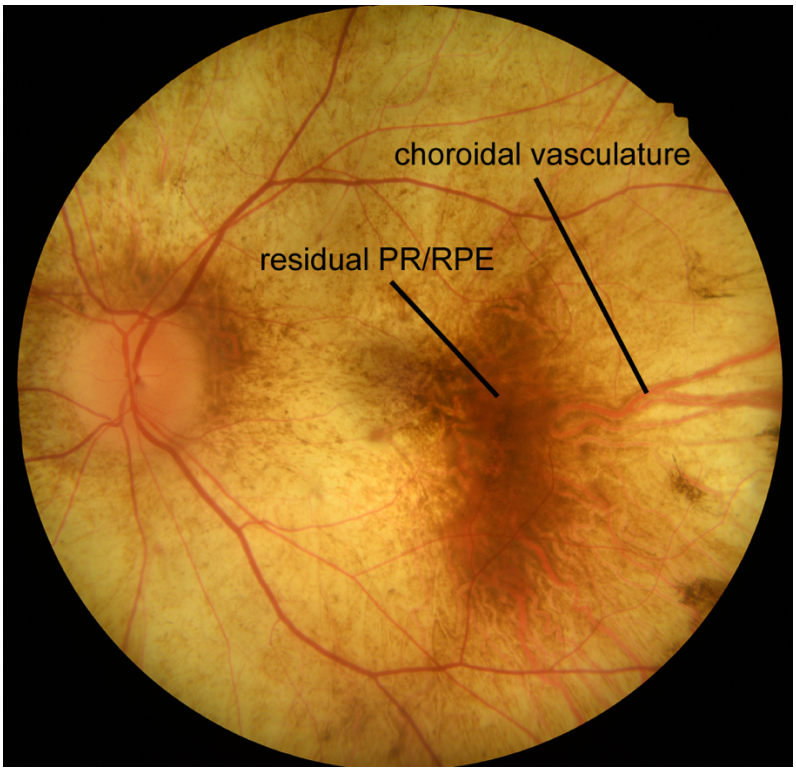

Figure 8: Fundus photograph in Choroideremia: peripheral RPE-atrophy leads to bright-yellowish fundus appearance, with visible choroidal vasculature contrasting against the sclera. In the macula, there is a residual island of intact PR/RPE, which is targeted in gene therapy. Source: Image modified from Fig2 in Chapter 2.3.

1.3.2. Achromatopsia

Achromatopsia (ACHM) is an autosomal-recessive, monogenetic inherited retinal degeneration, with a prevalence of approximately 1:30,000. Patients with ACHM display photophobia, nystagmus, an inability to discriminate colours and poor visual acuity. These symptoms correlate to a dysfunction and subsequent degeneration of cone photoreceptors. 80% of ACHM cases are caused by mutations in the cone cyclic nucleotide-gated channel subunit genes *CNGA3 (21)* or *CNGB3 (22)*. Further causative genes are cone phosphodiesterase genes *PDE6C (23)*, *PDE6H (24), GNAT2, and ATF6*. As depicted in figure 4c. these genes code for essential components of the cone phototransduction cascade. Historically, ACHM was regarded a stationary disease. This is due to the fact, that functional changes in ERG and visual acuity over the course of

ACHMs natural history are minor. With the advent of high-definition structural imaging there has been renewed discussion about this, with the consensus being that ACHM is mostly stationary, but a subset of patients shows minor changes over long periods of time (25,26). Regardless, there is a large therapeutic window with functionally impaired, but morphologically intact cones, that can be targeted with gene therapy. In addition, *CNGA3* and *CNGB3* are short enough to be eligible for AAV-based gene transfer. Chapter 2.1 of this dissertation reports and interprets pre-clinical data on shedding and biodistribution, that were gathered in NHP, prior to the first clinical phase I/II gene therapy trial for ACHM, which was conducted at Tübingen University in 2015 (NCT02610582) (27).

1.4. Gene Therapy

1.4.1. Concept

Gene therapy (GT) is an emerging therapeutic discipline, which conceptually encompasses all strategies that aim to alter the genetic makeup of a cell in order to achieve a therapeutic benefit. GT promises treatment strategies for a host of otherwise incurable diseases, and has already found applications in ophthalmology, neurology, and haematology. GT differs from traditional therapies, in that it has to be tailored to the underlying pathology, and to the treated individual. This makes GT a prime example of personalized medicine.

On a molecular level, GT constitutes an addition or subtraction of a cell's genetic information, with most current GTs being gene addition strategies. Gene addition can be used to substitute a deficient gene, as is the case in the correction of most monogenetic disease, or to introduce a novel, specifically engineered sequence into the target cell, like in CAR-T-cell generation. In gene addition, the therapeutic agent is a 'transgene', a piece of coding DNA, often flanked by regulatory sequences (promoters, enhancers, etc.). Subtraction of genetic information can be used to silence or skip negative dominant genes, or to outright delete pathogenic mutations or genes. The dominance of gene addition in current clinical trials can be attributed to the fact, that gene addition in principle requires

no sequence guiding, and can in some cases be achieved without cleavage of the native DNA (episomal transgene). In consequence gene addition introduces fewer variables and, especially if performed as episomal addition (i.e. no integration into the host genome), carries a favourable safety profile compared to other forms of GT. Nonetheless, given the advent of CRISPR as a breakthrough technology for high-precision, sequence-guided gene correction, a niche that was formerly occupied by zinc-finger nucleases and TALENs, other types of GT are expected to arrive in clinical studies in increasing numbers.

GT can be performed inside the patient (*in vivo*) or on cells extracted from the patient, which are then infused back (*ex vivo*). At the time of writing, *ex vivo* gene therapy is primarily used for CAR-T cell generation in cancer immunotherapy of B-cell mediated malignancies. Here, T-cells of a patient are extracted, purified, and treated with genetically modified lenti- or retroviruses to make them express a chimeric antigen receptor (CAR) with high affinity to CD19, an antigen specific to B-cells and therefore (to a clinically sufficient degree) to the tumour. Once infused back into the patient, this enables the so-armed T-cells to recognize and deplete malignant cells, at the cost of (transient) B-cell dysplasia. Despite its success in haematology, potential applications for *ex vivo* GT are narrow compared to *in vivo* GT. This is because in most disease, affected cells cannot be removed and reinstated as readily as in haematologic conditions, if at all.

In practice, successful GT requires the transgene to reach the target tissue (only relevant *in vivo*), enter the target cell, and express the resulting protein in an appropriate quantity. While gene expression inside the cell is usually modified via design of the transgene, getting there requires a specialized delivery system. These gene-shuttles are called vector systems, and they can be roughly divided into viral and non-viral vectors. Gene transfer via viral vectors is referred to as ‘transduction’, while gene transfer via non-viral vectors is referred to as ‘transfection’.

1.4.2. Challenges and Milestones

Scientists theorized about GT since the 1960s and 70s, when genetically marked cell lines became available and researchers found the first evidence, that exogenous DNA could be expressed in mammalian cells (28). This coincided with the discovery that the polyomavirus SV40 (29) was capable of gene transfer *in vitro*. A decade later, the finding that papillomavirus was able to cause malignant transformation in humans (30) clearly confirmed, that permanent genetic alteration of human cells through viruses was a common occurrence in nature (31). Despite the early interest (32), the necessary technology to achieve safe and efficient gene transfer is very recent. In fact, fatal complications related to the study drug in early clinical GT trials, among them the death of 18 years old Jesse Gelsinger (33), have set back GT clinical translation by decades (34).

The two leading safety concerns in GT are an excessive immune response, termed cytokine release syndrome (CRS), and malignant transformation of treated cells. In the first, a systemic application of supraphysiological quantities of (viral) vector particles causes an over-activation of T-cells, and subsequent release of pro-inflammatory cytokines. As these cytokines stimulate T-cells further, this can spark a deleterious feed-forward loop, a 'cytokine storm', which may escalate to multiple organ dysfunction and death. Naturally, acute immune reactions can also be limited to a treated tissue or organ. In the eye, acute immunogenic inflammatory reactions after gene therapy are referred to as gene therapy associated uveitis (GTAU). In the second major complication, integration of a transgene into the host genome can disrupt tumour suppressor genes or activate protooncogenes, sparking malignant disease. The most prominent example of this complication is a trial for severe combined immunodeficiency (SCID-X1), using an integrating gamma-retrovirus, in which 4 out of 9 treated children developed acute lymphatic leucaemia (ALL) in response to the treatment, one of which died (10 years follow-up) (35,36). Yet, it is important to provide the context: SCID-X1 carries a very poor prognosis, and the applied gene therapy had successfully treated the disease in 7 out of 9 children.

Crucially, the incidence of both major complications is heavily modified by the applied vector system. Using newer generations of viral vectors, safety of GT has improved

substantially (37). Regardless, fatal complications which are potentially related to the vector system still occur (38), and highlight the lasting importance of these fundamental complications. They also serve as a reminder to remain cautious regarding non-medical use of gene editing for the time being (39).

Despite these risks multiple GTs have demonstrated remarkable therapeutic benefit, and were recently able to pass key regulatory milestones. In August 2017, *ex vivo* gene therapy Kymriah®, became the first gene therapy to achieve full FDA approval for treatment of B-cell ALL. This was issued after a single infusion of Kymriah® demonstrated a spectacular 83% overall remission rate in patients suffering from relapsed or refractory disease. Kymriah® was closely followed in December 2019 by a GT in Ophthalmology, when Luxturna® was approved as a treatment for retinal dystrophies with biallelic mutations in *RPE65*. Based on an adeno-associated-virus (AAV) vector system, it was the first *in vivo* gene therapy to be granted full FDA approval, as well as the first approved causal treatment for any inherited disease. Another recent example of successful GT is Zolgensma®, another AAV-based *in vivo* GT for treatment of spinal muscular atrophy type 1, which was approved in 2019. While Zolgensma's® therapeutic effect has been lifesaving in most treated children, it has also gained infamy for being the most expensive drug ever approved at 2.1 million US$ per dose (Luxturna® 'only' costs 0.85 million US$ per patient).

1.4.3. Viral Vectors Overview

A multitude of viruses have been purposed as vectors for gene transfer. The most prominent among them are Adenovirus (Ad) (40–42), Retro- and Lentivirus (RV/LV) (43,44), and Adeno-Associated-Virus (AAV) (45,46)(47). They all come with specific advantages and drawbacks, predisposing them for different applications. The most important criteria regarding use as a vector are its capacity, immunogenicity, tropism and its integration behaviour.

The capacity of a vector is defined as the maximum length of a transportable sequence and is usually measured in kilobases. Larger capacities are generally favourable, to enable

the transfer of larger transgenes. The low capacity of some vector systems like AAV is currently one of the major obstacles in the development of GTs for certain diseases.

As viruses that can be used as vectors are also potential pathogens, they illicit an immune response. Yet, there is a considerable heterogeneity in the incidence and severity of immune-related complications, which is partly related to the virulence of the wildtype viruses. For example, the first generation of Ad vectors was considered particularly immunogenic, while AAV elicits mild immune response(48).

Viral tropism is a term that refers to the entirety of cell types which a virus can enter and replicate in. This is primarily dependent on the type of cellular receptors the particular viral surface can interact with to enter the cell. One such example are retroviruses which have been used extensively for GT, but are not able to transduce non-dividing cells. This led to the development of lentiviral vectors, which are similar to other retroviridae, but can also transduce non-dividing cells. Intracellular components that determine tropism in wildtype viruses can also be relevant in GT, but to a lesser degree, due to the heavily engineered nature of therapeutic transgenes. In gene therapy, the tropism of the vector ideally matches the cell types intended for treatment. A wide tropism reduces the specificity of the therapy through 'off-target' transduction of other tissues. Management of off-target transduction raises multiple challenges as it increases the risk of involuntary changes, increases the number of vector particles you need to administer to achieve the same therapeutic dose in the target tissue, and it creates the risk of germ line transduction. The current consensus in bioethics is that GT is supposed to be limited to an individual. Therefore, germ line transduction is to be prevented, as genetic changes made to gametes are potentially transmitted to offspring. This is one reason for which biodistribution and shedding analyses are paramount to determine the overall safety of a viral vector used in GT. Fortunately, the specificity of a GT is not singularly determined by its vector tropism. It can also be modified through the choice of adequate regulatory elements (i.e. tissue-specific promoters) during transgene design.

Another important distinction between vector groups lies in their integration pattern. Wild type AAV exhibits a low integration frequency, which is further reduced by removing certain elements of the viral genome in recombinant AAV used for GT applications. In contrast, RV, LV and Ad do integrate the transgene into the host genome. While

integration is a risk factor for malignant transformation it enables the transgene to be replicated with the rest of the genome during mitosis. It is therefore essential for treatment of rapidly dividing tissues, in which non-integrating gene transfer would quickly lead to a 'washout' of the therapeutic gene in the treated population of cells. In some vectors, like Ad, the integration site is random, while in RV, there are preferred loci for integration.

All properties discussed in this section can be extensively modified by introducing a variety of changes to the vector. All such efforts to optimize these parameters can be summarized as vector development. For example, the violent CRS caused by early Ad vectors (49,50), led to the development of new generations of Ad vectors, which are less immunogenic (51). Another example is the development of self-inactivating retroviruses in response to the high incidence of malignancy in the SCID-X1 trials (37). Yet, these examples are only the tip of the iceberg. Vector development is a constant, multi-faceted effort and lies at the core of pre-clinical GT development. With regards to ocular gene therapy, Adeno-Associated-Virus has established itself as the dominant vector system.

1.4.4. Adeno-Associated Virus in Gene Therapy

AAV is a small (20nm), non-enveloped virus, that belongs to the parvovirus family. It is also a dependovirus, meaning it is replication-deficient. Its name eludes to the fact, that AAV requires co-infection with a helper virus to replicate, and was consequently first encountered in Adenovirus samples (52). AAV is not known to cause disease in humans.

Wild type AAV (wtAAV) consists of a single-stranded, DNA genome just shy of 4.7 kilobases (kb), which can be either *plus* or *minus,* and is packaged inside an icosahedral capsid made up of 60 protein monomers (53,54). Its coding sequence contains two genes: *rep* and *cap*. Curiously, both *rep* and *cap* are adapted to the small genome size and are regulated and arranged in a way, that enables the expression of a multitude of proteins from only two genes. Preceded by two promoters, the *rep* gene can be transcribed into two, partly homogenous, mRNAs. Furthermore, each mRNA has a splice variant, resulting in a total of 4 possible Rep proteins. Rep proteins possess ATP-binding motifs, helicase activity (55) and regulate transcription (56). Hereby, they facilitate AAV replication and viral packaging into capsids. *cap* encodes the capsid proteins VP1, VP2

and VP3, which are all splice variants of the same mRNA. VP3 is the main constituent of the icosahedral capsid, and outnumbers VP1 and VP2 by a factor of 10:1:1. In an AAV vector system, a form of 'recombinant AAV' (rAAV), both *rep* and *cap* are replaced by the therapeutic transgene.

Flanking *rep* and *cap*, are two palindromic 145bp regions called inverted terminal repeats (ITR). Due to their palindromic structure, ITRs can loop around and form a double-stranded hairpin. These hairpins serve as origins of translation, that enable second-strand synthesis via interaction with host DNA polymerases. Once double strand synthesis is complete, ITRs also facilitate the formation of a double-stranded, circular, episomal loop of DNA, a concatemer. In wtAAV this episomal DNA loop allows the virus to remain dormant in the nucleus until a helper virus infects the cell and ignites replication. ITRs are also the only part of the wtAAV genome that has to be carried over to rAAV transgene cassettes (= *in cis* of the transgene during vector production).

Another beneficial property of AAV lies in the rapid evolution of its capsid surface, which is mediated by 12 hypervariable regions in the *cap* gene (57). At the time of writing 13 capsid variants, called serotypes, have been identified, of which AAV 2 is the most studied (54,58,59). With the large variety of serotypes comes a plethora of specific tropisms (60). AAVs most efficient targets include neurons, skeletal muscle cells, vascular smooth muscles cells and hepatocytes, but some AAVs have been found to also effectively transduce other dividing and non-dividing tissues, including in heart, lung and kidney. Known receptors and co-receptors for cell entry include heparan sulfate proteoglycan (HSPG), N- and O-linked sialic acids, galactose, several integrins, and several growth factors.

Another implication of this variety is, that AAV is quite malleable and can be engineered to transduce an array of different cells at high specificity. In practice, recombinant AAVs are produced using separate *rep* and *cap* plasmids, and a third plasmid containing the transgene cassette (= transgene + regulatory sequences + ITRs). If the *rep* and *cap* genes are sourced from different serotypes, the resulting hybrid rAAV is referred to as 'pseudotyped' (i.e. AAV2 *rep* + AAV8 *cap* = rAAV2/8). Two efficient methods which are used to modify serotypes further are targeted mutation approaches (61) and (*in* or *ex vivo*) directed evolution, for which AAV is quite transmissive (62). For example, one of

the preferred pseudotypes in retinal GT is rAAV2/8. A close variant, and a good example of targeted mutation in ocular gene therapy, is rAAV2/8(Y733F). In this vector, a capsid surface tyrosine (Y) residue at position 733 was deliberately substituted for a phenylalanine (F) residue. This was done after it was found that Y residues on the capsid surface were prone to phosphorylation by epidermal growth factor receptor protein tyrosine kinase (EGFR-PTK), and subsequent proteasomal degradation, which reduced transduction efficiency (63). As F residues are not phosphorylated by the enzyme, substation of Y with F was hypothesized to circumvent the intracellular loss of vector genomes, and increase transduction efficiency. indeed, this led to an improved transduction efficiency, and spurred development of multiple further iterations of Y-F vectors (64) (i.e. Quad Y-F). AAV2/2-7m8 (7m8 being the denominator for a peptide insertion in the capsid) one the other hand is an example for an approach called directed evolution, which is wildly different from targeted mutagenesis. In directed evolution, a *cap* genome library is generated through error-prone PCR. From this library a myriad of capsid-mutant vectors can be produced, from which individual strains are selected for desired traits, either *in vitro* or *in vivo* (62,65,66).

However, AAV has limitations which are more difficult to address, such as its low capacity. Many desirable transgene cassettes are larger than the 4.7kb capacity AAV can provide. On the larger end of the spectrum are genes like dystrophin in Duchenne's Muscular Dystrophy, with a cds of more than 11 kb. In retinal gene therapy, *ABCA4* (Stargardt's disease) and USH2A (Usher syndrome, coding sequence of approx. 15kb) are examples for desirable genetic targets too large for AAV. One strategy to transfer larger genes is co-infection of a cell with two vectors, each containing a part of the full sequence, as well as a set of recombination signals to ensure directional recombination (67).

But most importantly, AAV has demonstrated an overall excellent safety profile in animal and clinical studies. While wtAAV which still contain *rep* can occasionally integrate into the host genome (curiously this occurs specifically on chromosome 19), insertion events in rAAV only occur due to nonhomologous recombination and are very rare (68). Taken together the risk of insertional mutagenesis and malignant transformation is very low. Furthermore, while antibodies against AAV can be detected in a significant share of the population (i.e. AAV8: 32-65%,(69)), immune response against AAV is generally mild.

Critically, the notion that there is no immune response can be misleading and has come under increasing scrutiny (59,70–72). Administered systemically in very large doses AAV can potentially cause severe immune-related complications, and there is ample evidence for activation of the immune system, even in focal retinal gene therapy (73).

1.4.5. Specifics of Ocular Gene Therapy

As mentioned in section 1.4.2, voretigene neparvovec, was the first approved *in vivo* GT for eye diseases. It is not by chance, that Ophthalmology is one of the leading specialties in the clinical translation of GT, as the eye is in many ways a perfect match for current gene addition strategies. Regardless, ocular gene therapy comes with its own specific set of challenges, which need to be accounted for.

Firstly, the success of ocular gene therapy is part of AAV's success as a vector system. Photoreceptors, as post-mitotic neurons, rather undisturbed by the immune system, are impervious to most of AAVs drawbacks as a vector, and vice versa some AAV serotypes exhibit a natural tropism towards neurons. Also, there is a wealth of potential targets for GT, as there is a stunning number of monogenetic, inherited diseases which affect the retina, with more than 260 genes known to cause IRDs (74). From a clinical standpoint, the eye is easily accessible for both interventions and high-resolution imaging. The fact that it is a paired organ is also of benefit, as the fellow eye can potentially be used as an intraindividual control in interventional studies.

A more nuanced and constantly evolving aspect of retinal GT is optimal vector administration. While the blood-retina barrier is helpful in some regards (i.e. in reducing inflammation), it also prevents local tissue transduction after systemic application. Apart from gene therapy, the most common intraocular (i.e. non-topical) route of drug administration is intravitreal injection (IVT). IVT is a minimally invasive procedure, can be performed in an outpatient setting under local anaesthesia, and achieves much higher intraocular concentrations of an applied drug than topical or oral administration. Naturally, this makes IVT a desired route of administration for retinal GT. But despite the proximity of photoreceptors and vitreous, retinal transduction after IVT of rAAV is mostly limited to the inner retina (75), especially ganglion cells and Müller glia. A major barrier limiting transduction is the inner limiting membrane (ILM) (76). While this is

beneficial in certain diseases, which affect ganglion cells, most GT would require transduction of the PR and RPE. Another disadvantage of IVT lies in the eventual systemic drainage and dispersion of intraocular fluid, which can lead to off-target transduction and potentially compromises the ocular immune privilege. For these reasons, most current retinal gene therapies are administered via subretinal injection. In most current protocols, this procedure is performed in conjunction with a vitrectomy and thus requires a surgical theatre with operating microscope, vitrectomy machine and an experienced surgeon. The subretinal injection is performed with a very fine syringe (41 gauge) delivering vector solution into the otherwise virtual subretinal space. From this "bleb", vector particles have direct access to both RP and RPE. Creation of the bleb does assert mechanical (stretching force) and metabolic (detachment) stress, which, especially in vulnerable retina, can lead to complications such as atrophy of retinal tissue, macular hole formation and subsequent reflux of vector into the vitreous cavity (77). While more invasive and much more demanding in terms of required technology and surgical expertise (78,79), SR enables efficient transduction of the outer retina, and is the gold standard for retinal GT.

1.5. Aims

This thesis concentrates efforts directed towards a successful realisation of Germany's first phase I/II ocular GT trials. Challenges presented by the clinical reality of retinal GT were identified and addressed in three chapters, that draw equally from basic research and clinical expertise.

Chapter 2.1., titled "Vector Safety and Surgical Procedure: Superior Gene Transfer And Biodistribution Profile Of Subretinal Vs. Intravitreal Delivery Of AAV8 In Non-Human Primates", evolves around patient safety and environmental safety, through the lens of surgery technique. It aims to inform choice of surgical method, post-surgical quarantine of patients, handling of surgical complications in SR GT, and pre-clinical vector development. Critical questions to this end were:

1.) Does ocular administration of rAAV lead to germ line transduction? 2) Do patients need to be quarantined after GT to avoid shedding of gene-altering GMOs into the environment? 3.) Is significant reflux into the vitreous cavity, in case of a surgical complication (i.e. macular hole), problematic from a safety perspective? 4.) How do IVT and SR compare in terms of gene transfer, biodistribution and shedding? 5.) Is SR warranted, given the greater invasiveness compared to IVT?

To address these (among other) questions, 22 NHP (M. fascicularis) were chosen as a relevant model for biodistribution and shedding of vector particles after GT. They were divided into four groups and treated with clinical grade AAV in different doses and with different routes of administration (SR vs. IVT). Biofluids were sampled for 91 days post-surgery, after which the animals underwent necropsy. All biofluid and organ samples were then analysed for presence of vector genomes via qPCR.

Chapter 2.2., titled "Selecting Study Participants and Phenotyping in Ultra-Rare Disease: Multimodal Assessment Of Choroideremia Patients Defines Pre-Treatment Characteristics" is occupied with the evaluation of an ultra-rare patient collective under an intention to treat. It aims to inform patient selection and study design. It addresses the following questions:

1.) Can the partner eye of the treated eye be used as an internal, intraindividual control to measure therapeutic outcome (e.g. in which endpoints is the disease symmetrical, and to what degree)? 2.) What is the kinetics of vision loss in Choroideremia? 3.) Under the assumption that GT halts disease, how long of a follow-up is required to detect a therapeutic benefit? 4.) Which patients are suited to demonstrate a therapeutic benefit in an adequate time frame for approval? 5.) Are there any genotype-phenotype correlations in our cohort of potential patients?

Here, a retrospective analysis of potential study candidates suffering from Choroideremia was performed, with special attention to the symmetry between eyes, multimodality, and precise quantification of all endpoints.

After vector-development, patient safety, and cohort selection, chapter 2.3. "Defining Relevant Endpoints: Colour Discrimination Ellipses in Choroideremia" is concerned with determination of efficacy and adequate clinical endpoints required for approval:

1.) Which functional endpoints are useful for defining late-stage Choroideremia? 2.) Is there an alternative functional endpoint to visual acuity, which is also primarily affected in late disease? 3.) How can we best adapt clinical testing to the limitations of a heavily impaired patient collective?

The discrepancy in anatomical distribution of S vs. M/L cones led to the hypothesis, that S cones might be impaired to a larger degree in centripetally advancing Choroideremia. In this case tritan (blue)-discrimination might be a functional parameter in late stage Choroideremia. Due to the practical difficulties of Choroideremia patients in solving routine colour vision tests which require intense visual search, and in anticipation of the potential broad spectrum of ill-defined colour vision defects in this retinal degeneration, a cohort of CHM patients was investigated with an out-of-clinics colour vision test, the Cambridge Colour Test.

RESULTS

2.1. Vector Safety and Surgical Procedure: "Superior gene transfer and biodistribution profile of subretinal vs. intravitreal delivery of AAV8 in non-human primates"

Retina

Superior Retinal Gene Transfer and Biodistribution Profile of Subretinal Versus Intravitreal Delivery of AAV8 in Nonhuman Primates

Immanuel P. Seitz,[1,2] Stylianos Michalakis,[3] Barbara Wilhelm,[4] Felix F. Reichel,[1,2] G. Alex Ochakovski,[1,2] Eberhart Zrenner,[2] Marius Ueffing,[2] Martin Biel,[3] Bernd Wissinger,[2] Karl U. Bartz-Schmidt,[1] Tobias Peters,[4] and M. Dominik Fischer[1,2,4,5]; for the RD-CURE Consortium

[1]University Eye Hospital, Centre for Ophthalmology, University of Tübingen, Tübingen, Germany
[2]Institute for Ophthalmic Research, Centre for Ophthalmology, University of Tübingen, Tübingen, Germany
[3]Center for Integrated Protein Science Munich (CIPSM) at the Department of Pharmacy–Center for Drug Research, Ludwig-Maximilians-Universität München, Munich, Germany
[4]STZ Eyetrial at the Centre for Ophthalmology, University of Tübingen, Tübingen, Germany
[5]Nuffield Laboratory of Ophthalmology, Nuffield Department of Clinical Neurosciences, University of Oxford, Oxford, United Kingdom

Correspondence: Tobias Peters, STZ Eyetrial at the Centre for Ophthalmology, Elfriede-Aulhorn-Straße 7, 72076 Tübingen, Germany; Tobias.Peters@stz-eyetrial.de.

See the appendix for the members of the RD-CURE Consortium.

Submitted: June 20, 2017
Accepted: September 26, 2017

Citation: Seitz IP, Michalakis S, Wilhelm B, et al. Superior retinal gene transfer and biodistribution profile of subretinal versus intravitreal delivery of AAV8 in nonhuman primates. *Invest Ophthalmol Vis Sci*. 2017;58:5792–5801. DOI:10.1167/iovs.17-22473

Purpose. To investigate shedding and biodistribution characteristics of recombinant adeno-associated virus serotype 8 (rAAV8) after single-dose subretinal or intravitreal injection in nonhuman primates (NHP, *Macaca fascicularis*) as a surrogate for environmental hazard and patient safety.

Methods. In a study for regulatory submission, 22 NHP were divided into four cohorts receiving either single subretinal injections of vehicle or clinical grade rAAV8 (1×10^{11} or 1×10^{12} vector genomes [vg]) versus single intravitreal application of 1×10^{12} vg. Viral shedding and biodistribution were monitored in biofluids for up to 91 days, followed by necropsy and tissue harvesting of all major organs, the visual pathway, and lymphatic tissue. Quantification of vector genomes was done by quantitative (q)PCR.

Results. Shedding occurred in a dose-dependent manner in all biofluids and persisted for a maximum of 7 days. Intravitreal delivery led to increased and persistent (up to 13 weeks) distribution of vector genomes in blood and draining lymphatic tissue, increased off-target deposition, and inefficient gene transfer to the retina. No vector targeting of the germ line was observed in any cohort.

Conclusions. These data illustrate that subretinal application of rAAV8 leads to a more favorable biodistribution profile compared to intravitreal injections. Extraocular biodistribution is limited after subretinal delivery, while intravitreal injection leads to both greater and more persistent systemic exposure, evident in blood and lymphatic tissues. With the knowledge on the dynamics of shedding in a setting mimicking clinical application, guidelines can be developed to refine clinical trial protocols to reduce the risk for trial subjects and their environment.

Keywords: AAV8, nonhuman primates, biodistribution, shedding, subretinal versus intravitreal

This study was performed to meet the requirements for a regulatory submission of a "first in man" clinical trial, testing an investigational new drug (IND) for the treatment of achromatopsia (ACHM). ACHM is a hereditary retinal disorder with an estimated prevalence of 1:30,000[1] for which currently no treatment exists. The prevalence is greater in certain genetically isolated areas like the Micronesian atoll Pingelap, where up to 6% of the population are affected by the condition.[2] ACHM is a congenital disease that exclusively impairs cone function. Affected individuals suffer pronounced photopic defects such as total color blindness, reduced visual acuity, hemeralopia (day blindness), nystagmus, and photophobia.[3] To date, six genes have been identified that link to ACHM. Five of them constitute essential parts of the cone phototransduction cascade as they encode either for cyclic nucleotide–gated channels (*CNGA3*[4]/*CNGB3*[5]), phosphodiesterases (*PDE6C*[6]/*PDE6H*[7]), or a related G protein (*GNAT2*[8]). The sixth gene is *AFT6*. It encodes a protein that is part of the unfolded protein response in the endoplasmic reticulum.[9] At the University Eye Hospital Tübingen, we performed the first clinical gene therapy for ACHM caused by mutations in *CNGA3* using subretinal administration of rAAV8.hCNGA3 (NCT02610582) in 2015. Here, we describe findings from the preclinical biodistribution study, which evaluated safety aspects including the extent of biodistribution within the visual system, the extraocular tissues (e.g., germ line), and shedding of any genetically modified organism (GMO) into the environment after subretinal versus intravitreal injections. Cynomolgus monkeys were chosen because their ocular anatomy is rather humanlike (i.e., presence of a macula) and suited to mimic

Superior Retinal Gene Transfer and Biodistribution Profile of Subretinal Versus Intravitreal Delivery of AAV8 in Nonhuman Primates

Immanuel P. Seitz,[1,2] Stylianos Michalakis,[3] Barbara Wilhelm,[4] Felix F. Reichel,[1,2] G. Alex Ochakovski,[1,2] Eberhart Zrenner,[2] Marius Ueffing,[2] Martin Biel,[3] Bernd Wissinger,[2] Karl U. Bartz-Schmidt,[1] Tobias Peters,[4] and M. Dominik Fischer[1,2,4,5]; for the RD-CURE Consortium

[1]University Eye Hospital, Centre for Ophthalmology, University of Tübingen, Tübingen, Germany
[2]Institute for Ophthalmic Research, Centre for Ophthalmology, University of Tübingen, Tübingen, Germany
[3]Center for Integrated Protein Science Munich (CIPSM) at the Department of Pharmacy–Center for Drug Research, Ludwig-Maximilians-Universität München, Munich, Germany
[4]STZ Eyetrial at the Centre for Ophthalmology, University of Tübingen, Tübingen, Germany
[5]Nuffield Laboratory of Ophthalmology, Nuffield Department of Clinical Neurosciences, University of Oxford, Oxford, United Kingdom

Correspondence: Tobias Peters, STZ Eyetrial at the Centre for Ophthalmology, Elfriede-Aulhorn-Straße 7, 72076 Tübingen, Germany; Tobias.Peters@stz-eyetrial.de.

See the appendix for the members of the RD-CURE Consortium.

Submitted: June 20, 2017
Accepted: September 26, 2017

Citation: Seitz IP, Michalakis S, Wilhelm B, et al. Superior retinal gene transfer and biodistribution profile of subretinal versus intravitreal delivery of AAV8 in nonhuman primates. *Invest Ophthalmol Vis Sci.* 2017;58:5792–5801. DOI:10.1167/iovs.17-22473

Purpose. To investigate shedding and biodistribution characteristics of recombinant adeno-associated virus serotype 8 (rAAV8) after single-dose subretinal or intravitreal injection in nonhuman primates (NHP, *Macaca fascicularis*) as a surrogate for environmental hazard and patient safety.

Methods. In a study for regulatory submission, 22 NHP were divided into four cohorts receiving either single subretinal injections of vehicle or clinical grade rAAV8 (1×10^{11} or 1×10^{12} vector genomes [vg]) versus single intravitreal application of 1×10^{12} vg. Viral shedding and biodistribution were monitored in biofluids for up to 91 days, followed by necropsy and tissue harvesting of all major organs, the visual pathway, and lymphatic tissue. Quantification of vector genomes was done by quantitative (q)PCR.

Results. Shedding occurred in a dose-dependent manner in all biofluids and persisted for a maximum of 7 days. Intravitreal delivery led to increased and persistent (up to 13 weeks) distribution of vector genomes in blood and draining lymphatic tissue, increased off-target deposition, and inefficient gene transfer to the retina. No vector targeting of the germ line was observed in any cohort.

Conclusions. These data illustrate that subretinal application of rAAV8 leads to a more favorable biodistribution profile compared to intravitreal injections. Extraocular biodistribution is limited after subretinal delivery, while intravitreal injection leads to both greater and more persistent systemic exposure, evident in blood and lymphatic tissues. With the knowledge on the dynamics of shedding in a setting mimicking clinical application, guidelines can be developed to refine clinical trial protocols to reduce the risk for trial subjects and their environment.

Keywords: AAV8, nonhuman primates, biodistribution, shedding, subretinal versus intravitreal

This study was performed to meet the requirements for a regulatory submission of a "first in man" clinical trial, testing an investigational new drug (IND) for the treatment of achromatopsia (ACHM). ACHM is a hereditary retinal disorder with an estimated prevalence of 1:30,000[1] for which currently no treatment exists. The prevalence is greater in certain genetically isolated areas like the Micronesian atoll Pingelap, where up to 6% of the population are affected by the condition.[2] ACHM is a congenital disease that exclusively impairs cone function. Affected individuals suffer pronounced photopic defects such as total color blindness, reduced visual acuity, hemeralopia (day blindness), nystagmus, and photophobia.[3] To date, six genes have been identified that link to ACHM. Five of them constitute essential parts of the cone phototransduction cascade as they encode either for cyclic nucleotide–gated channels (*CNGA3*[4]/*CNGB3*[5]), phosphodiesterases (*PDE6C*[6]/*PDE6H*[7]), or a related G protein (*GNAT2*[8]). The sixth gene is *AFT6*. It encodes a protein that is part of the unfolded protein response in the endoplasmic reticulum.[9] At the University Eye Hospital Tübingen, we performed the first clinical gene therapy for ACHM caused by mutations in *CNGA3* using subretinal administration of rAAV8.hCNGA3 (NCT02610582) in 2015. Here, we describe findings from the preclinical biodistribution study, which evaluated safety aspects including the extent of biodistribution within the visual system, the extraocular tissues (e.g., germ line), and shedding of any genetically modified organism (GMO) into the environment after subretinal versus intravitreal injections. Cynomolgus monkeys were chosen because their ocular anatomy is rather humanlike (i.e., presence of a macula) and suited to mimic

surgical procedures used in patients. These data are expected to be relevant to all ocular gene therapies utilizing the adeno-associated virus serotype 8 (AAV8) capsid and possibly other serotypes with similar tropism, as the affinity of capsid surface epitopes toward local receptors helps to define their distribution pattern. Recent evidence of innate and adaptive immunity toward AAV epitopes increases the significance of these findings.[10,11]

Materials and Methods

Cynomolgus monkeys (nonhuman primates, NHP) were treated and cared for at the Covance Preclinical Services GmbH test facility in Muenster, Germany. The study was conducted with great care to ensure the well-being of the animals and was approved by the local authorities (Regierungspraesidium of North-Rhine Westphalia). All animal procedures were performed in accordance with the ARVO Statement for the Use of Animals in Ophthalmic and Vision Research, and in full compliance with the guidelines of the European Community (EUVD 86/609/EEC) for the care and use of laboratory animals, as well as in accordance with Good Laboratory Practice (GLP) standards as defined by German GLP monitoring authorities and in compliance with U.S. Food and Drug Administration and Good Laboratory Practice regulations.

Animals

A total of 22 NHP were assigned to four study cohorts. Six animals (three of each sex) were assigned to cohorts 1 to 3 and treated with subretinal injections (SR). Cohort 1 received vehicle only: balanced salt solution, BSS (Alcon Laboratories [UK] Ltd., Camberley, UK) with 0.001% PF-68 surfactant (BASF, Ludwigshafen, Germany). Cohorts 2 and 3 received single SR of either 1×10^{11} vector genomes (vg) (low dose) or 1×10^{12} vg (high dose), respectively. Cohort 4 consisted of four animals (two of each sex) and received single intravitreal injections (IVT) of 1×10^{12} vg (high dose) to mimic leakage from the subretinal space (e.g., through retinotomy or macular hole) or via falsa injection.

Production of Recombinant AAV8

Recombinant AAV8 carrying a transgene cassette based on an AAV2 genome (pseudotype AAV2/8) was manufactured according to good manufacturing practice (GMP) guidelines. It contained a cone-arrestin 3 promoter driving *CNGA3* expression that has been shown to have therapeutic effect in the Cnga3$^{-/-}$ mouse model.[12] GMP grade *cis* and *trans* plasmid DNA was provided by Aldevron (Fargo, ND, USA) using a high-quality characterized *Escherichia coli* master cell bank (MCB), and Atlantic BioGMP (Nantes, France) produced the GMP grade viral particles (rAAV.*hCNGA3*) utilizing a transient double-transfection protocol of an HEK293 MCB fully characterized according to the European Pharmacopeia. Harvested cells were lysed and supernatant PEG-precipitated, treated with benzonase, and purified by two rounds of caesium chloride gradient ultracentrifugation followed by a tangential flow filtration step for diafiltration and concentration. After formulation, the resulting drug substance was stored at ≤ -70°C until application.

Surgery and Postsurgical Care

Animals received general volatile anesthesia with isoflurane; (peri-)orbital regions were treated with 10% povidine iodine solution and sterile surgical drapes applied as in the clinical setting. A temporal canthotomy was performed for improved access, and three transconjunctival sclerotomies were made after transillumination confirmed the location of pars plana. Vitrectomy was performed as completely as possible without affecting the lens. A localized retinal detachment was induced through SR of 50 µL BSS (Alcon Laboratories) using a 41-gauge cannula (DORC 1270.EXT; Dutch Ophthalmic Research Center [International], B.V., Zuidland, The Netherlands). Virus solution (200 µL) was injected into the preformed bleb using a foot pedal–controlled injection system (PentaSys II; Ruck GmbH, Eschweiler, North Rhine-Westphalia, Germany). Before recovery, subconjunctival cefuroxime (125 mg; Ratiopharm GmbH, Ulm, Baden-Württemberg, Germany) and dexamethasone (2 mg; Ratiopharm Gmbh) were administered to the operated eye. Postoperative prophylactic treatment consisted of antibiotic (0.5% moxifloxacine; Ratiopharm GmbH), and antiphlogistic (1% prednisolone; Ratiopharm GmbH) eye drops given 3×/day each in the treated eye for 2 weeks and prednisone (Ratiopharm GmbH) 1 mg/kg intramuscularly from day −2 until day 5.

Biofluid and Tissue Sampling

Biofluid samples were harvested from all animals before dosing and on days 2, 3, 5, 7, and 31 for quantitative (q)PCR analysis. Blood was collected before dosing and 24, 48, 72, and 168 hours and at weeks 4 and 13 post dosing. Predose samples and samples collected on days 2 and 3 were analyzed in the first instance. The remaining samples were analyzed until there were two consecutive time points that were negative for vector genomes. Sample volumes used for analyses were 220 µL for blood, tear film, and nasal secretions, 100 µL for urine, and 50 µL for aqueous humor. For large organs, tissue samples were harvested at necropsy (91 days post dosing) with sterile, DNase-free single-use instruments and stored at <-70°C until DNA extraction. Where reported, whole organ weights, as well as individual sample weights, were documented. This enabled extrapolation of copy numbers per mg sample to copy numbers per (whole) organ.

DNA Extraction and qPCR

DNA was extracted from all tissue and blood samples prior to qPCR using QIAsymphony DSP DNA Mini kit with Qiagen Reagent DX, and the QIAsymphony DSP DNA Mini kit, respectively (Qiagen, Hilden, North Rhine-Westphalia, Germany). DNA concentrations were measured using spectrophotometry. Eight cryosections (20 µm thick) from whole eye cups were processed for each animal and pooled into one sample for extraction. Also, for heart, lung, and liver, three samples were extracted separately and the eluates pooled to result in one sample analyzed by qPCR. For all tissue samples and blood, 1 µg DNA was used per qPCR reaction. QIAsymphony DSP Virus/Pathogen kit for biofluids was used for the remaining samples. DNA concentration of these samples was not determined, due to the inclusion of carrier RNA in the extraction procedure. Here, samples of 5 µL were analyzed neat by qPCR. For presentation, results are normalized to 1 mL source material to improve interpretability. To validate the qPCR assay, a positive control (transgene plasmid) was serially diluted from 5×10^7 to 50 copies/reaction. The data generated from this dilution series were used to construct a standard curve for quantitative data analysis. Samples that tested positive after 40 cycles of amplification, but below 50 copies, were supposed to contain a nonquantifiable number of genomes per reaction (between 1 and 50), and thus deemed "<LLOQ." Samples without amplification after 40 cycles were deemed "negative." This validated qPCR assay was used to analyze each sample in

Table 1. Surrogates Relevant to Clinical Practice

Clinical Surrogates, Shedding		Maximal Shedding		Thresholds, Achieved in Days	
Sample	Cohort	On Day	Mean vg/mL	All < LLOQ	All Negative
Tear film	Low-dose SR	2	2.8 E+5	7	7
	High-dose SR	3	8.8 E+6	31	31
	High-dose IVT	3	3.7 E+4	31	31
Nasal secretions	Low-dose SR	2	1.2 E+5	31	>31
	High-dose SR	3	1.8 E+5	31	>31
	High-dose IVT	2	1.1 E+5	31	>31
Urine	Low-dose SR	2	3.3 E+3	3	3
	High-dose SR	2	6.1 E+4	7	>31
	High-dose IVT	2	2.3 E+4	31	31
Blood	Low-dose SR	0	0	0	0
	High-dose SR	1	1.1 E+4	7	>31
	High-dose IVT	1	5.1 E+6	91	>91

Tears and urine featured a response to both dose and route of administration. While dose escalation led to increased copy numbers and shedding duration, route of administration mostly affected copy numbers, rather than shedding duration, which was generally similar between subretinal and intravitreal injections. Blood samples did not show any vector presence after low-dose subretinal injections, and limited vector load after high-dose subretinal injections, while intravitreal administration led to immediate, strong, and persistent presence of vector in blood. First column: Groups. Second column: Time point of maximal shedding, vector genomes/mL of raw sample (cohort mean). Third column: Persistence of vector shedding, characterized by two thresholds: residual shedding = all samples testing at least below LLOQ, no shedding (none) = all samples negative.

triplicate, with one of the replicates spiked with a known quantity of the qPCR positive control to assess for the presence of any potential inhibitors in the sample.

Results

Animal Dosing

All randomly assigned animals successfully underwent dosing per protocol within 3 consecutive days. Complete subretinal placement was evident in direct visualization through the operating microscope and involved the targeted macular area in all animals. All biofluid and tissue sampling could be performed according to standard operating procedures and in strict accordance with GLP guidelines.

Animals Injected With Vehicle Only

All tissue and biofluid samples taken from animals in the control cohort injected with vehicle tested negative for presence of transgenic DNA, with exception of one tear sample and two nasal swabs taken from one female animal. In these samples, transgenic DNA quantities detected were all below the lower level of quantification (LLOQ = 50 copies per reaction). All consecutive tear samples and nasal swabs from this animal tested negative, as did all other biofluid and/or tissues samples at all time points.

Animals Injected With Vector Solution

Shedding occurred to some degree in all animals injected with vector solution and in all types of biofluids tested. An overview of maximal amount of detected vector genomes/mL biofluid and duration of shedding by route of administration and dose is given in Table 1. Of the biofluids that shed into the environment (tears, nasal secretions, and urine) no sample tested above the LLOQ later than day 7. Maximal shedding in most animals was observed 2 days after injection. After SR, shedding was most pronounced in tear fluid, followed by nasal secretions and urine. After IVT, the largest amount of vector was also shed via tears, but was followed by urine and lastly nasal secretions. Table 1 presents time points when shedding of all samples of a cohort were below LLOQ (residual shedding), or below level of detection (no shedding). Figure 1 summarizes the qualitative changes of shedding status (positive, residual, or negative) per cohort and biofluid over the observed time frame. To characterize time dependency it introduces $T_{1/2}$ as a semiquantitative "shedding status half-life": the point in time (in days) after administration on which ≥50% of a cohort's samples test below LLOQ. Individual shedding results of all animals are shown in Figures 2 to 4, plotted in log scale against time of harvest, capturing both the variability between animals of the same cohort and differences between cohorts.

Individual Lacrimal Shedding Results

Shedding via tear film was subject to a pronounced dose effect (Figs. 1, 2; Table 1). In animals from the low-dose group, fewer copies were found in positive samples, and tears were negative after a shorter time, compared to the high-dose group. Subretinal application of the high dose led to a 33-fold increase in maximal shedding (cohort mean) compared to the low dose, and shedding persisted at quantifiable levels for at least 1 week after surgery. Route of administration also had distinct effects on shedding via tears. While fewer copies were detected following intravitreal compared to SR (with the same amount of vector applied), both groups featured quantifiable samples after 1 week. Where only four out of six animals from the low-dose group shed vector via tears at any given time point, all (6/6) animals from the high-dose subretinal and (4/4) intravitreal cohorts shed vector via tears over the course of the study. Individual results are displayed in Figure 2 and copy numbers/mL are given in Supplementary Material S1.

Individual Shedding Results via Nasal Secretions

Shedding via nasal secretions was less dependent on dosage than shedding through tears and urine (Figs. 1, 3; Table 1). Shedding in the low-dose subretinal cohort receded more quickly ($T_{1/2}$ after 4 vs. 7 days for high dose) and was slightly less prevalent (5/6 animals), compared to the high-dose cohort (6/6). In line with the slightly increased prevalence after high-dose injection, dose escalation by one log unit also entailed a modest 1.4-fold increase in maximal copy numbers (cohort

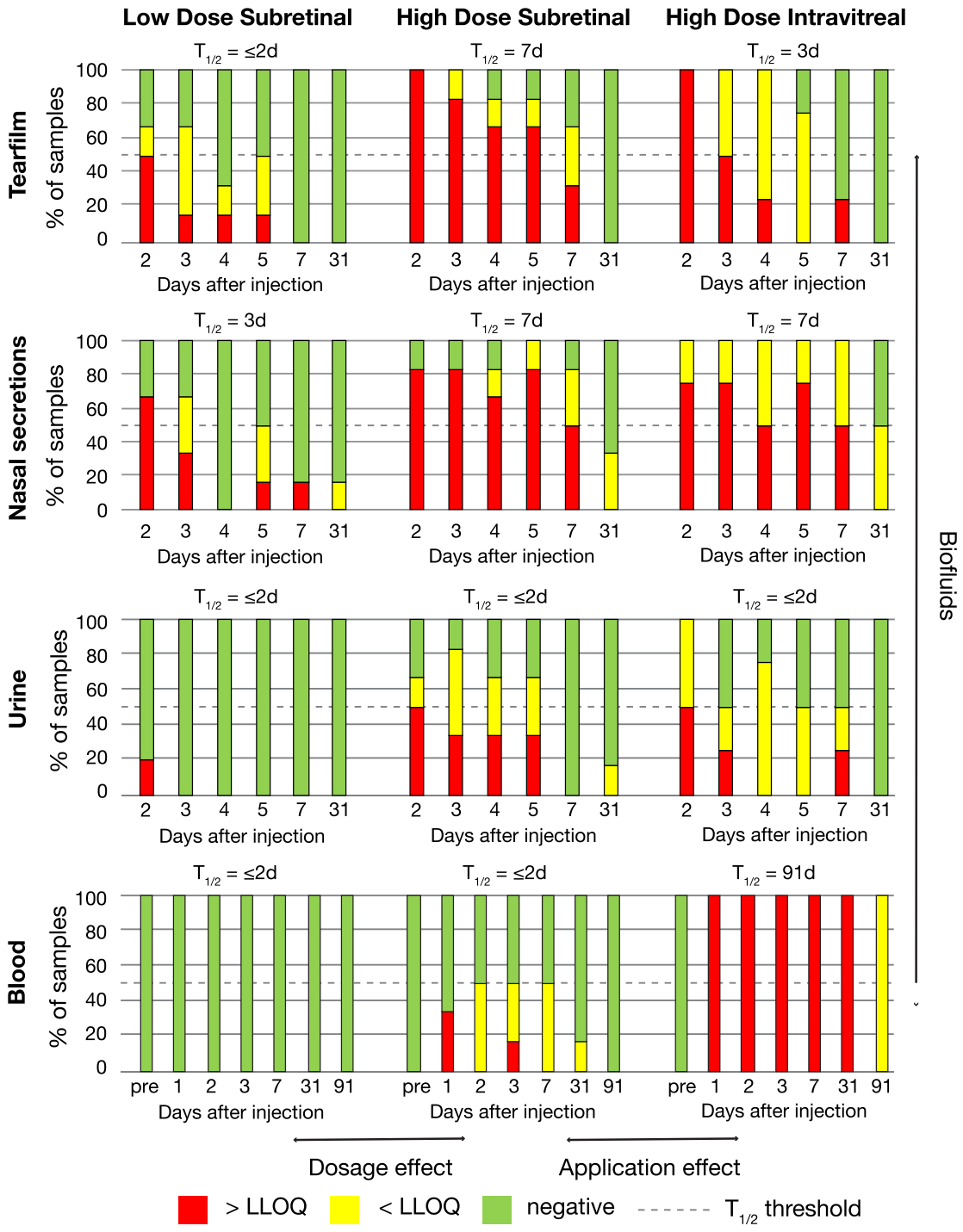

Figure 1. Shedding prevalence per cohort and biofluid during the observed time frame. Switching *between columns* compares results of the same sample type (i.e., shedding via tear) over different cohorts (i.e., subretinal low versus high dose), while switching *between rows* compares different sample types in the same cohort. The most notable difference is visible in the *bottom row* of the graph, displaying vector presence in blood across the three cohorts. *y*-axes: sample status in % of animals in the given cohort, *color-coded*. *x*-axes: days after injection. $T_{1/2}$: ≥50% of the cohort's samples test below LLOQ or negative. Individual sample status is *color-coded*.

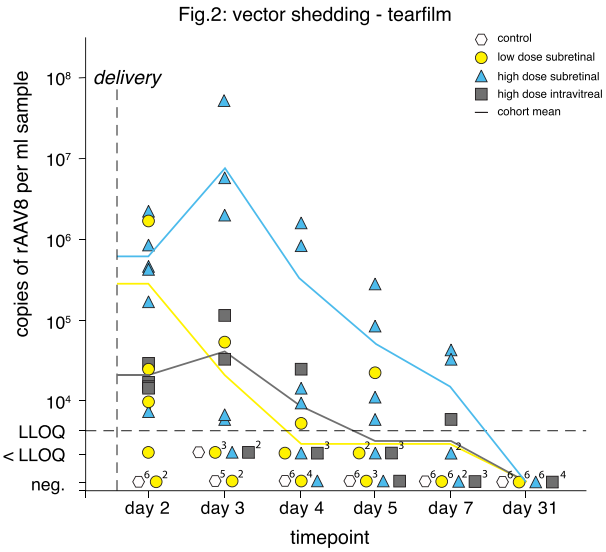

Figure 2. Vector genomes in tear film detected by qPCR plotted against time of harvest. Cohort means per time point indicated by *colored lines*. Of note, the high-dose subretinal cohort mean on day 3 was skewed by a single animal. It tested with 4.6 × 10 E+7 vg/mL on day 3, 53 times more than it tested on day 2, and 33 times more than it tested on day 4. The measurement was not omitted, although such variation was not seen in any other instance across the study. LLOQ = lower limit of quantification (50 copies/reaction).

mean). Like dose escalation, route of delivery had only a minor effect on shedding via nasal secretions. Between subretinal and intravitreal cohorts of the same dose, there was an equal prevalence (all animals in both groups) and duration of shedding, with 50% of animals in both cohorts featuring quantifiable qPCR results 7 days after surgery. A slight

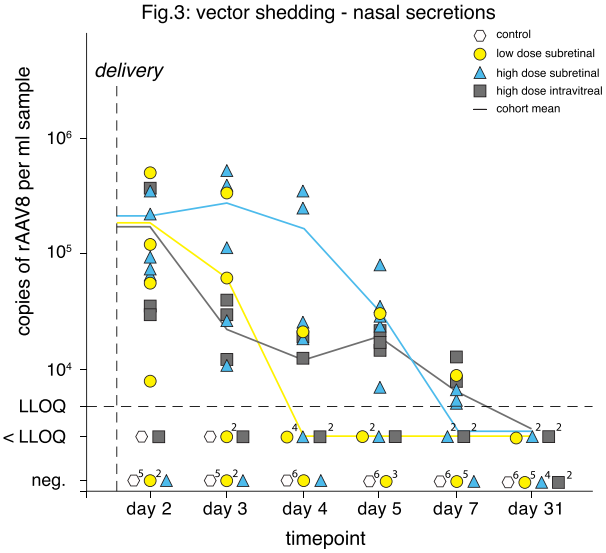

Figure 3. Vector genomes in nasal secretions detected by qPCR plotted against time of harvest. Dose escalation increased copy numbers and shedding duration. Intravitreal administration led to fewer copy numbers, but similar prevalence and duration compared to subretinal administration of the same dose. Cohort means per time point indicated by *colored lines*. LLOQ = lower limit of quantification (50 copies/reaction).

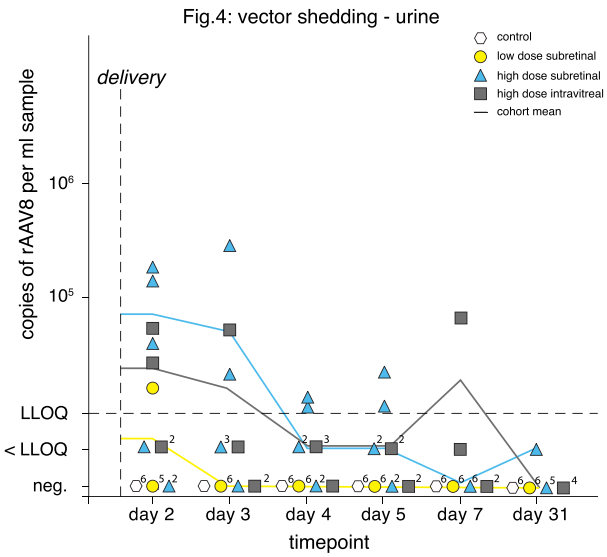

Figure 4. Vector genomes detected in urine by qPCR plotted against time of harvest. In the low-dose subretinal cohort, no relevant shedding was detected. Both high-dose cohorts displayed similar overall shedding via urine. Cohort means per time point indicated by *colored lines*. LLOQ = lower limit of quantification (50 copies/reaction).

difference between the high-dose groups was found in a 1.7-fold elevation of copy numbers after SR, relative to intravitreal administration. Individual results are displayed in Figure 3 and copy numbers/mL are given in Supplementary Material S1.

Individual Shedding Results via Urine

Shedding via urine was strongly dose dependent (Figs. 1, 4; Table 1). Foremost, it was barely detectable and nonpersistent in the low-dose cohort. Due to the low-dose cohort's low baseline, dose escalation by one log unit led to an 18.5-fold increase in maximal shedding (cohort mean) compared high-dose SR.

In contrast to the clear dose dependency, route of administration had subtler effects. Shedding prevalence was similar between IVT (4/4) and SR (5/6). Between these high-dose groups, copy numbers were moderately increased (2.7-fold) in subretinally injected animals, while shedding above LLOQ lasted 2 days longer after IVT. Individual results are displayed in Figure 4 and copy numbers/mL are given in Supplementary Material S1.

Transduction of the Visual System

At necropsy (91 days post injection), tissues of the visual pathway (Fig. 5; Table 2) were collected for formal biodistribution analyses. The segments of the visual system were sampled individually along the pathway taken by light (anterior segment, retina, optic nerve and chiasm, lateral geniculate nucleus [LGN], and visual cortex). Presence of vector in the aqueous humor was exclusively dependent on route of administration, while upstream distribution along the visual pathway was strongly associated with both dose and route of administration.

Ninety-one days after surgery, only one aqueous humor sample across both subretinal cohorts exhibited vector presence, while all samples in the intravitreal cohort were clearly above LLOQ. This was reversed within the eye, where compared to IVT, subretinal application of the same dose

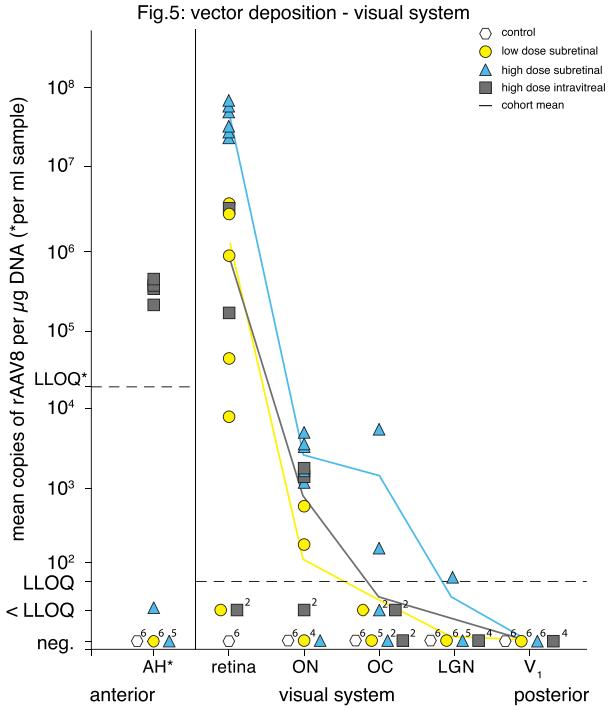

FIGURE 5. Individual visual pathway sample results (day 91) of all cohorts plotted anterior to posterior. Both aqueous humor deposition after IVT and retinal deposition after SR administration were highly uniform across their respective cohorts. Individual samples further up the optic pathway tested above LLOQ, with a single sample being positive at the level of the lateral geniculate nucleus. Cohort mean per segment indicated by *colored lines*. AH, aqueous humor; ON, optic nerve; OC, optic chiasm; LGN, lateral geniculate nucleus; V_1, visual cortex; LLOQ = lower limit of quantification (50 copies). *LLOQ for AH = 2.2 × 10 E+4 copies/mL sample.

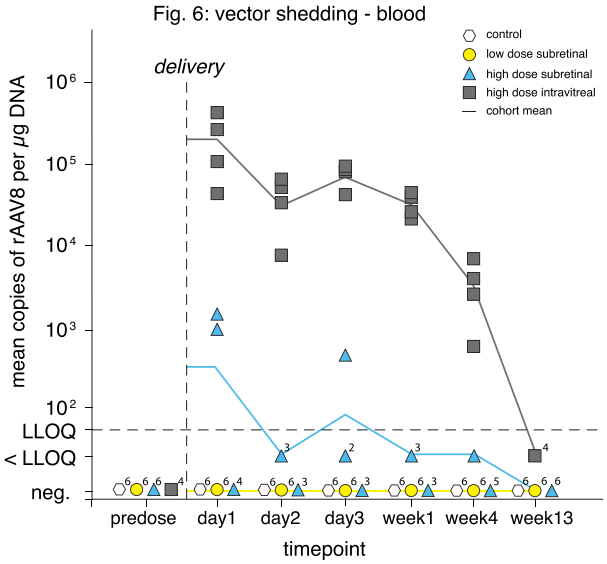

FIGURE 6. Vector genomes in blood detected by qPCR plotted against time of harvest. Blood samples did not show any vector genomes after low-dose subretinal injection, and only limited vector load after high-dose subretinal injection. Intravitreal administration led to immediate, strong, and persistent presence of vector in the blood. Cohort means per time point indicated by *colored lines*. 1 µg DNA = 40.1 ± 17.8 µL blood (mean ± SD). LLOQ = lower limit of quantification (50 copies).

resulted in 53 times higher copy numbers in whole retinal sections. A 10-fold dose escalation in SR caused a 37-fold increase of copy numbers detected in retinal tissue. The respective presence of vector in the retina carried over to following stations along the visual pathway. In optic nerve samples, dose escalation led to a 20-fold increase in copy numbers, while compared to IVT, SR resulted in 2.9-fold increased copy numbers. In line with the difference in copy numbers, five of six animals demonstrated vector presence in optic nerve samples after subretinal high-dose injections, as opposed to two of six animals in the low-dose cohort. A similar pattern, although with markedly lower copy numbers, also carried over to the optic chiasm, LGN, and visual cortex. Only one sample in the study (high-dose SR cohort) tested above the LLOQ at the level of the LGN, while not a single sample from the visual cortex tested positive for vector DNA. Table 2 shows copy numbers detected in each segment. Figure 5 illustrates the distribution of vector along the visual pathway in each cohort.

Biodistribution Outside the Visual System

The study also analyzed samples from blood (Figs. 1, 6; Table 1), major organs, and draining lymphatic tissue. Biodistribution in the systemic circulation and lymphatic tissues was strikingly dependent on the route of administration, but barely dose dependent. For example, while dosage had a moderate effect on biodistribution via blood, injecting intravitreally resulted in a 464-fold increased blood vector load compared to SR of the same dose, and vector presence in blood persisted in all animals of the IVT cohort until 91 days. Individual results are displayed in Figure 6 and copy numbers/mL are given in Supplementary Material S1.

Large Organs and Lymphatic Tissue

In line with elevated vector load in blood after IVT, draining lymph node and spleen contained significant amounts of vector genomes in animals of the IVT cohort, but virtually no copies after subretinal delivery (Figs. 7, 8). Relative amounts of vector genomes found in the lymph nodes (Table 3) after IVT were increased around 430-fold for deep cervical, 1000-fold for

TABLE 2. Vector Deposition Along the Visual Pathway in vg/µg Extracted DNA After 91 Days. Vector Deposition, Visual Pathway, and Vector Genomes per mL for Aqueous Humor

Cohort	Aqueous Humor	Retina	Optic Nerve	Optic Chiasm	LGN	Visual Cortex
Low-dose SR	0	1.3 E+6	1.2 E+2	<50	0	0
High-dose SR	<50	4.8 E+7	2.4 E+3	9.6 E+2	<50	0
High-dose IVT	3.2 E+5	9.1 E+5	8.4 E+2	<50	0	0

On day 91, relevant copy numbers were detected only in the aqueous humor of IVT animals. Vector deposition in the retina and upstream the visual pathway was most pronounced in high-dose SR animals.

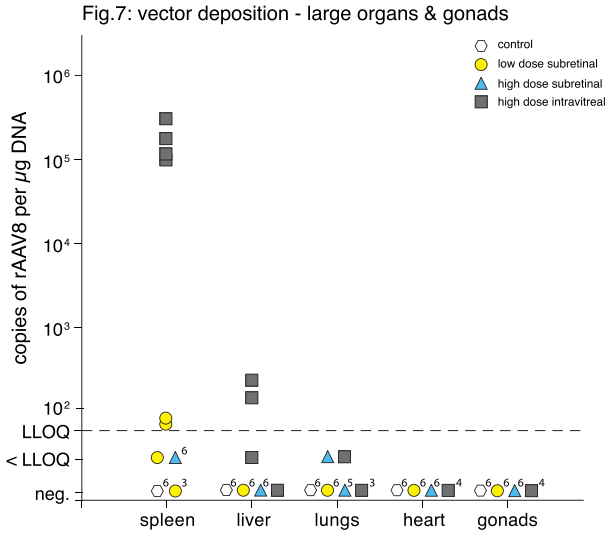

Figure 7. Individual internal large organ sample results of all cohorts. Off-target transduction of spleen and liver occurred to a similar degree in all animals from the intravitreal cohort. Corresponding tissue amounts are given in Supplementary Material S2. LLOQ = lower limit of quantification (50 copies).

retropharyngeal, 510-fold for mandibular, and 490-fold for mesenteric lymph nodes, compared to SR. IVT led to an approximately 7400-fold increase in copy numbers in spleen compared to SR. Liver samples were also positive in the intravitreal cohort, while heart, tongue, spinal cord, adrenal glands, and, importantly, the gonads were free of vector genomes in all animals of all cohorts (Table 4).

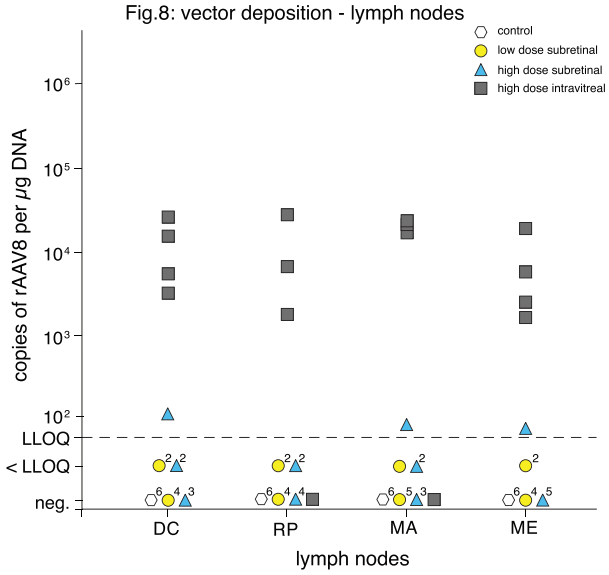

Figure 8. Individual lymph node sample results of all cohorts. Fourteen of 16 lymph node samples from the intravitreal group feature a noticeable degree of vector deposition. DC, deep cervical; RP, retropharyngeal; MA, mandibular; ME, mesenteric. Corresponding tissue amounts are given in Supplementary Material S2. LLOQ = lower limit of quantification (50 copies).

Table 3. Vector Deposition in Lymph Nodes Given as vg per Organ After 91 Days

Cohort	Deep Cervical	Retropharyngeal	Mandibular	Mesenteric
Low-dose SR	2.5 E+3	2.1 E+3	1.0 E+3	1.5 E+3
High-dose SR	8.1 E+3	2.3 E+3	7.0 E+3	4.5 E+3
High-dose IVT	3.5 E+6	2.4 E+6	3.6 E+6	2.2 E+6

At a similar dose, intravitreal delivery (bottom row) was associated with pronounced deposition in lymph nodes close to and far from the eye, compared to subretinal delivery. Assumed organ weight: 0.1 g per lymph node.

Summary

The study was designed to explore the shedding and biodistribution characteristics after subretinal delivery of AAV8 when mimicking the clinical scenario in patients. The IVT control group was added to test effects of inadvertent primary injection into the vitreous (via falsa) and/or a secondary delivery into the vitreous cavity through a retinal tear (e.g., macular hole formation) in the context of subretinal delivery. Both dose and route of delivery change the distribution profile, and Figure 9 shows a proposed model based on the major finding that intravitreal placement of AAV8 results in much higher viremia and contact with immune-competent cells. It highlights the potential of immune-competent effector cells to influence local reactions to the viral vector in the eye.

Discussion

To the best of our knowledge, this study reports the most comprehensive data on viral shedding and biodistribution of recombinant adeno-associated virus serotype 8 (rAAV8) after subretinal versus intravitreal injection (IVT) in nonhuman primates. This study was conducted in strict adherence to GLP guidelines and designed to generate data on biodistribution/shedding after subretinal and IVT in a protocol mimicking clinical application of rAAV8 gene therapy as closely as possible. In contrast to the protocol of the clinical trial, sclerotomies were not sutured in primates with the aim to reduce postsurgical irritation. However, this did not prevent digital manipulation of the treated eyes by the animals once transferred back to the cages. This may have affected biodistribution/shedding outcomes, and any such manipulation can easily be avoided in the clinical setting.

One important component of patient safety is avoidance of germ line transduction.[13,14] There was no vector presence in the germ line, regardless of sex, vector dosage, or route of administration. Shedding of GMO into the environment is another important aspect, and our data show that shedding to the environment receded below LLOQ by 1 week after surgery, with 21% of samples without detectable vector

Table 4. Vector Deposition in Large Organs Given as vg per Organ After 91 Days

Cohort	Spleen	Liver	Lungs	Heart	Gonads
Low-dose SR	4.6 E+5	0	0	0	0
High-dose SR	6.6 E+5	0	<LLOQ	0	0
High-dose IVT	4.9 E+9	3.2 E+6	<LLOQ	0	0

Significant off-target transduction of spleen and liver is observed after intravitreal administration.

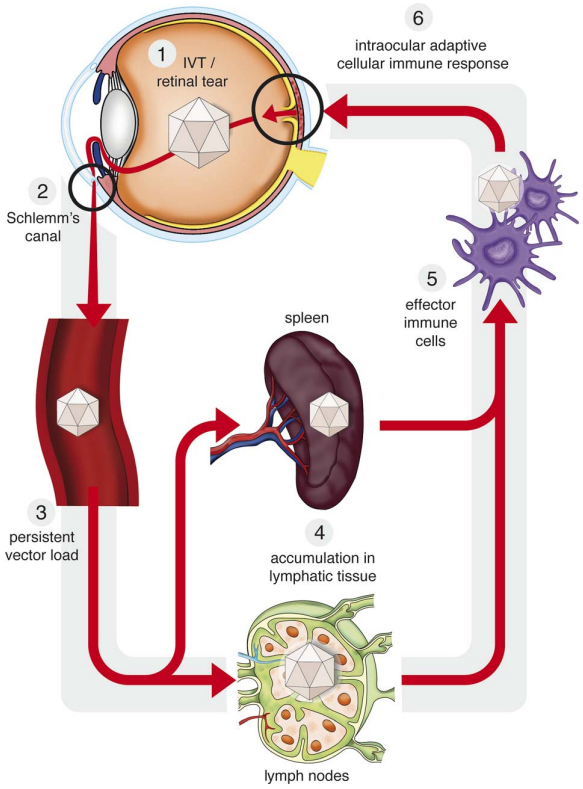

Figure 9. Summary and proposed model of biodistribution following intravitreal administration of AAV8. Intravitreal injection or retinal tear after subretinal injection leads to (**1**) persistent presence of vector in the aqueous humor and anterior chamber with (**2**) access to the venous system through Schlemm's canal. This study demonstrated long-term persistence of (**3**) vector in the blood and (**4**) deposition in lymphatic organs. The resulting prolonged and close contact with the immune system (**5**) might help to explain (**6**) acute or delayed inflammation observed after gene therapy.

genomes and 79% of all samples testing below LLOQ. In line with other reports, vector biodistribution and consequent deposition in internal organs were minimal in the subretinal cohorts.[15]

Both dose (1E+11 vs. 1E+12) and delivery (subretinal versus intravitreal) had an impact on biodistribution and shedding. Reducing the dose by one log unit resulted in 30% to 97% fewer copies off-target and shorter duration of shedding. Retinal gene transfer to the retina after IVT was at least one order of magnitude less compared to SR of the same vector dose. Vector genomes detected on day 1 in the intravitreal cohort's bloodstream accounted for 0.26% of the total dose applied, in contrast to 0.0006% after subretinal delivery of the same dose. This is in line with IVT leading to increased shedding into the systemic circulation via the anterior chamber. The observation that mesenteric lymph nodes, which do not drain from the injection site, did show a similar degree of vector deposition as deep cervical, retropharyngeal, and mandibular lymph nodes, also supports the notion of circulation-mediated biodistribution after IVT. Taken together, this evidence suggests a biodistribution profile not unlike what is described for intramuscular and intravenous injections.[16,17] Such a systemic visibility after IVT may promote vector recognition by the immune system and might help to explain any form of immune response after gene therapy.[11,18,19] Recent findings complement this hypothesis by showing a qualitative difference in immune response after IVT.[10]

It is important to note, however, that the absolute risk of any clinically relevant systemic toxicity in a patient after a retinal tear during subretinal delivery or IVT delivery can still be managed effectively. This is evident from clinical trials, where much higher dosages of rAAV8 were delivered primarily into the systemic circulation without causing serious adverse events.[20] However, these trials have shown that systemic exposure to significant numbers of any rAAV serotype can induce humoral and cellular immune response followed by directed removal of successfully transduced target cells by cytotoxic T lymphocytes.[21]

Previous studies in large animal models have demonstrated that rAAV8 gene therapy has a favorable safety profile[22] and efficiently transduces photoreceptors,[23,24] and that vector genome can be found along the visual pathway after subretinal delivery of rAAV.[25,26] Our data are in line with these reports and show that dose and route of application are important determinants of the extent of this distribution pattern.[27] While our data do not explain the mechanism of transduction along the visual pathway, they clearly show that both routes of application can lead to anterograde vector genome distribution along the axons of the ganglion cells up to the LGN. Intriguingly, this would indicate that subretinal rAAV8 does transduce ganglion cells. Alternative explanations would involve trans-synaptic mobility and/or vector solution traveling in the subretinal space to reach the optic nerve sheath and access to the cortex, for example, via cerebrospinal fluid. Both seem rather unlikely scenarios and are not supported by the fact that the visual cortex is free from vector genomes.

When taking all biodistribution and shedding data into consideration, we argue that SR offers the more favorable set of results. With constant improvements of subretinal surgery,[28,29] and the predominant intention of treating the retinal pigment epithelium and photoreceptors, we conclude that SR is therefore the preferable procedure in most current ocular gene therapy scenarios. This may of course change with the advent of new viral vectors[30–35] and improvements in intravitreal surgery,[36,37] which promise to efficiently transduce cells of the outer retina after intravitreal delivery.

While these results were generated using rAAV8, there is reason to believe that the mechanics underlying shedding and biodistribution are also applicable to other AAV serotypes with similar tropism. As most transgene cassettes in classic gene augmentation strategies feature target cell–specific promoters, off-target transduction with nonintegrating vectors such as AAV can still be regarded as fairly safe—especially as the germ line is shown not to be affected. However, in approaches using either ubiquitous promoters or immunogenic bacterial enzymes (e.g., CRISPR-Cas9) to edit genomic DNA with less than 100% specificity, off-target transduction may be more of a concern.[38]

Acknowledgments

The authors thank Apostolos Bezirgiannidis (University Eye Hospital Tübingen), Sven Korte, and Jörg Luft (both Covance Laboratories GmbH) for their help in the animal study and Daniel Pauleikhoff (Augenzentrum St. Franziskus, Münster) for the supply of 41-gauge needles on very short notice.

Supported by Tistou und Charlotte Kerstan Stiftung.

Disclosure: **I.P. Seitz**, None; **S. Michalakis**, P; **B. Wilhelm**, None; **F.F. Reichel**, None; **G.A. Ochakovski**, None; **E. Zrenner**, None; **M. Ueffing**, None; **M. Biel**, P; **B. Wissinger**, None; **K.U. Bartz-Schmidt**, None; **T. Peters**, None; **M.D. Fischer**, Nightstar

Ltd (C), Eyeserve GmbH (C), Regenxbio, Inc. (C), Bayer (R), Novartis (R)

References

1. Sharpe LT. Total colour-blindness: an introduction. In: Sharpe LT, ed. *Night Vision: Basic, Clinical and Applied Aspects*. Cambridge, UK: Cambridge University Press; 1990:253–289.
2. Sundin OH, Yang JM, Li Y, et al. Genetic basis of total colourblindness among the Pingelapese islanders. *Nat Genet*. 2000;25:289–293.
3. Aboshiha J, Dubis AM, Carroll J, Hardcastle AJ, Michaelides M. The cone dysfunction syndromes. *Br J Ophthalmol*. 2016; 100:115–121.
4. Kohl S, Marx T, Giddings I, et al. Total colourblindness is caused by mutations in the gene encoding the alpha-subunit of the cone photoreceptor cGMP-gated cation channel. *Nat Genet*. 1998;19:257–259.
5. Kohl S, Baumann B, Broghammer M, et al. Mutations in the CNGB3 gene encoding the beta-subunit of the cone photoreceptor cGMP-gated channel are responsible for achromatopsia (ACHM3) linked to chromosome 8q21. *Hum Mol Genet*. 2000;9:2107–2116.
6. Grau T, Artemyev NO, Rosenberg T, et al. Decreased catalytic activity and altered activation properties of PDE6C mutants associated with autosomal recessive achromatopsia. *Hum Mol Genet*. 2011;20:719–730.
7. Kohl S, Coppieters F, Meire F, et al. A nonsense mutation in PDE6H causes autosomal-recessive incomplete achromatopsia. *Am J Hum Genet*. 2012;91:527–532.
8. Kohl S, Baumann B, Rosenberg T, et al. Mutations in the cone photoreceptor G-protein alpha-subunit gene GNAT2 in patients with achromatopsia. *Am J Hum Genet*. 2002;71: 422–425.
9. Ansar M, Santos-Cortez RL, Saqib MA, et al. Mutation of ATF6 causes autosomal recessive achromatopsia. *Hum Genet*. 2015;134:941–950.
10. Kotterman MA, Yin L, Strazzeri JM, Flannery JG, Merigan WH, Schaffer DV. Antibody neutralization poses a barrier to intravitreal adeno-associated viral vector gene delivery to non-human primates. *Gene Ther*. 2015;22:116–126.
11. MacLachlan TK, Lukason M, Collins M, et al. Preclinical safety evaluation of AAV2-sFLT01—a gene therapy for age-related macular degeneration. *Mol Ther*. 2011;19:326–334.
12. Michalakis S, Mühlfriedel R, Tanimoto N, et al. Restoration of cone vision in the CNGA3(−/−) mouse model of congenital complete lack of cone photoreceptor function. *Mol Ther*. 2010;18:2057–2063.
13. Lanphier E, Urnov F, Haecker SE, Werner M, Smolenski J. Don't edit the human germ line. *Nature*. 2015;519:410–411.
14. Gyngell C, Douglas T, Savulescu J. The ethics of germline gene editing. *J Appl Philos*. 2016;34:498–513.
15. Deng WT, Dyka FM, Dinculescu A, et al. Stability and safety of an AAV vector for treating RPGR-ORF15 X-linked retinitis pigmentosa. *Hum Gene Ther*. 2015;26:593–602.
16. Ru Q, Li W, Wang X, et al. Preclinical study of rAAV2-sTRAIL: pharmaceutical efficacy, biodistribution and safety in animals. *Cancer Gene Ther*. 2017;24:251–258.
17. Tarantal AF, Lee CCI, Martinez ML, Asokan A, Samulski RJ. Systemic and persistent muscle gene expression in rhesus monkeys with a liver de-targeted adeno-associated virus vector. *Hum Gene Ther*. 2017;28:385–391.
18. Ye G, Budzynski E, Sonnentag P, et al. Safety and biodistribution evaluation in cynomolgus macaques of rAAV2tYF-PR1.7-hCNGB3, a recombinant AAV vector for treatment of achromatopsia. *Hum Gene Ther Clin Dev*. 2016;27:37–48.
19. Marangoni D, Wu Z, Wiley HE, et al. Preclinical safety evaluation of a recombinant AAV8 vector for X-linked retinoschisis after intravitreal administration in rabbits. *Hum Gene Ther Clin Dev*. 2014;25:202–211.
20. Nathwani AC, Reiss UM, Tuddenham EG, et al. Long-term safety and efficacy of factor IX gene therapy in hemophilia B. *N Engl J Med*. 2014;371:1994–2004.
21. Mingozzi F, Maus MV, Hui DJ, et al. CD8(+) T-cell responses to adeno-associated virus capsid in humans. *Nat Med*. 2007;13: 419–422.
22. Nathwani AC, Gray JT, McIntosh J, et al. Safe and efficient transduction of the liver after peripheral vein infusion of self-complementary AAV vector results in stable therapeutic expression of human FIX in nonhuman primates. *Blood*. 2007;109:1414–1421.
23. Manfredi A, Marrocco E, Puppo A, et al. Combined rod and cone transduction by adeno-associated virus 2/8. *Hum Gene Ther*. 2013;24:982–992.
24. Vandenberghe LH, Bell P, Maguire AM, et al. Dosage thresholds for AAV2 and AAV8 photoreceptor gene therapy in monkey. *Sci Transl Med*. 2011;3:88ra54.
25. Stieger K, Colle MA, Dubreil L, et al. Subretinal delivery of recombinant AAV serotype 8 vector in dogs results in gene transfer to neurons in the brain. *Mol Ther*. 2008;16:916–923.
26. Provost N, Le Meur G, Weber M, et al. Biodistribution of rAAV vectors following intraocular administration: evidence for the presence and persistence of vector DNA in the optic nerve and in the brain. *Mol Ther*. 2005;11:275–283.
27. Castle MJ, Gershenson ZT, Giles AR, Holzbaur EL, Wolfe JH. Adeno-associated virus serotypes 1, 8, and 9 share conserved mechanisms for anterograde and retrograde axonal transport. *Hum Gene Ther*. 2014;25:705–720.
28. Fischer MD, Hickey DG, Singh MS, MacLaren RE. Evaluation of an optimized injection system for retinal gene therapy in human patients. *Hum Gene Ther Methods*. 2016;27:150–158.
29. Ehlers JP, Kaiser PK, Srivastava SK. Intraoperative optical coherence tomography using the RESCAN 700: preliminary results from the DISCOVER study. *Br J Ophthalmol*. 2014;98: 1329–1332.
30. Ramachandran PS, Lee V, Wei Z, et al. Evaluation of dose and safety of AAV7m8 and AAV8BP2 in the non-human primate retina. *Hum Gene Ther*. 2017;28:154–167.
31. Dalkara D, Byrne LC, Klimczak RR, et al. In vivo-directed evolution of a new adeno-associated virus for therapeutic outer retinal gene delivery from the vitreous. *Sci Transl Med*. 2013;5:189ra179.
32. Kay CN, Ryals RC, Aslanidi GV, et al. Targeting photoreceptors via intravitreal delivery using novel, capsid-mutated AAV vectors. *PLoS One*. 2013;8:e62097.
33. Cronin T, Vandenberghe LH, Hantz P, et al. Efficient transduction and optogenetic stimulation of retinal bipolar cells by a synthetic adeno-associated virus capsid and promoter. *EMBO Mol Med*. 2014;6:1175–1190.
34. Khabou H, Desrosiers M, Winckler C, et al. Insight into the mechanisms of enhanced retinal transduction by the engineered AAV2 capsid variant -7m8. *Biotechnol Bioeng*. 2016; 113:2712–2724.
35. Woodard KT, Liang KJ, Bennett WC, Samulski RJ. Heparan sulfate binding promotes accumulation of intravitreally delivered adeno-associated viral vectors at the retina for enhanced transduction but weakly influences tropism. *J Virol*. 2016;90:9878–9888.
36. Takahashi K, Igarashi T, Miyake K, et al. Improved intravitreal AAV-mediated inner retinal gene transduction after surgical internal limiting membrane peeling in cynomolgus monkeys. *Mol Ther*. 2017;25:296–302.

37. Da Costa R, Roger C, Segelken J, Barben M, Grimm C, Neidhardt J. A novel method combining vitreous aspiration and intravitreal AAV2/8 injection results in retina-wide transduction in adult mice. *Invest Ophthalmol Vis Sci*. 2016;57:5326–5334.
38. Chew WL, Tabebordbar M, Cheng JKW, et al. A multifunctional AAV-CRISPR-Cas9 and its host response. *Nat Methods*. 2016;13:868–874.

Appendix

RD-CURE Consortium: Bernd Wissinger; Martin Biel; Eberhart Zrenner; Karl Ulrich Bartz-Schmidt; M. Dominik Fischer; Susanne Kohl; Stylianos Michalakis; Francois Paquet-Durand; Tobias Peters; Mathias Seeliger; Marius Ueffing; Nicole Weisschuh; Barbara Wilhelm; Ditta Zobor; Stephen Tsang; Laura Kühlewein; Christian Johannes Gloeckner; Nadine A. Kahle.

2.2. Selecting Study Participants and Phenotyping in ultra-Rare Disease: "Multimodal assessment of Choroideremia patients defines pre-treatment characteristics"

Graefes Arch Clin Exp Ophthalmol (2015) 253:2143–2150
DOI 10.1007/s00417-015-2976-4

RETINAL DISORDERS

Multimodal assessment of choroideremia patients defines pre-treatment characteristics

Immanuel P. Seitz · Ahmad Zhour · Susanne Kohl · Pablo Llavona · Tobias Peter · Barbara Wilhelm · Eberhart Zrenner · Marius Ueffing · Karl Ulrich Bartz-Schmidt · M. Dominik Fischer

Received: 28 August 2014 / Revised: 5 February 2015 / Accepted: 18 February 2015 / Published online: 7 March 2015

Abstract
Purpose Choroideremia (CHM) is a X-chromosomal disorder leading to blindness by progressive degeneration of choroid, retinal pigment epithelium (RPE), and retinal neurons. A current clinical gene therapy trial (NCT01461213) showed promising safety and efficacy data in a carefully selected patient population. The present study was performed to shed light on pre-treatment characteristics of a larger cohort of CHM patients using a high resolution multi-modal approach.
Methods In a retrospective cross-sectional study, data from 58 eyes of 29 patients with clinically confirmed CHM were analysed including best-corrected visual acuity (BCVA), refractive error, spectral-domain optical coherence tomography (SD-OCT), fundus autofluorescence (FAF), perimetry, and tonometry. Residual retinal volume, area of residual RPE, and foveal thickness were quantified to further define natural disease progression and assess symmetry.
Results We evaluated 98 data points of BCVA [0.34±0.06 (logMAR); mean±95 % confidence interval], 80 of IOP (14.6±0.6 mmHg), and 98 of refraction (−2.16±1.08 spherical equivalent). Visual fields (n =76) demonstrated variable degrees of concentric constriction (54 % <10°, 25 % 10–30°, 21 % >30°). Mean residual RPE area on FAF (n =64) measured 8.47±1.91 mm^2 (range 0.30–38.5 mm^2), while mean neuroretinal volume (n =42) was found to be 1.76±0.12 mm^3. Age at examination was exponentially associated with BCVA, while logarithmic functions best described progressive loss of retinal area and volume. A high degree of left to right symmetry was found in all modalities with structural markers showing the best correlation (r^2_{area}=0.83; r^2_{volume}=0.75).
Conclusion Analysis of these widely available clinical data defines the natural disease characteristics of a relevant patient population eligible for gene therapeutic intervention. In the wake of preliminary reports on safety and efficacy of CHM gene therapy (NCT01461213), this multi-modal assessment of a cohort of CHM patients provides important evidence of the natural rate of disease progression and degree of symmetry between eyes.

Keywords Choroideremia · Gene therapy · Autofluorescence · Symmetry

I. P. Seitz · A. Zhour · E. Zrenner · K. U. Bartz-Schmidt · M. D. Fischer
University Eye Hospital, University of Tübingen, Tübingen, Germany

I. P. Seitz · S. Kohl · P. Llavona · E. Zrenner · M. Ueffing
Institute for Ophthalmic Research, University of Tübingen, Tübingen, Germany

T. Peter · B. Wilhelm
STZ Eyetrial, Centre for Ophthalmology, University of Tübingen, Tübingen, Germany

M. D. Fischer
Nuffield Laboratory of Ophthalmology, University of Oxford, Oxford, UK

M. D. Fischer
Oxford Eye Hospital, Oxford University Hospitals NHS Trust, Oxford, UK

M. D. Fischer (✉)
Merton College, University of Oxford, Oxford OX1 4JD, UK
e-mail: dominik.fischer@ndcn.ox.ac.uk

Introduction

Choroideremia (CHM) is a monogenic X-linked disorder causing progressive loss of vision. The clinical entity was recognised in the late 19th century, when a 32-year-old miller from the Puster valley in today's Italy (South Tyrol) presented in Prof. Mauthner's outpatient clinic in Innsbruck on 1 June

Graefes Arch Clin Exp Ophthalmol (2015) 253:2143–2150
DOI 10.1007/s00417-015-2976-4

RETINAL DISORDERS

Multimodal assessment of choroideremia patients defines pre-treatment characteristics

Immanuel P. Seitz · Ahmad Zhour · Susanne Kohl · Pablo Llavona · Tobias Peter · Barbara Wilhelm · Eberhart Zrenner · Marius Ueffing · Karl Ulrich Bartz-Schmidt · M. Dominik Fischer

Received: 28 August 2014 / Revised: 5 February 2015 / Accepted: 18 February 2015 / Published online: 7 March 2015

Abstract
Purpose Choroideremia (CHM) is a X-chromosomal disorder leading to blindness by progressive degeneration of choroid, retinal pigment epithelium (RPE), and retinal neurons. A current clinical gene therapy trial (NCT01461213) showed promising safety and efficacy data in a carefully selected patient population. The present study was performed to shed light on pre-treatment characteristics of a larger cohort of CHM patients using a high resolution multi-modal approach.
Methods In a retrospective cross-sectional study, data from 58 eyes of 29 patients with clinically confirmed CHM were analysed including best-corrected visual acuity (BCVA), refractive error, spectral-domain optical coherence tomography (SD-OCT), fundus autofluorescence (FAF), perimetry, and tonometry. Residual retinal volume, area of residual RPE, and foveal thickness were quantified to further define natural disease progression and assess symmetry.
Results We evaluated 98 data points of BCVA [0.34±0.06 (logMAR); mean±95 % confidence interval], 80 of IOP (14.6±0.6 mmHg), and 98 of refraction (−2.16±1.08 spherical equivalent). Visual fields (n =76) demonstrated variable degrees of concentric constriction (54 % <10°, 25 % 10–30°, 21 % >30°). Mean residual RPE area on FAF (n =64) measured 8.47±1.91 mm^2 (range 0.30–38.5 mm^2), while mean neuroretinal volume (n =42) was found to be 1.76±0.12 mm^3. Age at examination was exponentially associated with BCVA, while logarithmic functions best described progressive loss of retinal area and volume. A high degree of left to right symmetry was found in all modalities with structural markers showing the best correlation (r^2_{area}=0.83; r^2_{volume}=0.75).
Conclusion Analysis of these widely available clinical data defines the natural disease characteristics of a relevant patient population eligible for gene therapeutic intervention. In the wake of preliminary reports on safety and efficacy of CHM gene therapy (NCT01461213), this multi-modal assessment of a cohort of CHM patients provides important evidence of the natural rate of disease progression and degree of symmetry between eyes.

Keywords Choroideremia · Gene therapy · Autofluorescence · Symmetry

I. P. Seitz · A. Zhour · E. Zrenner · K. U. Bartz-Schmidt · M. D. Fischer
University Eye Hospital, University of Tübingen, Tübingen, Germany

I. P. Seitz · S. Kohl · P. Llavona · E. Zrenner · M. Ueffing
Institute for Ophthalmic Research, University of Tübingen, Tübingen, Germany

T. Peter · B. Wilhelm
STZ Eyetrial, Centre for Ophthalmology, University of Tübingen, Tübingen, Germany

M. D. Fischer
Nuffield Laboratory of Ophthalmology, University of Oxford, Oxford, UK

M. D. Fischer
Oxford Eye Hospital, Oxford University Hospitals NHS Trust, Oxford, UK

M. D. Fischer (✉)
Merton College, University of Oxford, Oxford OX1 4JD, UK
e-mail: dominik.fischer@ndcn.ox.ac.uk

Introduction

Choroideremia (CHM) is a monogenic X-linked disorder causing progressive loss of vision. The clinical entity was recognised in the late 19th century, when a 32-year-old miller from the Puster valley in today's Italy (South Tyrol) presented in Prof. Mauthner's outpatient clinic in Innsbruck on 1 June

1871. The patient complained of nyctalopia and visual field constrictions, and showed all phenotypic hallmarks of the disease with centripetal atrophy of choroid, retinal pigment epithelium, and outer neuroretina [1].

Cremers and colleagues characterised the underlying genetic defect in the late 20th century [2–7]. In affected patients, the CHM locus (Xq21.2) may feature either pathogenic frameshift mutations or even larger deletions/insertions in *CHM*. Interestingly, CHM is uniquely coherent on a genetic level in that the vast majority of CHM is caused by null mutations, with complete absence of stable protein products [8]. *CHM* encodes for Rab escorting protein 1 (REP1), an ubiquitous enzyme important for intracellular vesicular transport [9]. Its homologue REP2 can compensate for *CHM* mutations in most other tissues, preventing a syndromic phenotype [10].

Despite more than 100 years of clinical observation, it is not entirely clear whether CHM primarily causes atrophy of the choroidal vasculature with secondary degeneration of retinal pigment epithelium (RPE) and photoreceptors, which rely on choroidal perfusion (as suggested first by Mauthner), or whether REP1 deficiency primarily causes death of RPE and photoreceptors with secondary atrophy of the choroid. Studies in mouse models of selective REP1 deficiency in photoreceptors, RPE, or both pointed to a potential cumulative pathogenic effect from both cell populations contributing to dysfunction and degeneration [11]. This prompted the use of a ubiquitous promoter for proof of concept studies, leading to a clinical safety study that would allow expression of the therapeutic coding sequence in all affected cell types [12].

Today, less than 25 years after the genetic cause was characterised, the first patients have been successfully treated in a pioneering clinical safety trial (NCT01461213) featuring a strategy of gene supplementation by adenovirus-associated viral vector delivery [13]. Preliminary data from this trial suggests that gene therapy is able to slow if not halt progression of degeneration in the treated eyes and possibly even reverse some previously under-recognised functional defects in areas not (yet) affected by the progressive atrophy associated with deficiency of REP1 [13]. While this study sets a milestone in the translational efforts in ophthalmology, it also highlights the importance to continuously review patients with hereditary retinal disorders (HRD) potentially suitable for future treatment options. Key questions during pre-treatment characterization of patients with choroideremia and HRDs in general concern: i) the precise spatial and temporal sequences of functional and structural defects in the natural disease progression to help determine windows of opportunity for intervention or maximal discriminatory power, ii) which parameters best serve as sensitive, specific, and robust outcome measures of therapeutic safety and efficacy, and furthermore, iii) how symmetric are those findings and is the fellow eye a suitable internal control?

This study was performed to address these questions by multi-modal clinical analysis of a cohort of patients with confirmed CHM. Only relatively recent data (recorded after January 2000) from 58 eyes (29 patients) were used in a retrospective cross-sectional study. We found evidence for exponential best fits for both functional and structural biomarkers over time, reflecting the centripetal disease progression on retinal level. Symmetry was high between right and left eyes and most robustly assessed by objectively quantifying the area of remaining retinal pigment epithelium in fundus autofluorescence recordings.

Materials and methods

Patients

This was a retrospective cross-sectional study in 58 eyes of 29 patients with clinically confirmed choroideremia (CHM), who were referred to the University Eye Hospital Tübingen between 2000 and 2014. The diagnosis of CHM was established based on a family history reflecting X-linked inheritance pattern and the characteristic fundus appearance. The study was performed in accordance with the tenets of the Declaration of Helsinki 1975 (1983 revision). Institutional review board approval was not required for this retrospective study as regulated by the data protection law of the state Baden–Württemberg, Germany.

Molecular assessment

Study participants were recruited over 20 years from the University Eye Hospital Tuebingen within the special day clinic for inherited retinal diseases. This and all our studies are performed according to the tenets of the Declaration of Helsinki, and all genetically tested participants gave written consent, approved by the local research and ethical review boards. Genomic DNA was extracted from peripheral blood samples using standard protocols. Genetic testing was performed in different laboratories with different research and diagnostic genetic setups. Recent testing in P15, P18, P20, and P23 followed the procedure published by Furgoch et al. [14]. All coding exons and flanking intron-exon boundaries of *CHM* were PCR-amplified with the primers described therein and sequenced. PCR fragments were purified by ExoSAP-IT treatment (USB, Cleveland, OH, USA), sequenced using Big Dye Termination chemistry (Applied Biosystems [ABI], Weiterstadt, Germany), and products separated on a DNA capillary sequencer (ABI 3100 genetic analyzer, Weiterstadt, Germany). Sequences were assembled and analysed with the SeqMan program (DNASTAR Lasergene Co., London, UK).

Clinical examinations

All subjects underwent slit-lamp examination, measurement of best-corrected distance visual acuity (D-BCVA) using Snellen charts, and visual field (VF) testing with semiautomated kinetic perimetry (SKP) using an Octopus 900 perimeter (Haag–Streit, Switzerland) or Goldmann perimetry as described previously [15, 16]. Briefly, the peripheral visual field boundary and blind spot were assessed using a size I4e target. A minimum of twelve vectors were assessed for the peripheral visual field inclusive of vectors offset from the vertical and horizontal meridia moving centripetally at 5°/sec (3°/sec for determination of the blind spot). Following assessment, the response points along each vector were joined to form the isopter for the I4e target. Average extend of this isopter in each eye was categorized as <10°, 10–30° or >30°.

Retinal imaging was performed on the same day after bilateral pupil dilation, and included spectral-domain optical coherence tomography (SD-OCT) and autofluorescence imaging (AF) using the Spectralis™ HRA+OCT platform (Heidelberg Engineering, Heidelberg, Germany) as described previously [17]. Pupillary mydriasis was induced using tropicamide eye drops 5 mg/ml (Mydriaticum Stulln, Pharma Stulln, Germany). For SD-OCT, multiple high-speed B-scans were recorded to assess central retinal architecture and quantify thickness of remaining neuro-retinal tissue. To improve signal to noise ratio (SNR), $n \geq 9$ scans were averaged for each B-scan recording, whereby SNR improved by the square root of n (i.e., SNR was at least tripled). Non-voluntary eye movements during averaging were corrected using the proprietary TruTrack™ function. AF data were recorded in the same session and settings (averaging and eye-tracking) using the same platform after switching from the SD-OCT mode to the HRA mode, which essentially records confocal scanning laser ophthalmoscopic (cSLO) images, after exciting retinal tissue at λ=488 nm and introducing a barrier filter to collect light above λ=500 nm [18]. For cSLO imaging, either the 30° or 55° optics of the Spectralis™ HRA+OCT platform was used depending on the extend of the residual central island. Proprietary software (Heidelberg Eye Explorer v1.6.4.0 and Spectralis Viewing Module 5.3.2.0) was used to quantify residual RPE islands and retinal thickness values (Fig. 1). For this, the border between the island of intact central retinal tissue and the atrophic periphery was determined by an experienced investigator (IPS) and reviewed by a fellow investigator (AZ), before area measurements produced by the proprietary software were recorded for statistical analysis. The border between the AF signal from remaining RPE and atrophic periphery was usually well defined and easy to delineate. In cases of any doubt, OCT scans recorded at the same time point were used to confirm location of the transitional zone between intact RPE/retina and atrophic area.

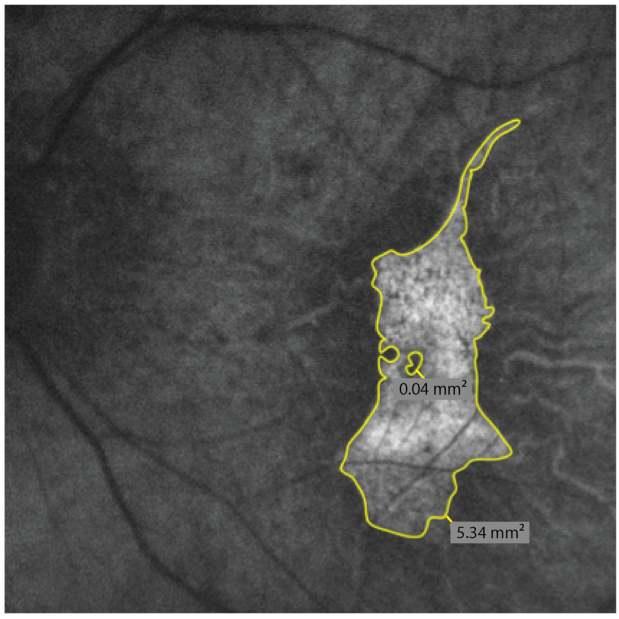

Fig. 1 Representative 30° autofluorescence recording from a patient with choroideremia (CHM). A *yellow line* was manually drawn around the area of remaining autofluoresecent islands of retinal pigment epithelium using the lasso tool of the proprietary software (Heidelberg Eye Explorer), which automatically reports the absolute area measurements. Note that any discontinuations (e.g., the small "hole" of 0.04 mm^2) within the island were subtracted from the overall area measurement

Statistical analysis

Bivariate correlation, *t*-tests and linear regression analyses were performed between modalities for cross-sectional progression analysis and between right and left eyes for symmetry analysis using Statistical Package for Social Sciences (SPSS) version 21 by IBM (SPSS Inc., Chicago, IL, USA) or Microsoft Excel version 14.1.0 (Microsoft, Redmond, Washington, USA), both for Macintosh OSX. Conversion of decimal BCVA data into logMAR was achieved by using the following formula: LogMAR=− Log (decimal acuity) [19]. Statistical significance was defined as $p < 0.05$.

Results

Overall cohort characteristics

Retrospective analysis of clinical data from the University Eye Hospital of Tübingen digital database revealed approximately 500 data points on visual function and retinal structure from 29 clinically confirmed CHM patients recorded between 2000 and 2014. Patients were either sporadic cases or presented with a family history consistent with X-linked inheritance. Clinical presentation was heterogeneous with respect to

disease severity. Age at examination ranged from 5 to 63 years. Mean and median age at examination were 42.5 and 48.0 years respectively.

Most patients reported about onset of nyctalopia in their teens, while central visual acuity typically remained largely unchanged until the fifth decade. All showed clear signs of peripheral and/or mid-peripheral atrophy of choroid, retinal pigment epithelium (RPE) and thinning of the retina due to photoreceptor loss, all in line with CHM.

Genetic test results

Genetic test results confirming the clinical diagnosis CHM were available for 25 patients at the time of publication (four patients did not consent to molecular diagnostics and/or did not send blood samples). A list of the recorded mutations and their predicted effect is given in Table 1. The mutations observed in our patients most likely present null alleles, as they represent large deletions, nonsense mutations, or frame-shifting insertion/deletion mutations resulting in premature termination codons, all of which most likely undergo nonsense-mediated decay. This is in line with previous reports, which also show that the vast majority of CHM is caused by null mutations with complete absence of or instable protein products [8]. Novel mutations were observed in seven cases. The mutation spectrum comprises three nonsense mutations, two small frame-shifting deletions, three small frame-shifting duplications, two larger deletions covering exon 1 in patient 19 and exons 3–15 in the brothers 4 and 5, respectively, and two mutations resulting in missplicing.

Table 1 Results from molecular testing in patients with clinically confirmed choroideremia (CHM)

Patient	Hemizygote mutations in *CHM*		Comment
	Nucleotide level	Protein level	
1	c.924 T>G	p.Tyr308*	van den Hurk et al. 2003
2	c.715C>T	p.Arg239*	Francis et al. 2005
3	c.124_133dup	p.Gly45Valfs*10	novel
4	deletion of exons 3-15	null	novel, brother of patient 5
5	deletion of exons 3-15	null	novel, brother of patient 4
6	c.1446delA	p.Gly483Glufs*15	van den Hurk et al. 1992
7	c.616dupA	p.T206NfsX17	brother of patient 8
8	c.616dupA	p.T206NfsX17	brother of patient 7
9	c.941-1G>T	splice defect / null	novel
10	c.924 T>G	p.Tyr308*	van den Hurk et al. 2003
11	n.a.	n.a.	no consent and/or no sample
12	n.a.	n.a.	no consent and/or no sample
13	c.314+10127 T>A	splice defect / null	van den Hurk et al. 2003, Hum Genet
14	n.a	n.a	no consent and/or no sample
15	c.1036G>T	p.Glu346*	novel
16	c.1531_1532delinsTCTTCT AAACAGCAT	p.Thr511Serfs*8	van den Hurk et al. 2003
17	c.924 T>G	p.Tyr308*	van den Hurk et al. 2003
18	c.1116_1117del	p.Leu374Valfs*43	novel
19	del Exon 1	null	confirmed; extent not defined
20	c.645del	p.Thr216Leufs*16	novel
21	c.715C>T	p.Arg239*	Francis et al. 2005
22	n.a.	n.a.	no consent and/or no sample
23	c.1476_1477dup	p.Cys493Tyrfs*6	novel
24	c.877C>T	p.R293X	van den Hurk et al. 2003
25	c.800delT	pT288Lfs*3	van den Hurk et al. 2003
26	deletion of exons 1-15	null	van den Hurk et al. 1992
27	c.653C>G	p.Ser218x	van den Hurk et al. 2003
28	c.757C>T	p.Arg253*	van den Hurk et al. 2003
29	c.116C>G	p.S39X	van den Hurk et al. 2003

Clinical outcome measures

Mean and 95 % confidence interval (CI) of 98 entries on logMAR visual acuity was 0.34±0.06. Intraocular pressure (n=80) was 14.6±0.6 mmHg, and refractive error (n =98) calculated as spherical equivalent was −2.16±1.08 overall. Visual fields (n= 6) demonstrated variable degrees of visual field loss, with half of the cohort (54 %) showing severe visual field constrictions (<10°), and two equal-sized groups (25 % and 21 %) with 10–30° and>30° remaining fields respectively. Mean residual RPE/neuroretinal area as quantified by fundus autofluorescence imaging (n =64) was 8.47±1.91 mm^2 (range 0.30–38.5 mm^2). Residual neuroretinal volume within the central macular area defined by the 3 mm ERTDS grid was 1.76±0.12 mm^3 (n=42).

Degree of intraindividual symmetry

In order to determine symmetry between right and left eyes in CHM patients at various disease stages, we firstly compared visual acuity measurements of the right and left eyes taken at the same time point and by the same experienced ophthalmologist. Linear regression analysis showed a good fit (r^2=0.64) indicating a rather symmetric development of visual acuity (Fig. 2a).

The objective quantification of residual area of fundus autofluorescence showed an even higher degree of symmetry (r^2=0.83) between right and left eyes of CHM patients (Fig. 2b). Using the 3-mm ETDRS grid, quantification of central retinal volume also showed a good degree of symmetry (r^2=0.75, Fig. 2c).

Disease progression and age

Rate of progression was tested in a cross-sectional fashion, correlating key biomarkers of visual function and retinal structure with age at examination in all patients. Central visual acuity and age at examination shows a relatively poor, exponential correlation (r^2=0.23) with good visual function until the 4th decade and subsequent rapid reduction of visual acuity as the degeneration encroaches the central retina (Fig. 3a).

Structural disease progression was determined directly and objectively by quantifying the residual area of intact fundus autofluorescence (Fig. 3b), which indicates metabolically active, viable retinal pigment epithelium. This biomarker consists of an area measurement in square mm, and bivariate correlation analysis with the linear measure age at examination indeed revealed a good logarithmic fit (r^2=0.67, Fig. 3). Analysis with volumetric data from the central 3 mm showed again only relatively poor correlation (r^2=0.25, Fig. 3c).

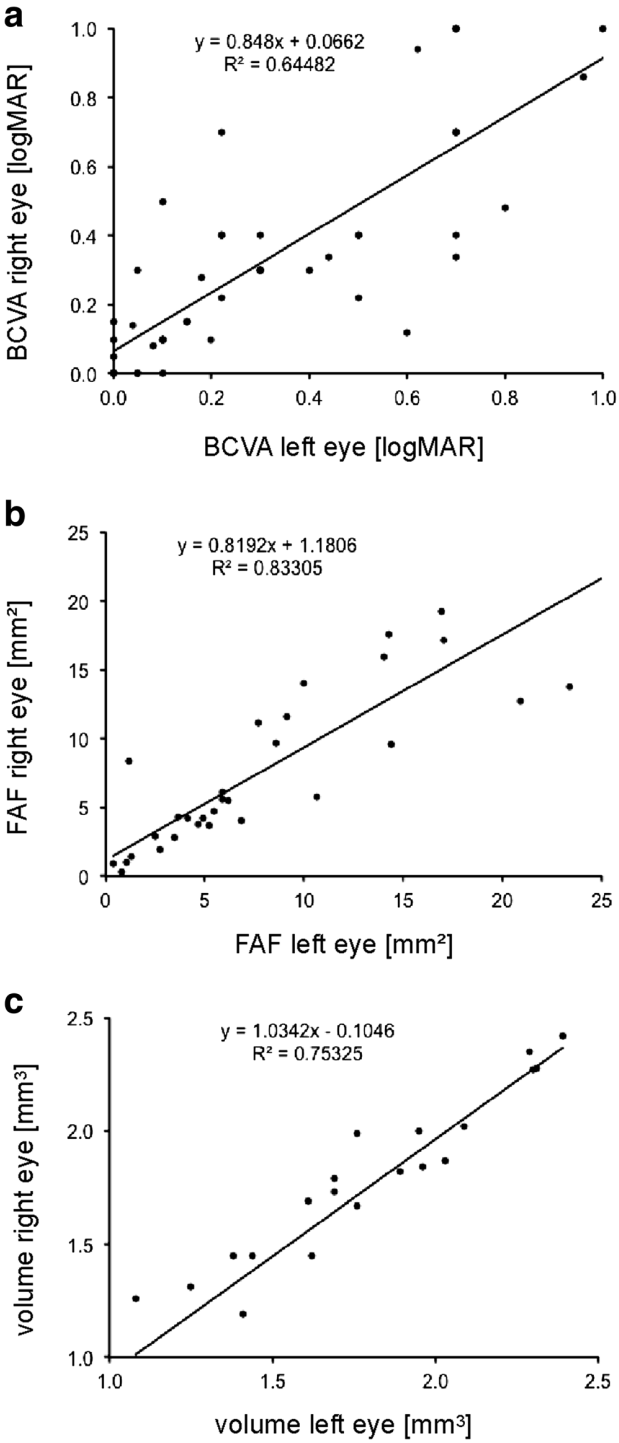

Fig. 2 Analysis of intraindividual symmetry in patients with choroideremia. **a** Best-corrected visual acuity (BCVA) as logarithm of the minimal angle of resolution (LogMAR) show high symmetry between right and left eyes (r^2=0.64). **b** Area of residual islands of intact fundus autofluorescence (FAF) was compared between right and left eyes (r^2=0.83). **c** Residual neuroretinal volume within the central 3 mm also correlated fairly well between eyes (r^2=0.75)

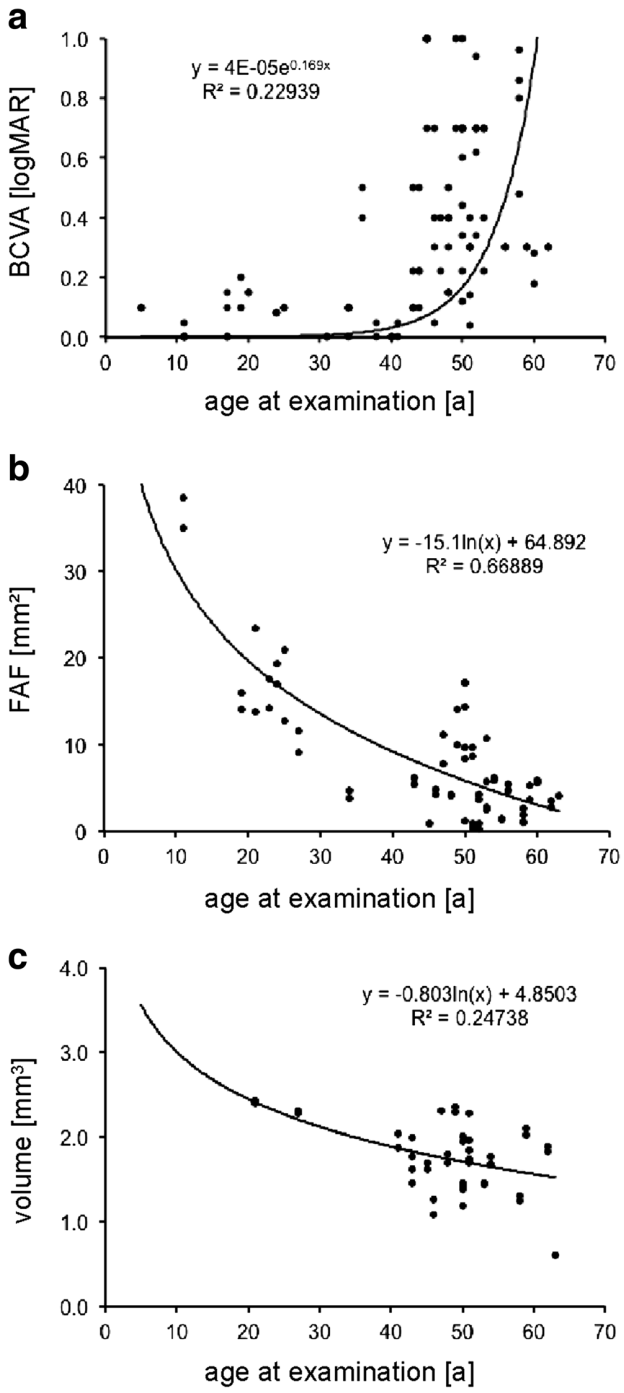

Fig. 3 Analysis of natural disease progression in patients with choroideremia. **a** Functional progression measured by best-corrected visual acuity (BCVA) in LogMAR (Logarithm of the minimal angle of resolution) vs age at examination describes an exponential function with visual acuity rapidly declining in later disease stages as the fovea becomes affected. Pearson correlation efficient r^2=0.23. **b** Structural markers of disease progression, such as size of the remaining island of intact fundus autofluorescence (FAF) measured in mm^2 best fit a logarithmic trend line (r^2=0.69) . **c** Volume measurements correlate with age at examination only marginally better then BCVA (r^2=0.25)

Discussion

The advent of gene therapeutic and other promising strategies for previously untreatable blinding disorders leads to a shift in management of patients with HRD. While previously considered of more or less purely academic interest, providing an accurate phenotypic and genetic characterisation now enables patients to potentially be selected for clinical trials aimed to help transfer the field of gene therapy into clinical reality.

Next to this, there are still a number of questions to be addressed by careful phenotyping, genotyping, and longitudinal follow up of patients with HRDs. As such, rate of progression is among the key questions, traditionally asked for prognostic reasons. With the advent of supplementation gene therapy and other potential strategies developed to slow or even stop progression, detailed knowledge of rate of progression can also provide information on the 'window of therapeutic opportunity' and help define end- and timepoints with high discriminatory power. In order to design interventional clinical trials, these data are essential in the process of defining eligibility of patients (e.g., when to treat), relevant efficacy measures, and time schedules for study visits during follow-up. Here, knowledge on the rate of natural disease progression and degree of symmetry becomes paramount.

This study contributes to this knowledge in CHM patients by testing the relationship of key functional and structural biomarkers with age of the respective patient and assessing symmetry of these biomarkers between the right and left eye of CHM patients. To the best of our knowledge, there is currently no quantitative analysis published on the intra-individual symmetry of important clinical parameters, which may serve as surrogate markers for therapeutic efficacy after unilateral intervention in a clinical trial setting. Given that (for example) additive gene therapy is applied locally and to the benefit of the treated eye only, knowledge of the degree of symmetry between eyes is of strategic value. Analysis of data between right and left eyes showed high degrees of symmetry, with data on area measurements of fundus autofluorescence outperforming residual retinal volume and the psychophysical measurement of visual acuity showing the least symmetry (FAF: r^2=0.83; volume: r^2=0.75; BCVA: r^2=0.64). This may simply reflect the higher level of integration present in psychophysical measures (optical media, cognition, et cetera) compared to simple bio-morphological quantification, which is bound to introduce more variability in the outcome measure.

In terms of visual acuity and age at examination, our study showed a poor linear correlation (r^2=0.16) and only slightly better fit for an exponential trend line (r^2=0.23). This pattern of VA deterioration has been described previously, and precisely reflects the non-uniform distribution of resolving power in the retina, with the fovea being the most important contributor to Snellen visual acuity and the last to be affected in the

centripetal course of degeneration. Rate of progression was 0.0103 logMAR per year in the linear model, which is very similar to what Coussa et al. reported (0.0072) in a slightly younger cohort (36±17.7) [20]. Roberts et al. found an annual loss of 0.09 logMAR in a retrospective longitudinal study with data sets from different tertiary referral centres [21] Interestingly, Coussa et al. reported a higher annual loss of visual acuity (0.06±0.08 log MAR) for patients in the >50 age group, indicating a more rapid vision loss in older patients. This supports our observation of an exponential, rather than linear decline of VA with age. Thus, the above linear predictions probably overestimate progression until ca. age 40, and underestimate the development beyond, and differences in reported functional progression may stem from differences in cohort characteristics such as age. The improvement of fit with choosing an exponential trend line reflects the known clinical course of CHM patients, maintaining a good visual function until approximately the 5th decade of life, with a subsequent rapid reduction of visual acuity as the degeneration starts to affect the fovea. Importantly, fundus autofluorescence provided a structural biomarker with a markedly closer fit (r^2=0.67) with regard to the relationship to age at examination, possibly benefiting from the lack of increasing variability, which affect psychophysical outcome measures to a greater extent in advanced disease stages [22].

These data suggest that treatment at a later stage of the disease would give the best discriminatory power between treated and untreated eyes, as the exponential curve is steepest due to rapid loss of remaining retinal tissue and disproportionally large impact on visual acuity. While this is scientifically plausible, it poses an ethical dilemma for the physician, who retains a safe and potentially efficacious treatment from the patient with certain progression to blindness. The study design of the phase II trial for Leber's congenital amaurosis (LCA) in Philadelphia addresses this problem by allowing the treatment of the second eye after a certain time period of following the natural disease progression (personal communication Dr. Bennett).

This compromise follows the reasoning that the untreated fellow eye is an appropriate internal control in LCA patients, which is likewise true for CHM as confirmed by this study. More specifically, our data indicate that while symmetry is high for both structural and functional biomarkers, quantitative assessment of residual RPE area might be a superior outcome measure compared to visual acuity from a scientific point of view. Firstly, it is easier to mask readout, as quantification can be performed without patient interaction by experts outside the trial unit (e.g., reading centre). In contrast, masking strategies for BCVA assessment will always be incomplete. Even if the examiner recording the BCVA was successfully masked for the treatment, the patient would not be. Therefore, one has to assume confounding effects by motivation and expectation that may influence efficacy results.

There is ample evidence with regard to the increased variability of BCVA results in patients with low visual acuity [22]. Alas, increasing the numbers of successfully identified ETDR S letters remains the gold standard treatment goal — especially in the pursuit of gaining market approval and complying with the checklists of regulatory agencies.

It will remain an important challenge for clinicians and scientists to provide a solid body of evidence supporting the argument that interventions such as gene therapy are efficacious if they stop further degeneration, rather than leading to an improvement of visual acuity. This even more so in disorders similar to CHM, where patients maintain very good central visual acuity until the very end of the disease course. We argue that preventing the degeneration at an earlier time point might be the more viable approach, rather than waiting for foveal involvement, when gene therapy has only limited remaining therapeutic potential, as most target cells have already undergone degeneration.

Acknowledgments The authors wish to acknowledge the help from all colleagues who helped obtain the clinical data on CHM patients in the "RP Sprechstunde" (outpatient clinic for hereditary retinal disorders) over previous decades. Drs. S Biskup, M Preisig, B Weber, and JA van den Hurk contributed to this work by verifying the diagnosis on a genetic level in some of the patients.

Conflict of interest statement All authors certify that they have NO affiliations with or involvement in any organization or entity with any financial interest (such as honoraria; educational grants; participation in speakers' bureaus; membership, employment, consultancies, stock ownership, or other equity interest; and expert testimony or patent-licensing arrangements), or non-financial interest (such as personal or professional relationships, affiliations, knowledge or beliefs) in the subject matter or materials discussed in this manuscript.

Grant support Gesellschaft zur Förderung der Neuroophthalmologie e.V., Tistou & Charlotte Kerstan Foundation, Pro Retina e.V., UK Medical Research Council (MR/K003690/1);

References

1. Mauthner L (1872) Ein Fall von Chorioideremie. Bericht des Naturwissenschaftlich-Medizinischen Vereins Innsbruck:191–197
2. Cremers FP, Brunsmann F, van de Pol TJ, Pawlowitzki IH, Paulsen K, Wieringa B, Ropers HH (1987) Deletion of the DXS165 locus in patients with classical choroideremia. Clin Genet 32:421–423
3. Cremers FP, van de Pol DJ, Diergaarde PJ, Wieringa B, Nussbaum RL, Schwartz M, Ropers HH (1989) Physical fine mapping of the choroideremia locus using Xq21 deletions associated with complex syndromes. Genomics 4:41–46
4. Cremers FP, van de Pol DJ, Wieringa B, Collins FS, Sankila EM, Siu VM, Flintoff WF, Brunsmann F, Blonden LA, Ropers HH (1989) Chromosomal jumping from the DXS165 locus allows molecular characterization of four microdeletions and a de novo chromosome X/13 translocation associated with choroideremia. Proc Natl Acad Sci U S A 86:7510–7514
5. Cremers FP, Sankila EM, Brunsmann F, Jay M, Jay B, Wright A, Pinckers AJ, Schwartz M, van de Pol DJ, Wieringa B et al (1990)

Deletions in patients with classical choroideremia vary in size from 45 kb to several megabases. Am J Hum Genet 47:622–628
6. Cremers FP, Molloy CM, van de Pol DJ, van den Hurk JA, Bach I, Geurts van Kessel AH, Ropers HH (1992) An autosomal homologue of the choroideremia gene colocalizes with the Usher syndrome type II locus on the distal part of chromosome 1q. Hum Mol Genet 1:71–75
7. Cremers FP, Armstrong SA, Seabra MC, Brown MS, Goldstein JL (1994) REP-2, a Rab escort protein encoded by the choroideremia-like gene. J Biol Chem 269:2111–2117
8. Coussa RG, Traboulsi EI (2012) Choroideremia: a review of general findings and pathogenesis. Ophthalmic Genet 33:57–65
9. Rak A, Pylypenko O, Niculae A, Pyatkov K, Goody RS, Alexandrov K (2004) Structure of the Rab7:REP-1 complex: insights into the mechanism of Rab prenylation and choroideremia disease. Cell 117:749–760
10. Moosajee M, Ramsden SC, Black GC, Seabra MC, Webster AR (2014) Clinical utility gene card for: choroideremia. Eur J Hum Genet 22(4)
11. Wavre-Shapton ST, Tolmachova T, Lopes da Silva M, Futter CE, Seabra MC (2013) Conditional ablation of the choroideremia gene causes age-related changes in mouse retinal pigment epithelium. PLoS One 8:e57769
12. Tolmachova T, Tolmachov OE, Barnard AR, de Silva SR, Lipinski DM, Walker NJ, Maclaren RE, Seabra MC (2013) Functional expression of Rab escort protein 1 following AAV2-mediated gene delivery in the retina of choroideremia mice and human cells ex vivo. J Mol Med 91:825–837
13. MacLaren RE, Groppe M, Barnard AR, Cottriall CL, Tolmachova T, Seymour L, Clark KR, During MJ, Cremers FP, Black GC, Lotery AJ, Downes SM, Webster AR, Seabra MC (2014) Retinal gene therapy in patients with choroideremia: initial findings from a phase 1/2 clinical trial. Lancet 383:1129–1137
14. Furgoch MJ, Mewes-Ares J, Radziwon A, Macdonald IM (2014) Molecular genetic diagnostic techniques in choroideremia. Mol Vis 20:535–544
15. Fischer MD, Fleischhauer JC, Gillies MC, Sutter FK, Helbig H, Barthelmes D (2008) A new method to monitor visual field defects caused by photoreceptor degeneration by quantitative optical coherence tomography. Invest Ophthalmol Vis Sci 49:3617–3621
16. Wiethoff S, Zhour A, Schols L, Fischer MD (2012) Retinal nerve fibre layer loss in hereditary spastic paraplegias is restricted to complex phenotypes. BMC Neurol 12:143
17. Fischer MD, Willmann G, Schatz A, Schommer K, Zhour A, Zrenner E, Bartz-Schmidt KU, Gekeler F (2012) Structural and functional changes of the human macula during acute exposure to high altitude. PLoS One 7:e36155
18. Bellmann C, Rubin GS, Kabanarou SA, Bird AC, Fitzke FW (2003) Fundus autofluorescence imaging compared with different confocal scanning laser ophthalmoscopes. Br J Ophthalmol 87:1381–1386
19. Holladay JT (1997) Proper method for calculating average visual acuity. J Refract Surg 13(4):388–391
20. Coussa RG, Kim J, Traboulsi EI (2012) Choroideremia: effect of age on visual acuity in patients and female carriers. Ophthalmic Genet 33:66–73
21. Roberts MF, Fishman GA, Roberts DK, Heckenlively JR, Weleber RG, Anderson RJ, Grover S (2002) Retrospective, longitudinal, and cross sectional study of visual acuity impairment in choroideraemia. Br J Ophthalmol 86:658–662
22. Bittner AK (2011) Variability in vision and photopsias in retinitis pigmentosa are related to disease severity and psychosocial factors. Dissertation. The Johns Hopkins University

2.3. Defining Relevant Endpoints: "Colour discrimination ellipses in Choroideremia"

Graefe's Archive for Clinical and Experimental Ophthalmology (2018) 256:665–673
https://doi.org/10.1007/s00417-018-3921-0

RETINAL DISORDERS

Colour discrimination ellipses in choroideremia

Immanuel P. Seitz[1,2] · Jasleen K. Jolly[3] · M. Dominik Fischer[1,2,3] · Matthew P. Simunovic[3,4,5]

Received: 14 August 2017 / Revised: 8 January 2018 / Accepted: 24 January 2018 / Published online: 5 February 2018

Abstract
Purpose The purpose of this study was to characterise alterations in colour discrimination in a cohort of patients with choroideremia prior to gene therapy, using a test previously validated for use in patients with retinal dystrophies.
Methods We tested 20 eyes of 10 patients with a diagnosis of choroideremia and an age-matched cohort of 10 eyes of 10 normal controls using the "Cambridge Colour Test" (CCT), in which subjects are required to distinguish the gap in a C presented in one of 4 orientations in a Stilling-type array. Colour discrimination was probed along eight axes in the CIE L*u*v* colour space, and the resulting data were plotted in the CIE 1976 chromaticity diagram and fitted with least-squares ellipses. Subsequently, we estimated the achromatic area for each subject by calculating the area of the resultant discrimination ellipse and calculated sensitivity thresholds along relevant colour confusion axes.
Results Colour discrimination—as quantified by $\log_{10}$ of the ellipse area expressed in square 1/1000th^2 units in CIE 1976—was 2.26 (range 1.82 to 2.67) for normal subjects and 3.85 (range 2.35 to 5.41) for choroideremia patients. There was a statistically significant correlation between both achromatic area and red-green colour discrimination at the CCT and BCVA, and to a lesser degree between blue colour discrimination at the CCT and BCVA. The majority of ellipses in choroideremia were aligned close to the tritan axis, and loss of sensitivity was significantly larger in the tritan direction than in the red-green.
Conclusions The majority of our patients demonstrated greater loss in tritan discrimination than in red-green colour discrimination using the CCT. There was a significant correlation between achromatic area and BCVA. In keeping with our current understanding of the machinery of colour vision, there was a significant correlation between BCVA and colour discrimination thresholds, which was stronger for red-green colour discrimination, than for tritan colour discrimination. We propose that this and similar tests of colour discrimination may prove to be suitable tools for assessing functional outcomes in gene therapy trials for choroideremia.

Keywords Choroideremia · Colour vision · Colour discrimination · Colour vision deficiency

✉ Matthew P. Simunovic
mps23@cantab.net

[1] University Eye Hospital Tübingen, Elfriede-Aulhorn Straße 7, 72076 Tübingen, Germany
[2] Institute for Ophthalmic Research, Elfriede-Aulhorn Straße 7, 72076 Tübingen, Germany
[3] Nuffield Laboratory of Ophthalmology, John Radcliffe Hospital West Wing, University of Oxford, Oxford OX3 9DU, UK
[4] Sydney Eye Hospital, 8 Macquarie St, Sydney, NSW 2000, Australia
[5] Save Sight Institute, Discipline of Ophthalmology, University of Sydney, 8 Macquarie St, Sydney, NSW 2000, Australia

Introduction

Choroideremia is an X-linked recessive chorioretinal dystrophy first described by Mauthner in 1871 [1]. The condition is characterised by centripetal loss of the choroid, retina and retinal pigment epithelium (RPE): the functional correlates of these structural changes are nyctalopia and loss of peripheral visual field. Typically, the onset of symptoms is in the second decade of life: Foveomacular integrity and central vision are relatively preserved until the fifth decade. The causative *CHM* gene codes for Rab escort protein 1 (REP1), a protein vital for intracellular trafficking within the eye: the majority of causative mutations have been demonstrated to be null, with no evidence for phenotype-genotype correlation

Graefe's Archive for Clinical and Experimental Ophthalmology (2018) 256:665–673
https://doi.org/10.1007/s00417-018-3921-0

RETINAL DISORDERS

Colour discrimination ellipses in choroideremia

Immanuel P. Seitz[1,2] · Jasleen K. Jolly[3] · M. Dominik Fischer[1,2,3] · Matthew P. Simunovic[3,4,5]

Received: 14 August 2017 / Revised: 8 January 2018 / Accepted: 24 January 2018 / Published online: 5 February 2018

Abstract

Purpose The purpose of this study was to characterise alterations in colour discrimination in a cohort of patients with choroideremia prior to gene therapy, using a test previously validated for use in patients with retinal dystrophies.

Methods We tested 20 eyes of 10 patients with a diagnosis of choroideremia and an age-matched cohort of 10 eyes of 10 normal controls using the "Cambridge Colour Test" (CCT), in which subjects are required to distinguish the gap in a C presented in one of 4 orientations in a Stilling-type array. Colour discrimination was probed along eight axes in the CIE L*u*v* colour space, and the resulting data were plotted in the CIE 1976 chromaticity diagram and fitted with least-squares ellipses. Subsequently, we estimated the achromatic area for each subject by calculating the area of the resultant discrimination ellipse and calculated sensitivity thresholds along relevant colour confusion axes.

Results Colour discrimination—as quantified by $\log_{10}$ of the ellipse area expressed in square 1/1000th^2 units in CIE 1976—was 2.26 (range 1.82 to 2.67) for normal subjects and 3.85 (range 2.35 to 5.41) for choroideremia patients. There was a statistically significant correlation between both achromatic area and red-green colour discrimination at the CCT and BCVA, and to a lesser degree between blue colour discrimination at the CCT and BCVA. The majority of ellipses in choroideremia were aligned close to the tritan axis, and loss of sensitivity was significantly larger in the tritan direction than in the red-green.

Conclusions The majority of our patients demonstrated greater loss in tritan discrimination than in red-green colour discrimination using the CCT. There was a significant correlation between achromatic area and BCVA. In keeping with our current understanding of the machinery of colour vision, there was a significant correlation between BCVA and colour discrimination thresholds, which was stronger for red-green colour discrimination, than for tritan colour discrimination. We propose that this and similar tests of colour discrimination may prove to be suitable tools for assessing functional outcomes in gene therapy trials for choroideremia.

Keywords Choroideremia · Colour vision · Colour discrimination · Colour vision deficiency

Introduction

Choroideremia is an X-linked recessive chorioretinal dystrophy first described by Mauthner in 1871 [1]. The condition is characterised by centripetal loss of the choroid, retina and retinal pigment epithelium (RPE): the functional correlates of these structural changes are nyctalopia and loss of peripheral visual field. Typically, the onset of symptoms is in the second decade of life: Foveomacular integrity and central vision are relatively preserved until the fifth decade. The causative *CHM* gene codes for Rab escort protein 1 (REP1), a protein vital for intracellular trafficking within the eye: the majority of causative mutations have been demonstrated to be null, with no evidence for phenotype-genotype correlation

✉ Matthew P. Simunovic
mps23@cantab.net

1 University Eye Hospital Tübingen, Elfriede-Aulhorn Straße 7, 72076 Tübingen, Germany

2 Institute for Ophthalmic Research, Elfriede-Aulhorn Straße 7, 72076 Tübingen, Germany

3 Nuffield Laboratory of Ophthalmology, John Radcliffe Hospital West Wing, University of Oxford, Oxford OX3 9DU, UK

4 Sydney Eye Hospital, 8 Macquarie St, Sydney, NSW 2000, Australia

5 Save Sight Institute, Discipline of Ophthalmology, University of Sydney, 8 Macquarie St, Sydney, NSW 2000, Australia

[2]. Currently, phase II trials of gene-replacement therapy for choroideremia are underway, with both short-term and sustained benefits evident in the phase I/II cohort reported to date [3, 4]. Colour vision has anecdotally and empirically [5] been reported to improve in some subjects following gene therapy for choroideremia; therefore, colour vision may prove to be a suitable functional assay of the effects of such treatment. Normal colour discrimination is proposed to rely on two phylogenetically distinct processing pathways [6]. The oldest of these pathways compares quantum catches from short-wavelength sensitive cones to medium- and long-wavelength sensitive cones (tritan colour discrimination). The newer pathway compares quantum catches from medium- and long-wavelength sensitive cones and is proposed to be parasitic upon a mechanism specialised for spatial resolution (red-green colour discrimination) [6]. The former subsystem appears to be especially vulnerable to insult from ocular and visual pathway pathology [7] via a variety of putative mechanisms [8]. The assessment of colour discrimination in patients with choroideremia is problematic. Many tests of colour discrimination suitable for those with acquired colour vision deficiency require an element of visual search (e.g., the FM 100Hue test): therefore, poor performance at such tests may partially reflect difficulties in visual search secondary to limited visual field, rather than altered colour vision alone. Hence, we sought to establish colour discrimination using a test—the Cambridge Colour Test—which is likely to be less vulnerable to such effects.

Methods

A total of 20 subjects were tested as part of the investigation. Ten subjects with a clinical diagnosis of choroideremia (mean age 45.5 years, range 21–58 years) had 20 eyes tested monocularly (right eye first), whilst 10 colour normal subjects who were all able to pass the Ishihara Plate Test (mean age 38.4 years, range 26–70 years) served as a control group. In nine of ten patients with choroideremia, the genotype was established by sequencing and/or multiplex ligation-dependent probe amplification [9]. Clinical assessment to revalidate the established diagnosis was conducted by an ophthalmologist experienced in assessing patients with inherited retinal disease. It included best corrected visual acuity (BCVA) using a Bailey-Lovie style letter chart, applanation tonometry, slit-lamp biomicroscopy and fundus examination. To ensure sufficient foveal integrity, all choroideremia patients underwent an intensified structural characterisation, consisting of fundus photography, fundus autofluorescence and optical coherence tomography (Spectralis, Heidelberg Engineering, Germany). Colour vision assessment was conducted using the CCT (Cambridge Research Systems, UK), a computer-controlled test of colour discrimination described in detail previously [10]. The subject's task in the CCT is to discriminate the gap in a coloured C presented in one of four orientations in a grey Stilling-type array. The C itself subtends 4.3 deg. at the corneal surface and its gap subtends 1 deg. The subject indicates their response via a button box connected to the computer. The saturation of the test discs is varied using an interleaved staircase where the chromaticity of the C is varied along 8 axes spaced 45 degrees apart in the CIE L*u*v* colour space. In order to eliminate the possibility of defeating the test through brightness cues, the luminance of the discs in the array is selected to lie semi-randomly at a value between 7.6 and 17 cd.m^{-2}. The generated individual data were plotted in the CIE 1976 u' v' chromaticity diagram and fitted with least-squares ellipses. Subsequently, we calculated sensitivity thresholds along relevant colour confusion axes, as well as achromatic area, which was estimated by calculating the ellipse area in the CIE 1976 u' v' chromaticity diagram (Fig. 1).

Results

All patients displayed structural anomalies consistent with the clinical and genetic diagnosis of choroideremia.

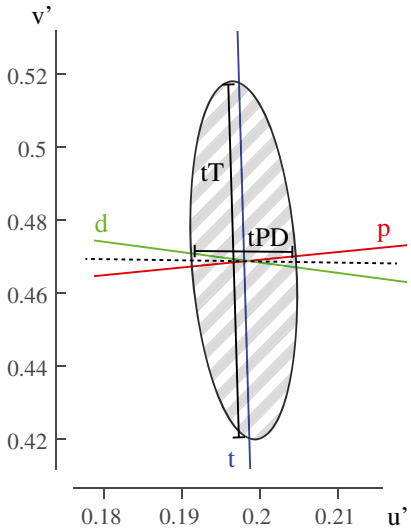

Fig. 1 Illustration of colour discrimination ellipse measurements used for further analysis: sample ellipse of a tritanopic patient, plotted in the CIE1976 chromaticity diagram. Grey stripes: colour discrimination ellipse area. Colour confusion axes are labelled d (deutan), p (protan) and t (tritan). A combined protan/deutan axis is noted as dashed line. tT: ellipse length along the tritan axis (tritan sensitivity threshold). tPD: ellipse length along a combined protan/deutan axis (protan/deutan sensitivity threshold)

Characteristic findings in mid to late stage disease are assembled in Fig. 2. Table 1 summarises the underlying genotype, BCVA, ellipse dimensions and qualitative colour deficiency findings for each subject with choroideremia. Genotypes were determined for nine of ten patients. Causative mutations included three exon-wide deletions, two single-nucleotide deletions, one two-nucleotide duplication and three single-nucleotide nonsense substitutions. In line with variation in age and disease progression, BCVA amongst patients ranged from 0 to 0.8 LogMAR. Colour discrimination thresholds were age-appropriate in all control subjects and elevated along at least one axis in all patients. Disproportionally elevated thresholds (by a factor of 2 or greater, compared to thresholds along the other axes) were deemed to be the dominant deficiency. Tritan detection thresholds were elevated in all patients, and the dominant deficiency in 14 of 20 eyes. Protan/deutan deficits were more common, but not exclusive to, patients with advanced disease progression. They were detected in 9 of 20 eyes, yet dominant in only one eye. Five of 20 eyes did not exhibit a dominant deficiency. Figure 3 illustrates colour discrimination ellipses of four patients and two healthy controls. The mean $\log_{10}$ achromatic area was 2.26 (range 1.82 to 2.67) for normal subjects and 3.85 (range 2.35 to 5.41) for choroideremia patients. This difference between patients and normals was significant for achromatic area (Fig. 4; Welch-Satterthwaite t test: $t(25.4) = 6.9$, $p = 2.6$ E-7) as well as for red-green sensitivity (mean of protan and deutan detection thresholds, Fig. 5; Mann-Whitney U: $p =$ 0.006) and blue sensitivity (Fig. 6; Mann-Whitney U: $p =$ 2.3 E-5). In the choroideremia patients, we found a significant

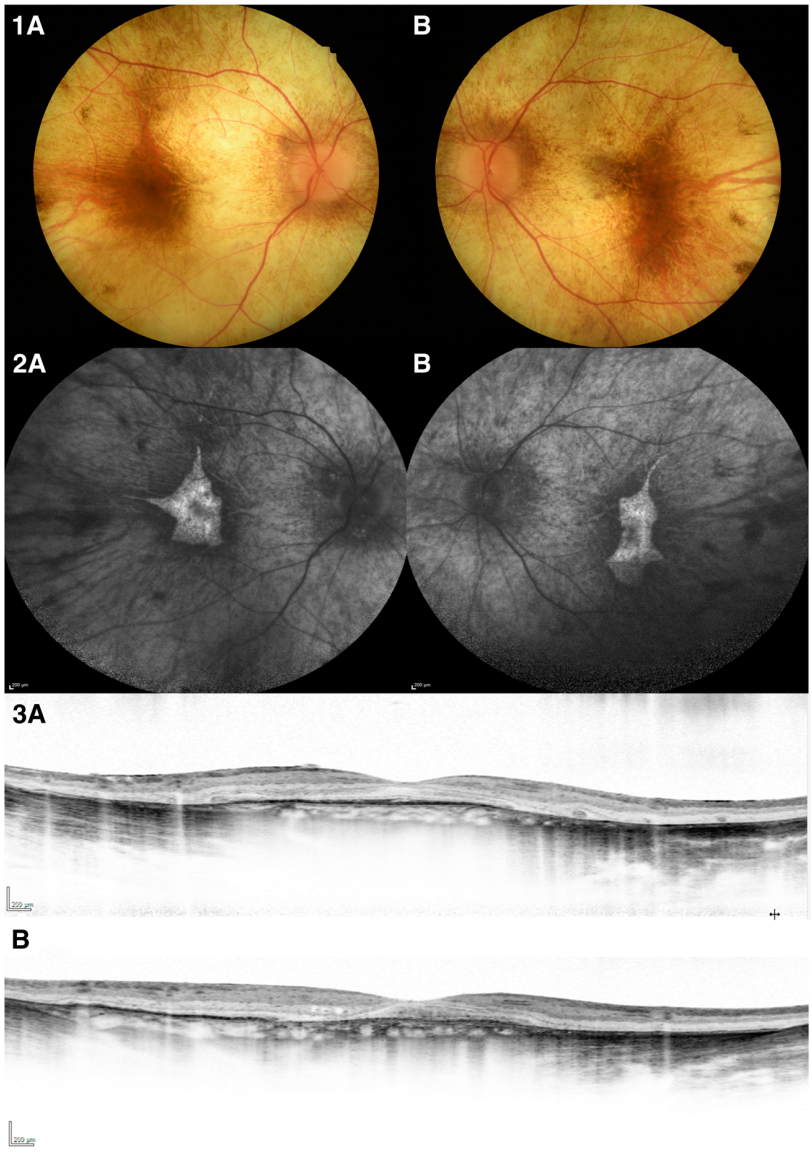

Fig. 2 Structural findings in mid to late stage choroideremia. Right (**a**) and left (**b**) eyes of patient 9. Fundus photography (1) shows comprehensive degeneration of the retina, RPE and choroid, leaving only parts of the inner retina, and the sclera intact (yellow area). Autofluorescence (2) highlights foveal residual islands, with reduced to normal function. OCT (3) scans confirm both peripheral degeneration and remaining foveal integrity

Table 1 Summary of BCVA, genotypes, ellipse data and qualitative colour deficiency findings in choroideremia patients. Ellipse lengths expressed in 1/1000th units in the CIE 1976 chromaticity diagram. Ellipse areas are expressed as $\log_{10}$ square 1/1000th units in the CIE 1976 chromaticity diagram. All patient eyes exhibited reduced colour discrimination along one or more colour confusion axis, denoted as T: Tritan, P: Protan, D: Deutan. When multiple axes are affected, ">"was used to denote dominance (threshold/threshold ratio > 2) of a specific defect

Patient #	Eye	Genotype	Visual acuity logMAR	$\log_{10}$ ellipse area	Ellipse length	Ellipse angle	Axial ratio	Reduced discrimination along
1	OD	c.757C > T (p.Arg253*)	0.8	4.43	0.22	109.74	1.36	T = PD
	OS	c.757C > T (p.Arg253*)	0.48	4.40	0.20	95.83	1.28	T = PD
2	OD	deletion of exons 1–15	0.14	3.33	0.18	96.41	11.72	T
	OS	deletion of exons 1–15	0.06	3.02	0.10	91.72	7.27	T
3	OD	c.116C > G (p.S39X)	0.08	2.95	0.13	85.98	15.88	T
	OS	c.116C > G (p.S39X)	0.08	2.77	0.07	91.60	5.87	T
4	OD	c.1446delA	0.04	3.27	0.13	87.89	7.54	T
	OS	c.1446delA	0.14	5.41	11.37	101.60	394.71	T > PD
5	OD	N/A	0.04	3.96	0.19	89.10	3.10	T > PD
	OS	N/A	0.46	4.39	0.23	118.51	1.69	T = PD
6	OD	deletion of exons 1–15	0.7	4.23	0.16	160.92	1.15	T = PD
	OS	deletion of exons 1–15	0.34	3.98	0.17	16.44	2.50	PD > T
7	OD	c.800delT (pT288Lfs*3)	0.44	5.03	11.81	82.91	1017.04	T
	OS	c.800delT (pT288Lfs*3)	0.34	2.85	0.07	93.40	6.04	T
8	OD	deletion of exon 12	0.02	2.35	0.03	82.22	4.03	T
	OS	deletion of exon 12	0	2.55	0.05	86.60	4.85	T
9	OD	c.314 + 10,127 T > A	0.18	4.92	4.59	75.56	199.09	T
	OS	c.314 + 10,127 T > A	0.28	5.39	13.50	76.08	581.64	T
10	OD	c.498_499dupGC (p.Leu167Argfs*2)	0.6	3.83	0.18	93.51	3.59	T > PD
	OS	c.498_499dupGC (p.Leu167Argfs*2)	0.2	4.00	0.15	93.51	1.80	T = PD

tendency (Mann-Whitney U: $p = 0.004$) towards tritan deficiency (threshold mean, ±SD, ± 95%CI; 0.112, ± 0.083, ± 0.039) rather than to red-green deficiency (0.064, ± 0.060, ± 0.028) (Fig. 7). Significant intra-individual symmetry in patients was limited to the M and L cone function (Fig. 8; Pearson $r = 0.707$, $p = 0.022$) and not found along the tritan axis (Fig. 9; Pearson $r = 0.382$, $p = 0.276$) or with total achromatic area (Fig. 7; Pearson $r = 0.408$, $p = 0.121$). As anticipated from the natural history of the condition, colour discrimination was found to decline with declining visual acuity. There was a significant correlation between the achromatic area, as estimated from the ellipse area and visual acuity (Fig. 10; Spearman $P = 0.586$, $p = 0.007$). Of note, BCVA also correlated significantly to the individual colour detection thresholds. BCVA was found to be correlated to sensitivity along a red-green axis (Fig. 11; Spearman $P = 0.587$, $p = 0.007$) and the tritan axis (Fig. 12; Spearman $P = 0.469$, $p = 0.037$). However, the correlation between tritan discrimination and BCVA was weaker than for red-green colour discrimination, a finding that is in keeping with current understanding of the machinery of colour vision and the effects of retinal pathology [8].

Discussion

Patients in later disease stages are preferred early treatment candidates in clinical gene therapy trials [3]. Therefore, this study aims to highlight translationally relevant alterations of colour vision in choroideremia patients with mid- to late-stage disease. This stage is marked by degeneration of the parafoveal region [11], which contains a high density of S-cones [12], whilst central M- and L-cones are relatively preserved within the fovea (where they have their peak density). These observations may help to explain the preponderance of tritan deficiencies in our cohort of patients with choroideremia. Previous observations that disorders of the tritan mechanism are common in a variety of retinal diseases [7] in which central fixation is maintained support this hypothesis [7, 8].

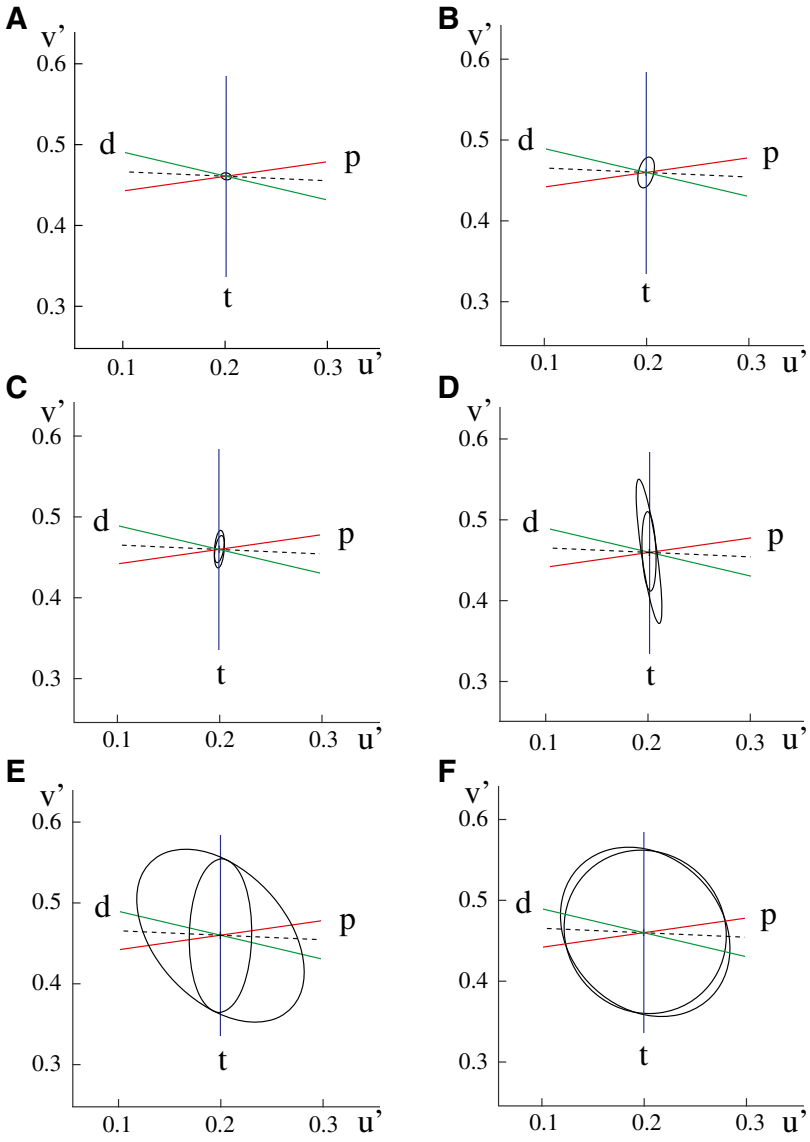

Fig. 3 Sample achromatic ellipses plotted in the CIE 1976 chromaticity diagram. Panels **a** and **b** show the range of results in control subjects. Panels **c**–**f** illustrate patient results. **a** 26-year-old control subject, normal colour sensitivity. **b** 70-year-old control subject, age-related decrease of sensitivity across all axes. **c** 21-year-old patient, highest sensitivity (=lowest thresholds) recorded in the patient cohort, non-age-appropriate subnormal tritan sensitivity. **d** 38-year-old patient, pronounced tritan deficiency. **e** 55-year old patient, asymmetric colour discrimination defects between both eyes. **f** 58-year-old patient, subtotal loss of colour discrimination in end stage choroideremia. Colour confusion axes are labelled d (deutan), p (protan) and t (tritan). The combined protan/deutan axis is marked as a dashed line

Of note, we found a flatter slope of correlation between BCVA and tritan discrimination, compared to BCVA and red-green discrimination. These results are also in agreement with previous empirical observations that tritan discrimination may be affected independently of spatial vision, whilst red-green discrimination is generally unaffected by disease processes until spatial resolution declines [13, 14]. Furthermore, these findings concur with our current understanding of the underlying pathways involved in spatial and spectral discrimination [8]. However, the observations in our patient cohort for the CCT are in contrast to some of the previously published studies (using the FM 100Hue) [15] which found no predilection for selective loss of either tritan or red-green discrimination in choroideremia [16, 17]. This discrepancy might arise from a variety of factors which may affect the assessment of colour discrimination in patients with inherited retinal degenerations. First, such patients may lack the necessary spatial resolution to perform standard tests of colour discrimination. Second, this problem may be compounded by visual field loss, which can make it difficult for certain patients to perform tests often considered to be ideal for testing patients with acquired colour vision deficiency [15]. A good example is the abovementioned FM 100Hue test, which is often considered to be the gold-standard for assessing patients with acquired colour vision deficiency and which is accordingly recognised by the US Federal Drugs Administration (FDA) as a suitable outcome measure in clinical trials. The test consists of a total of 85 caps which are separated into four boxes. In this test, the subject is required to order the caps in a gradual progression in perceived colour. Typically, the patient will

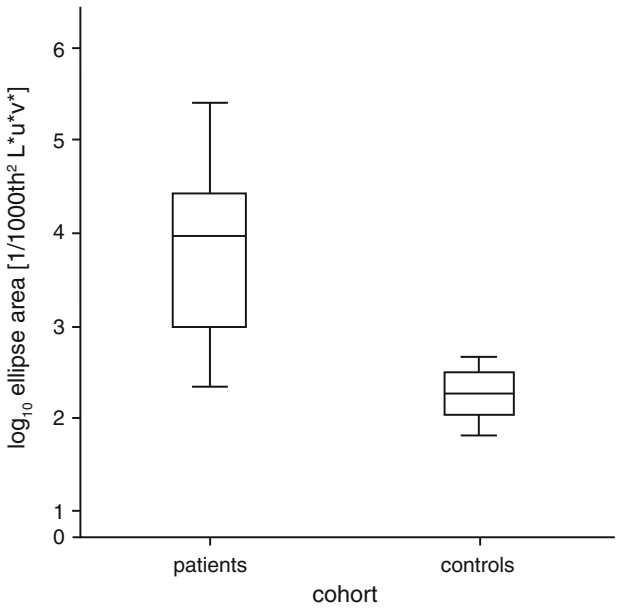

Fig. 4 Colour discrimination ellipse area (log10 1/1000th^2 $L^*u^*v^*$ units) of choroideremia patients vs age-matched controls. Boxes show the interquartile range, including the cohort's median denoted as a horizontal line. Bars denote the cohort's minimal and maximal values

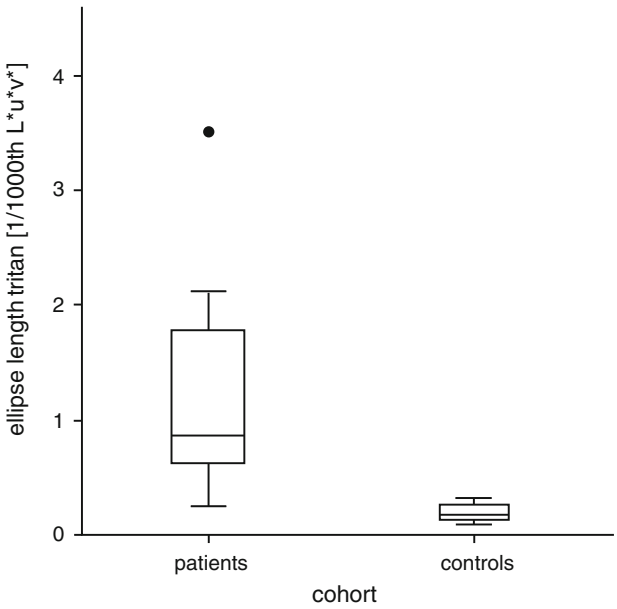

Fig. 6 Colour discrimination ellipse length (1/1000th $L^*u^*v^*$ units) along tritan axis of choroideremia patients vs age-matched controls. Coloured boxes show the interquartile range, including the cohort's median denoted as a horizontal line. Whiskers denote the cohort's minimal and maximal values. Outliers are marked as dots

do this by progressively matching: that is, they will commence with one of the "fixed" caps at either end of the box and match one of the moveable caps to this fixed cap. Once this is done, the task begins again, except this time the match is between the recently placed cap and the remaining caps. Given that the colour aperture of the FM 100Hue subtends about 2 degrees (depending on viewing distance), and the fact that there are 21–22 caps per box which are typically scattered to allow the patient to perform their ordering, this is a lengthy and complex task for patients with a significant visual field defect, as

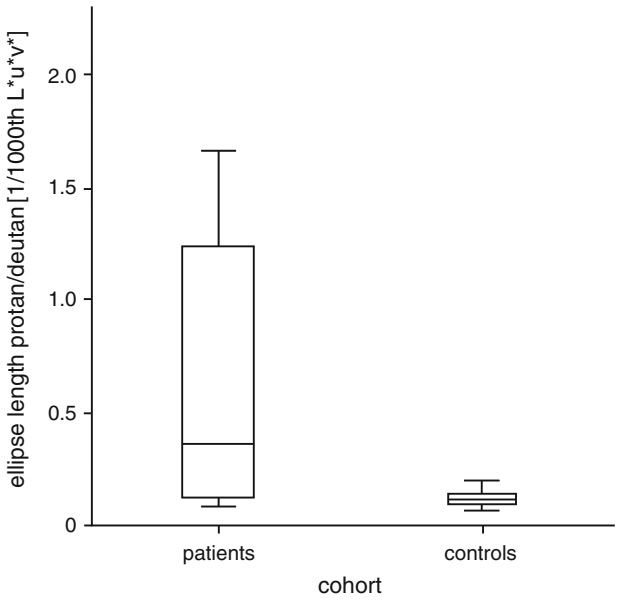

Fig. 5 Colour discrimination ellipse length (1/1000th $L^*u^*v^*$ units) along a combined protan/deutan axis of choroideremia patients vs age-matched controls. Boxes show the interquartile range, including the cohort's median denoted as a horizontal line. Bars denote the cohort's minimal and maximal values

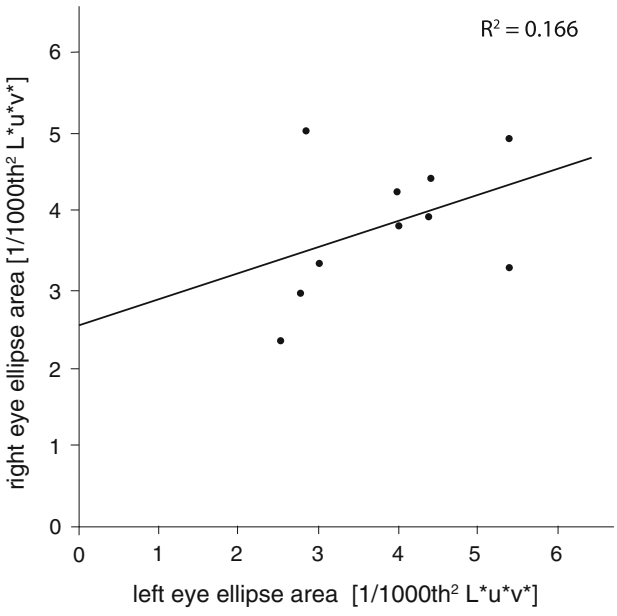

Fig. 7 Colour discrimination ellipse area (log10 1/1000th^2 $L^*u^*v^*$ units): intraindividual symmetry in choroideremia patients

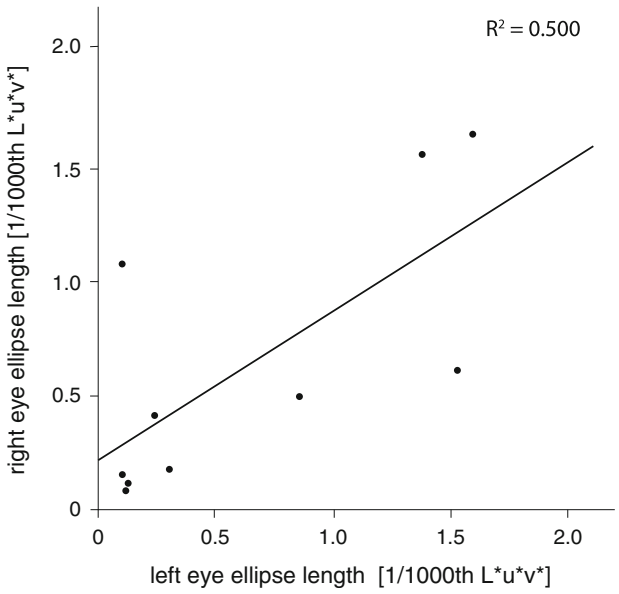

Fig. 8 Colour discrimination ellipse length (1/1000th $L^*u^*v^*$ units) along a combined protan/deutan axis: intraindividual symmetry in choroideremia patients

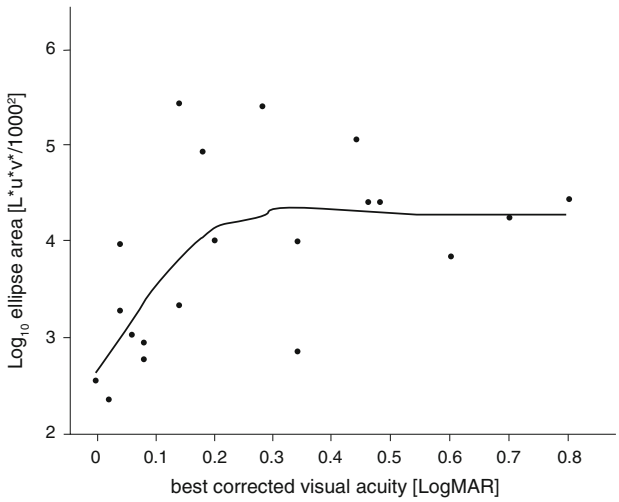

Fig. 10 Colour discrimination ellipse area (log10 1/1000th^2 $L^*u^*v^*$ units) vs BCVA (logMAR). Epanechnikov kernel function illustrates differing degrees of monotonic correlation. Spearman $\rho = 0.586$, $p = 0.007$; Kendall $\tau = 0.394$, $p = 0.016$

there is an attendant degree of visual search required. Although previous studies utilising the FM 100Hue have demonstrated functional defects, even when visual acuity is normal [15], this may partially reflect difficulties with visual search and the associated stress and/or fatigue, rather than underlying difficulties with colour discrimination. To provide a suitable means of assessing colour discrimination in patients with choroideremia, we used the Cambridge Colour test, which would be anticipated to be less subject to such effects. Furthermore, identifying an axis of maximum confusion in acquired colour vision deficiency is inherently more precise in the CCT than in the FM 100Hue. Although our subjects were able to perform the standard CCT, patients with lower levels of spatial discrimination are better assessed with the low vision version of the test, in which subjects must discriminate a 4 degree coloured disc from 3 grey discs presented in a diamond shaped array [18]. The latter test has been validated for use in patients with retinal degenerations [19, 20].

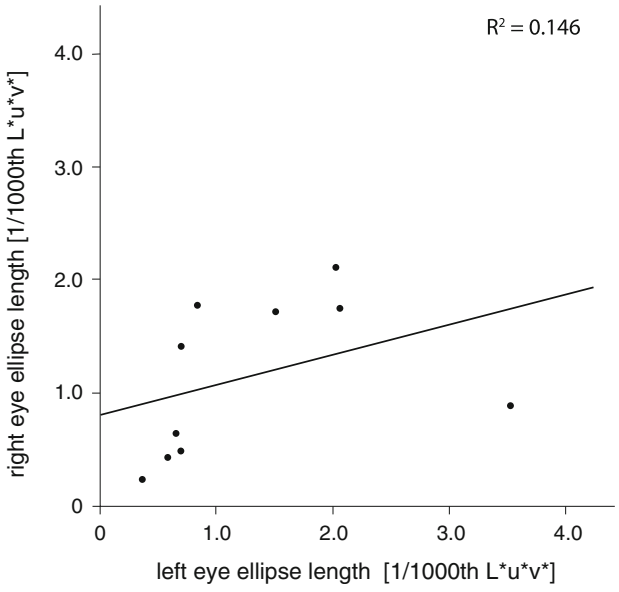

Fig. 9 Colour discrimination ellipse length (1/1000th $L^*u^*v^*$ units) along tritan axis: intraindividual symmetry in choroideremia patients

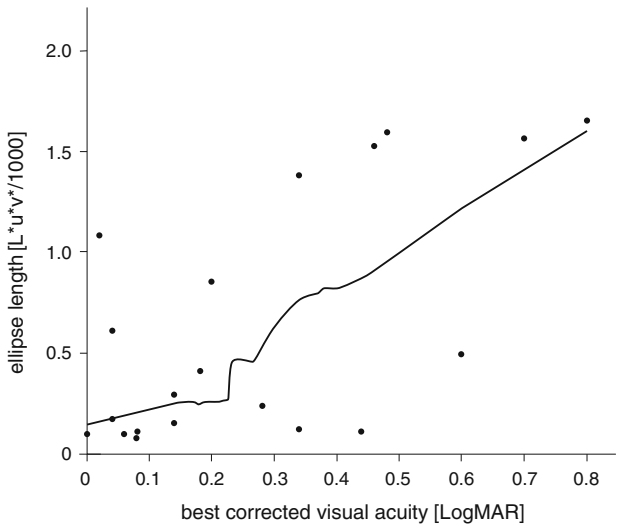

Fig. 11 Colour discrimination ellipse length (1/1000th $L^*u^*v^*$ units) along a combined protan/deutan axis vs BCVA (logMAR). Epanechnikov kernel function illustrates different degrees of monotonic correlation. Spearman $\rho = 0.587$, $p = 0.007$; Kendall $\tau = 0.447$, $p = 0.006$

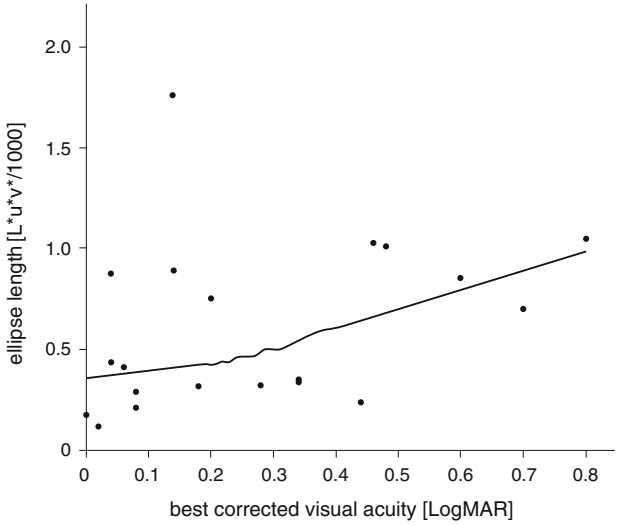

Fig. 12 Colour discrimination ellipse length (1/1000th $L^*u^*v^*$ units) along tritan axis vs BCVA (logMAR). Epanechnikov kernel function illustrates different degrees of monotonic correlation. Spearman $\rho = 0.469$, $p = 0.037$; Kendall $\tau = 0.330$, $p = 0.044$

Conclusion

In summary, we used a computer-controlled test of colour discrimination suitable for assessing patients with low vision and field loss to derive colour discrimination ellipses [10]. We found that colour discrimination is sub-normal in our cohort of patients with choroideremia when compared to a group of age-matched controls. Furthermore, the achromatic area—as estimated by the area of the fitted discrimination ellipses in the CIE 1976 chromaticity diagram—correlates to BCVA. The majority of choroideremia patients demonstrated ellipses that were aligned closely to the tritan confusion axis. We found a significant correlation between both BCVA and red-green colour discrimination, and to a lesser degree between BCVA and blue colour discrimination. In keeping with previous reports, our data suggest that the assessment of colour discrimination may be a suitable outcome measure for assessing the effects of gene therapy. [15]

Funding No funding was received for this research. MPS is supported by a Foundation Fighting Blindness Career Development Fellowship.

Compliance with ethical standards

Conflict of interest All authors certify that they have no affiliations with or involvement in any organisation or entity with any financial interest (such as honoraria; educational grants; participation in speakers' bureaus; membership, employment, consultancies, stock ownership or other equity interest; and expert testimony or patent-licencing arrangements), or non-financial interest (such as personal or professional relationships, affiliations, knowledge or beliefs) in the subject matter or materials discussed in this manuscript.

Ethical approval The study was performed in accordance with the tenets of the Declaration of Helsinki 1975 (1983 revision). Institutional review board approval was not required for this study as regulated by the data protection law of the state Baden–Württemberg, Germany.

References

1. Mauthner L (1871) Ein Fall von Choroideremia. Berichte des Naturwissenschaftlich-medizinischen Vereins in Innsbruck 11
2. Simunovic MP, Jolly JK, Xue K, Edwards TL, Groppe M, Downes SM, MacLaren RE (2016) The Spectrum of CHM gene mutations in Choroideremia and their relationship to clinical phenotype. Invest Ophthalmol Vis Sci 57(14):6033–6039. https://doi.org/10.1167/iovs.16-20230
3. MacLaren RE, Groppe M, Barnard AR, Cottriall CL, Tolmachova T, Seymour L, Clark KR, During MJ, Cremers FP, Black GC, Lotery AJ, Downes SM, Webster AR, Seabra MC (2014) Retinal gene therapy in patients with choroideremia: initial findings from a phase 1/2 clinical trial. Lancet (London, England) 383(9923):1129–1137. https://doi.org/10.1016/s0140-6736(13)62117-0
4. Edwards TL, Jolly JK, Groppe M, Barnard AR, Cottriall CL, Tolmachova T, Black GC, Webster AR, Lotery AJ, Holder GE, Xue K, Downes SM, Simunovic MP, Seabra MC, MacLaren RE (2016) Visual acuity after retinal gene therapy for Choroideremia. N Engl J Med 374(20):1996–1998. https://doi.org/10.1056/NEJMc1509501
5. Simunovic MP, Xue K, Jolly JK, MacLaren RE (2017) Structural and functional recovery following limited iatrogenic macular detachment for retinal gene therapy. JAMA Ophthalmol 135(3):234–241. https://doi.org/10.1001/jamaophthalmol.2016.5630
6. Mollon JD (1989) "Tho' she kneel'd in that place where they grew..." the uses and origins of primate colour vision. J Exp Biol 146:21–38
7. JD M (1982) What is odd about the short-wavelength mechanism and why is it disproportionately vulnerable to acquired damage. Doc Ophthalmol Proc Ser 33:145–149
8. Simunovic MP (2016) Acquired color vision deficiency. Surv Ophthalmol 61(2):132–155. https://doi.org/10.1016/j.survophthal.2015.11.004
9. Bailey IL, Lovie JE (1976) New design principles for visual acuity letter charts. Am J Optom Physiol Optic 53(11):740–745
10. Regan BC, Reffin JP, Mollon JD (1994) Luminance noise and the rapid determination of discrimination ellipses in colour deficiency. Vis Res 34(10):1279–1299
11. Seitz IP, Zhour A, Kohl S, Llavona P, Peter T, Wilhelm B, Zrenner E, Ueffing M, Bartz-Schmidt KU, Fischer MD (2015) Multimodal assessment of choroideremia patients defines pre-treatment characteristics. Graefe's archive for clinical and experimental ophthalmology = Albrecht von Graefes Archiv fur klinische und experimentelle. Ophthalmologie 253(12):2143–2150. https://doi.org/10.1007/s00417-015-2976-4
12. Curcio CA, Allen KA, Sloan KR, Lerea CL, Hurley JB, Klock IB, Milam AH (1991) Distribution and morphology of human cone photoreceptors stained with anti-blue opsin. J Comp Neurol 312(4):610–624. https://doi.org/10.1002/cne.903120411
13. Verriest G (1963) Further studies on acquired deficiency of color discrimination. J Opt Soc Am 53:185–195
14. Pinckers A, Marre M (1983) Basic phenomena in acquired colour vision deficiency. Doc Ophthalmol Adv Ophthalmol 55(3):251–271
15. Jolly JK, Groppe M, Birks J, Downes SM, MacLaren RE (2015) Functional defects in color vision in patients with Choroideremia. Am J Ophthalmol 160(4):822–831.e823. https://doi.org/10.1016/j.ajo.2015.06.018
16. Heon E, Alabduljalil T, McGuigan IIIDB, Cideciyan AV, Li S, Chen S, Jacobson SG (2016) Visual function and central retinal

structure in Choroideremia. Invest Ophthalmol Vis Sci 57(9): OCT377–OCT387. https://doi.org/10.1167/iovs.15-18421
17. Hayakawa M, Fujiki K, Hotta Y, Ito R, Ohki J, Ono J, Saito A, Nakayasu K, Kanai A, Ishidoh K, Kominami E, Yoshida K, Kim KC, Ohashi H (1999) Visual impairment and REP-1 gene mutations in Japanese choroideremia patients. Ophthalmic Genet 20(2):107–115
18. Simunovic MP, Votruba M, Regan BC, Mollon JD (1998) Colour discrimination ellipses in patients with dominant optic atrophy. Vis Res 38(21):3413–3419
19. Jeffrey B, Zein W, Falsini B, Nigam D, Sieving P (2013) Quantitative measurement of color discrimination in cone-rod dystrophies and inherited maculopathy. Invest Ophthalmol Vis Sci 54(15):2793–2793
20. Jeffrey BG, Knighten DA, Cukras CA, Brooks BP, Zein WM (2014) Quantitative measurement of color discrimination with a low vision color test in patients with retinitis Pigmentosa. Invest Ophthalmol Vis Sci 55(13):1399–1399

DISCUSSION

After decades of setbacks and steady improvements of GT technology, the recent move back into clinical experimentation put considerable pressure on clinician scientists to "get GT right" this time. Due to its history and ethical implications (80–82), GT is a subject of fascination and scrutiny, both in the public eye and for regulators. At the same time, clinical translation of GT is a daunting task: highly complex and ridden with pitfalls.

Naturally, there are large overlaps between development of GT and that of more traditional drugs, but some challenges have been unique to GT. After all, once administered, GT cannot be discontinued. If it sheds or enters the germ line, it can permanently alter the environment, bystanders, or the unborn progeny of the patient. In addition to these concerns about GT in general, current ocular GT is largely aimed at rare disease. This gives rise to another set of challenges (i.e. patient selection, detection of efficacy) which are magnified, when contrasted against the unknowns of GT. It is this area of conflict, that is tackled by this thesis.

Regarding efficacy and safety of ocular GT, this thesis investigated shedding and biodistribution of an rAAV8 vector, destined for clinical use, after intraocular administration. Non-human primates (NHP, *M. fascicularis*) were used as a model, due to its similar ocular anatomy and physiology compared to humans. Multiple biofluids that spill into the environment in a clinical setting (i.e. tears, nasal secretions, urine and blood) were sampled and analysed for vector genome copies over a 90-day period. After 90 days the animals underwent necropsy, and all tissues of interest were analysed for vector genome copies.

Another point of interest was the influence of the surgical procedure, chosen as SR (at two dosages) vs. IVT (high dose). This is relevant for two reasons: Firstly, macular holes are a relevant complication in SR (77). In clinical practice, macular hole management is well defined, but in GT a macular hole also incurs heavy vector reflux from the bleb into the vitreous. The consequences of such a leakage with regards to patient handling and GT safety had not been elucidated prior to our work, and therefore this complication was simulated in this thesis by an IVT application. Secondly, development of IVT-based GT is a hot topic in vector development, as IVT promises a less invasive means to deliver

ocular GT, and the possibility to treat the whole retina with one injection (which is not possible in SR). While the overwhelming majority of papers in the area of IVT GT are occupied with improvement of its efficacy (76,83–87), the implications of IVT GT from a safety and biodistribution standpoint (i.e. systemic distribution, immune response) are comparatively understudied (88). To the authors best knowledge, this thesis contains the first work to investigate biodistribution and shedding after IVT of rAAV2/8 in NHP.

Regarding germ line safety, this thesis has demonstrated that ocular GT using rAAV8, independently of route of administration, has a low risk of germ line transduction, as no vector genome copies were detected in gonad samples. In addition, the episomal transgene transferred by AAV is not replicated along the chromosomes and would therefore quickly dilute to the point of negligence in potential progeny.

Shedding analyses, which capture the duration and magnitude of shedding, were used to guide patient handling in a clinical setting. These analyses revealed, that shedding via biofluids does occur in all biofluids and in a dose-dependent manner but is transient. Combined with the high specificity of the vector, favourable safety data, and validated germ line safety, this meant that no strict isolation of the patient is required after ocular GT surgery, even in the case of significant reflux intro the vitreous during surgery. Yet, these results prompted separate collection and destruction of materials that had been in close contact with patient biofluids, in the first clinical ocular GT trials. Due to a low risk of clinically significant off-target effects mediated by shed particles in ocular AAV GT, this practice has since been abandoned. Regardless, these considerations will resurface given changing circumstances, such as the use of novel integrating vectors, that can transduce exposed tissues of bystanders, like skin, mucosa, or lung cells. Rightfully so, biofluid sampling up to this date remains part of most current study protocols.

While germ line and environmental safety were independent of the route of administration, other biodistribution parameters revealed stark, qualitative differences between IVT and SR, which had not been described before.

As expected, more vector genome copies (vg) were detected in the retina after equal-dose SR vs. IVT (53x more), which indicates superior gene transfer after SR. Depending on the dose-effect relation (which is still largely unknown) this also implies, that occurrence of significant reflux can decrease GT efficacy.

For tissues other than the retina, vg numbers were reversed, with IVT showing massive systemic deposition compared to SR, by up to almost four orders of magnitude. Vector deposition in different lymph node compartments, including nodes far away from the eye, such as mesenteric lymph nodes, was 400-1000 times higher after IVT, while the number of vg in another immune mediator, the spleen, was more than 7000x higher. The hypothesized distribution of vector particles via Schlemm's channel, and into the systemic circulation was supported by a remarkable persistence of vg in the blood of IVT animals, with a large number of vg detected in blood samples, even after 90 days. Taken together, this massive deposition of vector in plain sight of the immune system may stir an adaptive immune response, compromise the eye's immune privilege, and leave treated cells vulnerable to CD8-mediated decay. This notion, for which this thesis was among the first to present solid evidence, has since been emphasized by reports from a clinical trial for Leber Hereditary Optic Neuropathy, in which a concerning 13 out of 15 treated individuals developed intraocular inflammation after IVT application of AAV-GT (89).

Another large organ, which curiously revealed significant vg deposition after IVT was the liver. This implies that rAAV8 retains parts of its wild type tropism. While luckily, these biodistribution results have proven inconsequential in cases of significant reflux in ocular GT trials, it is prudent not to take them lightly. For example, although the circumstances have not been made fully transparent at the time of writing, three children in an ongoing clinical GT trial for the treatment of X-linked Myotubular Myopathy (XLMTM), which received $3x10^{14}$ vg of rAAV8 targeting muscle tissue via intravenous administration, have died from pre-existing liver failure (38), which apparently had been exacerbated by the study drug. Taken together, this part of the thesis, instead of purely feeding forward into our clinical trials, also had clear implications for pre-clinical vector-development.

Returning to the clinical considerations, it was found that ocular administration of rAAV does not cause germ line transduction. Regarding environmental safety, the results indicated that materials in close contact with biofluids of patients should be handled with care in the days after surgery, but quarantine is not required. In addition, it was shown that SR is superior to IVT in terms of on-target gene transfer, but that SR's efficacy might decrease in case of significant reflux (i.e. macular hole). And finally, biodistribution after IVT, but not after SR, was surprisingly similar to systemic administration, and carries an

increased risk of immune-mediated complications, and off-target transduction. In conclusion, SR was confirmed as the surgical method of choice.

With fundamental questions of safety and surgical technique addressed, the focus of this thesis shifts to patient selection. Patient selection is one of the core components of any clinical study design, and closely tied to the chosen primary and secondary clinical endpoints. After all, therapies aim to improve certain clinical endpoints, be it survival, specific biomarkers, or severity of symptoms. Therefore, phase II clinical trials tend to include patients, in which a possible positive treatment effect will be unconfounded, and most readily detectable.

Applied to a disease like Choroideremia (CHM), this is not easy to achieve. In theory, the primary goal of GT in CHM is not to improve function, but to slow, or ideally halt degeneration. Because of this, early treatment candidates are patients who show rapid degeneration. In this subset of patients, the limited follow-up period provided by a clinical trial is long enough, to detect a difference in disease progression between treated and untreated eyes. In contrast, if you were to treat into a period of naturally stable disease, it would be much more difficult to detect a protective effect of therapy. In order to identify patients with rapid degeneration, and to successfully control for a treatment effect in this scenario, you need a precise understanding of the natural progression of the disease. Other aspects that become relevant in this context are genotype-phenotype correlation (i.e. how dependent is the individual natural history on the genotype) and intraindividual symmetry (i.e. how similar the progression is between both eyes of the same patient). Yet, CHM is an ultra-rare disease, with no approved therapy. As such, at the time of writing (of chapter 2.2.), natural history of the disease was a niche subject, and studies to answer these questions were sparse. Even more so, if you were interested in more recent clinical modalities like OCT and fundus autofluorescence.

Therefore, clinical data from a set of CHM patients which had visited the University Eye Hospital Tübingen were analysed in retrospect, to cover the largest possible timeframe of observation. Key advantages of this dataset were the large number of genetically confirmed patients, the use of state-of-the-art modalities, and the fact that most of these patients were followed up over multiple visits and many years. The latter seems trivial, but regular visits were not typical for this patient collective, which was traditionally told

that there is no treatment available, and that prognosis is rather bleak, but at the same time not well defined. In recent years, the advent of gene therapy for CHM has spurred a host of new natural history studies and helped elucidate the phenotype further (90,91).

This thesis demonstrated, that visual acuity loss is initially slow, until the degeneration affects the fovea in the 4th or 5th decade of life. From here on, there is an accelerated loss of visual acuity. This is in contrast to previous studies, which assumed a linear loss of visual acuity, and therefore likely overestimated loss of visual acuity in early disease, and underestimated loss of visual acuity in late CHM (92,93). This has led to the proposal of a clinical two-stage, exponential model of disease progression (94), which has since been adopted by other groups (95), including a large meta-analysis (96). Furthermore, size of the central residual RPE/PR island was found to be highly symmetrical in structural parameters such as OCT, and FAF, with a quadratic function best describing the kinetics of total RPE/PR area loss (in accordance with almost linear radial loss). While the size of the central residual island was highly symmetrical between eyes, residual islands displayed unique silhouettes, each with variable foveal involvement. Due to this, symmetry of visual acuity was less robust compared to structural endpoints.

Overall, it was found that the untreated fellow eye is eligible as a high-quality, internal, intraindividual control to measure therapeutic outcome in treated eyes after GT. Regarding patient selection, it was found that accelerated disease progression occurs in the 4th to 5th decade of life, and that patients in this age cohort are likely to have discernible natural progression in the fellow eye over the course of a clinical trial. In accordance with previous literature no relevant variation in genotype-phenotype correlation was observed, as most cases are due to *null* alleles. The elevated importance of natural history studies in rare and ultra-rare retinal disease is further highlighted by the fact, that many current and upcoming GT clinical trials are flanked by prospective natural history studies.

Regardless, even in a carefully selected patient cohort, and given a well-described natural progression, changes in clinically relevant endpoints can still be too gradual to serve as discriminators of therapeutic efficacy within e.g. 12 months follow up. In mid-stage CHM this is especially true for one of the most clinically relevant endpoints in Ophthalmology: Visual acuity. It hinges on the very central cones in the fovea and can be relatively unaffected in CHM until the disease encroaches the fovea. Yet, a gain in visual acuity has

traditionally been the main functional parameter for regulatory approval of new therapies in Ophthalmology. In the case of GT for CHM, and other retinal GTs, these circumstances result in an 'endpoint dilemma':

A CHM patient with 20/20 or 20/16 vision, driven by an intact central residual island, might be treated with GT in order to prolong survival of the central cells, and preserve visual acuity. Given the theory behind GT for CHM, a gain in visual acuity is not likely to happen, as REP-1 is essential for PR survival, but not necessarily for PR function. However, demonstration of a delayed decline in the treated eye can take years, even in a well-defined cohort. To overcome this quandary, clinician scientists were encouraged to identify new, clinically relevant, functional endpoints, which are better suited to capture the benefits of GT in CHM.

Therefore, this thesis asked whether there is another functional endpoint, that might be more sensitive to the previously established pattern of degeneration in mid to late stage CHM than visual acuity. As mentioned previously, the most affected part of the retina in late stage CHM is the parafoveal region. Based on the assumption that blue-cones, located in the parafoveal region, are affected earlier by the centripetal degeneration in CHM, and are potentially more vulnerable to injury (10), it was hypothesized, that tritanopia (blue-deficiency) might be a clinically relevant endpoint in mid to late stage CHM, and would progress into a non-selective (global) colour vision deficit in terminal disease. While previous literature had shown a diffuse decline of colour vision in line with general cone degeneration, selective tritan deficiency had not been reported previously (97,98). Given that CHM patients demonstrate very constricted visual fields and therefore have practical difficulties in solving commonly used colour vision tests, and in an attempt to capture the hypothesized gradual change in colour vision (normal colour vision -> selective tritan-deficit -> global deficit), a colour vision test outside of clinical practice was deemed necessary to test the tritan-deficiency hypothesis. Due to its limited need for visual search, and colour-confusion-axes-independent testing capabilities, the CCT was chosen as the ideal instrument to detect a tritan deficiency in CHM and potentially validate the suitability of tritan-deficiency as a clinical endpoint for GT trials. Using the CCT, we indeed found a preponderance of tritan-deficits in a mixed-stage cohort of CHM patients, which broadened into a global defect in a terminal disease stage. This was the first description of specific tritan defects in CHM. The results are well in line with our

understanding of the disease, and have validated colour vision as a possible, functional endpoint in CHM trials. Of note, another group found the same pattern of defects in phenotypically similar LCA using the same methodology (99).

Other successful outcome measures which resulted from the same push towards new clinical endpoints were microperimetry and mobility tests such as the multi-luminance mobility test (MLMT) (100). Microperimetry is a recent variant on classic perimetry, which uses eye tracking to measure central retinal sensitivity with high spatial resolution. Due to its superior correlation between function and anatomy, as well as its high sensitivity, microperimetry has become one of the main outcome measures in retinal GT, including CHM (101–103). Mobility tests attacked the problem from another angle, letting patients navigate obstacle courses which are designed to mimic everyday tasks, in varying light conditions. Drastic improvements in completion time and error score in such courses helped illustrate the clinical benefit of voretigene neparvovec, and contributed to its regulatory approval (104,105). Moreover, they highlight the creativity that goes into clinical endpoint development in retinal GT.

In summary, this thesis has helped bridge the gap between the pre-clinical setting and clinical reality in Germany's first ocular GT trials. Crucial questions regarding safety, efficacy, surgical technique, patient selection, and endpoint validity were identified and addressed through experimental data from NHP, a retrospective natural history study, and clinical data generated with an out-of-clinics colour vision assessment. Figure 9 summarizes the overlap of scientific expertise and clinical perspective, which guided the work in each chapter.

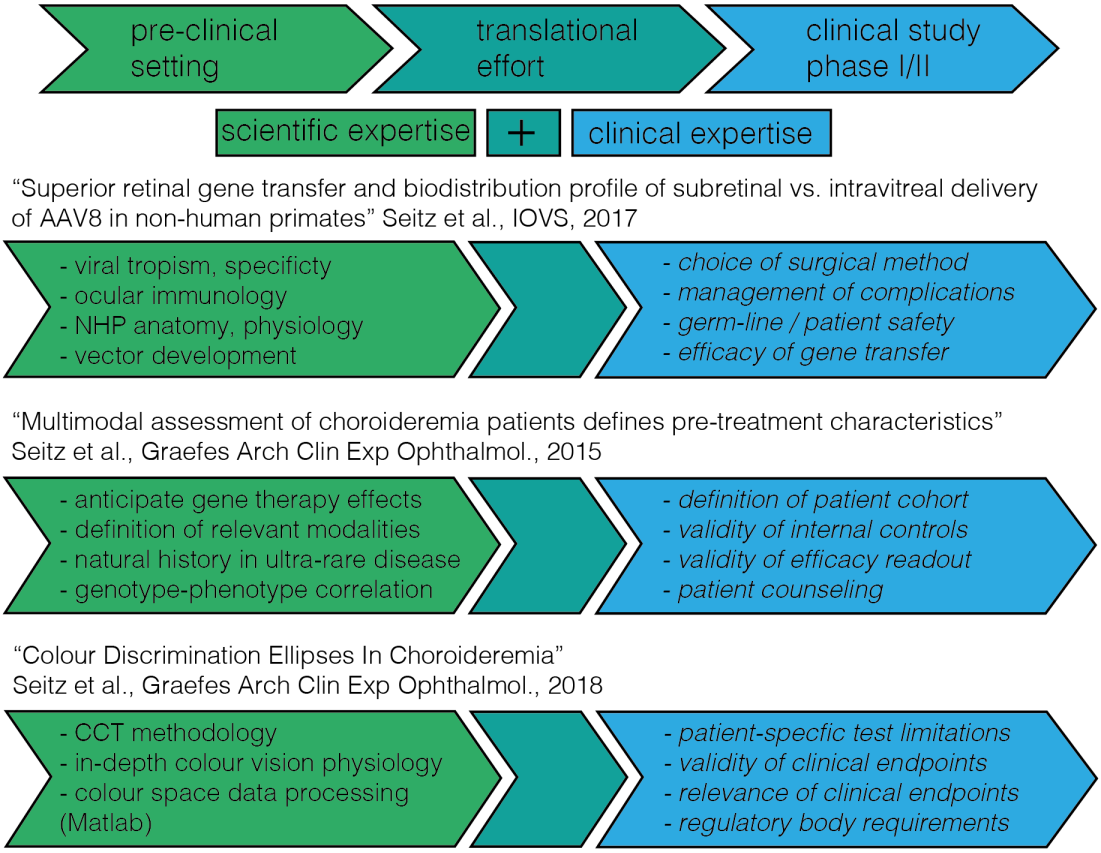

Figure 9 Summary of the translational efforts presented in this work: In each individual chapter, pre-clinical and clinical expertise were required to identify and overcome some of the challenges presented to clinician scientists by Germany's first ocular gene therapy trials.

It was demonstrated that subretinal gene therapy using AAV displayed a favourable safety profile in NHPs, and that the ethical implications of germ line transduction are minor in this use case of GT. It was also confirmed, that the fellow eye can be used as an internal control for the treated eye, which enabled a robust efficacy readout, despite slow disease progression. Furthermore, the results of this thesis were used to inform patient selection in Germany's first ocular GT trial.

In addition, the thesis generated auxiliary data to inform further pre-clinical and clinical developments in the field. Among these are management of surgical complications leading to significant reflux into the vitreous cavity, which were found to be associated

with significantly increased immune exposition and lower efficacy of gene transfer, as well as recommendations for patient isolation and contamination management after GT surgery. It also furthered our knowledge about the colour vision phenotype and natural history of CHM, which was used to improve patient counselling and future trial designs. Apart from feeding forward into clinics, the results also had implications for vector development, by highlighting the risk of off-target transduction and increased immunogenicity when using IVT vector systems. It also illustrates how problem solving in the area overlapping pre-clinical research and early clinical adoption can stir creativity, and how it is crucial for achieving regulatory approval. Lastly, the thesis aims to convey a perspective on how medical professionals can use their trained skills and clinical expertise in an attempt not to mimic basic research, but to bring a practical perspective into advanced pre-clinical research. Thus, they can identify the most relevant aspects for clinical translation, and carefully apply new therapies, to the benefit of the patient.

Outside of scientific and clinical convention, which this thesis is certainly a product of, it must not be forgotten that this is the first time in history humans selectively engineer their own genetic code. Undoubtedly, the successful translation of gene therapy into clinical practice marks the beginning of a long road ahead for scientists, physicians, regulatory bodies, ethicists, politicians and eventually all of society. Along this way it will be paramount to remember that, even in its very infancy, gene therapy has demonstrated its capacity for great promise, and peril. Especially once the “ethically low hanging fruit” of therapeutic targets (i.e. high lethality, significant burden, readily eligible for GT) have been explored, further development of gene therapy and gene engineering will necessitate broad discussion and legislation. Until then, more careful and rigorous research is required.

SUMMARY

After 50 years of gradual progress, the last decade has seen gene therapy shaping up to be a transformational technology for the treatment of previously untreatable monogenetic disorders. After being set back by several decades, crucial improvements to vector safety have again propelled gene augmentation therapy into translational reality, with monogenetic retinal disorders on the forefront of the development. This dissertation aimed to inform translational efforts towards Germany's first ocular gene therapy trials, which were conducted at the Centre for Ophthalmology in Tübingen. The individual chapters discuss the candidate's work along a trajectory from pre-clinical to clinical stages of these trials. It starts with the analysis and interpretation of comprehensive findings regarding patient, germline, and environmental safety of gene augmentation therapy, gathered from non-human primates, which led to important new hypotheses, regarding vector development and delivery, as well as patient management. Moving closer to Germany's first ocular gene therapy surgery, the thesis presents a careful, multi-modal analysis of Choroideremia patients' phenotypes, that factored into subject selection, validated the trial design, and helped to further define this rare disease. Spurred by the challenge to define novel clinical endpoints, and based on the phenotype, which was characterized in the second section, this work concludes with the investigation of a recent, computer-based colour vision test in treatment candidates, to establish its adequacy as an endpoint in retinal gene therapy trials. This dissertation is complemented by multiple reviews regarding inherited retinal disorders, as well as multiple second- and co-authorships in related literature. In its entirety, this thesis aims to paint a comprehensive picture of translational efforts in the dawn of potentially transformational advances in gene therapy.

GERMAN SUMMARY

Nach 50 Jahren schrittweisen Fortschritts hat sich die Gentherapie im letzten Jahrzehnt zu einer transformativen Technologie in der Behandlung bisher nicht behandelbarer monogenetischer Erkrankungen entwickelt. Nach Rückschlägen um die Jahrtausendwende haben entscheidende Verbesserungen der Vektorsicherheit die Gen-Addition binnen kurzer Zeit zur Anwendung in klinischen Studien gebracht, mit den monogenetischen Netzhauterkrankungen an der Spitze dieser Entwicklung. Die vorliegende Dissertation umfasst präklinische, sowie klinische Arbeiten, die im Umfeld der ersten klinischen okularen Gentherapiestudien Deutschlands an der Universität Tübingen geleistet wurden und darauf abzielen, die Kluft zwischen "Werkbank und Patient" erfolgreich zu überbrücken. Die einzelnen Kapitel diskutieren die Arbeit des Promovenden entlang einer Achse von präklinischen Untersuchungen der Therapieform, hin zur konkreten Umsetzung am Patienten. Dementsprechend öffnet die Arbeit mit ausführlichen Experimenten an Nicht-Menschenaffen bezüglich der Patienten-, Erblinien- und Umweltsicherheit der okularen Gentherapie, sowie der OP-Methodik. Aus diesen Erkenntnissen ergaben sich wichtige und neue Hypothesen mit Bezug zur Vektorentwicklung und -Anwendung, sowie zur intra- und postoperativen Versorgung behandelter Patienten. Im Vorfeld der ersten okularen Gentherapie-OPs in Deutschland, wurde im Rahmen der Dissertation zudem eine eingehende, multimodale Untersuchung des klinischen Phänotyps von Choroideremie-Patienten durchgeführt, deren Ergebnisse das Studiendesign validieren konnten, zur Auswahl der ersten Studienteilnehmer herangezogen wurden, und signifikant zur genaueren Beschreibung dieses seltenen Krankheitsbildes beitrugen. Die Gesamtarbeit schließt mit einer durch den Promovenden klinisch durchgeführten Untersuchung des Farbensehens von Gentherapie-Kandidaten mittels eines außerklinischen, computergestützten Verfahrens, um die Eignung der Methode als Endpunkt für klinische Gentherapie-Studien zu validieren. Flankiert wird die Dissertation von mehreren Übersichtsartikeln zu den hierfür relevanten Erkrankungen, sowie durch Zweit- und Ko-Autorenschaften in weiteren themennahen Arbeiten. Zusammengenommen zeichnet diese Dissertation, im Lichte potenziell umwälzender Fortschritte, ein umfassendes Bild der klinischen Forschung im Bereich der retinalen Gentherapie.

BIBLIOGRAPHY

1. Plateri F. De corporis humani structura et usu Felicis Plateri libri III: tabulis methodicè explicati, iconibus accuratè illustrati. p.187: Froben; 1583. 316 p.

2. Häggström M. Medical gallery of Mikael Häggström 2014. WikiJournal Med. 1((2)).

3. Yanoff D. Opthalmology. In: 5th ed. Elsevier; 2018. p. 428.

4. Wässle H, Grünert U, Röhrenbeck J, Boycott BB. Cortical magnification factor and the ganglion cell density of the primate retina. Nature. 1989 Oct;341(6243):643–6.

5. Daniel PM, Whitteridge D. The representation of the visual field on the cerebral cortex in monkeys. J Physiol. 1961 Dec;159(2):203–21.

6. Hendrickson A. Organization of the Adult Primate Fovea. In: Penfold PL, Provis JM, editors. Macular Degeneration [Internet]. Berlin, Heidelberg: Springer Berlin Heidelberg; 2005. p. 1–23. Available from: https://doi.org/10.1007/3-540-26977-0_1

7. Young RW. THE RENEWAL OF ROD AND CONE OUTER SEGMENTS IN THE RHESUS MONKEY. J Cell Biol. 1971 May 1;49(2):303–18.

8. Bowmaker JK, Dartnall HJ. Visual pigments of rods and cones in a human retina. J Physiol. 1980 Jan;298:501–11.

9. Mollon JD. 'Tho' she kneel'd in that place where they grew...' The uses and origins of primate colour vision. J Exp Biol. 1989 Sep;146:21–38.

10. Simunovic MP. Acquired color vision deficiency. Surv Ophthalmol. 2016 Apr;61(2):132–55.

11. Guild J, Petavel JE. The colorimetric properties of the spectrum. Philos Trans R Soc Lond Ser Contain Pap Math Phys Character. 1931 Jun 24;230(681–693):149–87.

12. Wright WD. A re-determination of the trichromatic coefficients of the spectral colours. Trans Opt Soc. 1929 Mar;30(4):141–164.

13. Seabra MC, Ms B, Jl G. Retinal degeneration in choroideremia: deficiency of rab geranylgeranyl transferase [Internet]. Vol. 259, Science (New York, N.Y.). Science; 1993 [cited 2020 Oct 14]. Available from: https://pubmed.ncbi.nlm.nih.gov/8380507/

14. Seabra MC, Yk H, Js A. Deficient geranylgeranylation of Ram/Rab27 in choroideremia [Internet]. Vol. 270, The Journal of biological chemistry. J Biol

Chem; 1995 [cited 2020 Oct 14]. Available from: https://pubmed.ncbi.nlm.nih.gov/7592656/

15. Zhang AY, Mysore N, Vali H, Koenekoop J, Cao SN, Li S, et al. Choroideremia Is a Systemic Disease With Lymphocyte Crystals and Plasma Lipid and RBC Membrane Abnormalities. Invest Ophthalmol Vis Sci. 2015 Dec;56(13):8158–65.

16. Strunnikova NV, Barb J, Sergeev YV, Thiagarajasubramanian A, Silvin C, Munson PJ, et al. Loss-of-function mutations in Rab escort protein 1 (REP-1) affect intracellular transport in fibroblasts and monocytes of choroideremia patients. PloS One. 2009 Dec 22;4(12):e8402.

17. Coussa RG, Traboulsi EI. Choroideremia: a review of general findings and pathogenesis. Ophthalmic Genet. 2012 Jun;33(2):57–65.

18. Simunovic MP, Jolly JK, Xue K, Edwards TL, Groppe M, Downes SM, et al. The Spectrum of CHM Gene Mutations in Choroideremia and Their Relationship to Clinical Phenotype. Invest Ophthalmol Vis Sci. 2016 Nov 1;57(14):6033–9.

19. NightstaRx Ltd, a Biogen Company. A Randomised, Open Label, Outcomes-Assessor Masked, Prospective, Parallel Controlled Group, Phase 3 Clinical Trial Of Retinal Gene Therapy For Choroideremia Using An Adeno-Associated Viral Vector (AAV2) Encoding Rab Escort Protein 1 (REP1) [Internet]. clinicaltrials.gov; 2020 Feb [cited 2020 Oct 14]. Report No.: NCT03496012. Available from: https://clinicaltrials.gov/ct2/show/NCT03496012

20. Fischer MD, Ochakovski GA, Beier B, Seitz IP, Vaheb Y, Kortuem C, et al. CHANGES IN RETINAL SENSITIVITY AFTER GENE THERAPY IN CHOROIDEREMIA. RETINA. 2020 Jan;40(1):160–168.

21. Kohl S, Marx T, Giddings I, Jägle H, Jacobson SG, Apfelstedt-Sylla E, et al. Total colourblindness is caused by mutations in the gene encoding the alpha-subunit of the cone photoreceptor cGMP-gated cation channel. Nat Genet. 1998 Jul;19(3):257–9.

22. Kohl S, Baumann B, Broghammer M, Jägle H, Sieving P, Kellner U, et al. Mutations in the CNGB3 gene encoding the beta-subunit of the cone photoreceptor cGMP-gated channel are responsible for achromatopsia (ACHM3) linked to chromosome 8q21. Hum Mol Genet. 2000 Sep 1;9(14):2107–16.

23. Grau T, Artemyev NO, Rosenberg T, Dollfus H, Haugen OH, Cumhur Sener E, et al. Decreased catalytic activity and altered activation properties of PDE6C mutants associated with autosomal recessive achromatopsia. Hum Mol Genet. 2011 Feb 15;20(4):719–30.

24. Kohl S, Coppieters F, Meire F, Schaich S, Roosing S, Brennenstuhl C, et al. A nonsense mutation in PDE6H causes autosomal-recessive incomplete achromatopsia. Am J Hum Genet. 2012 Sep 7;91(3):527–32.

25. Hirji N, Georgiou M, Kalitzeos A, Bainbridge JW, Kumaran N, Aboshiha J, et al. Longitudinal Assessment of Retinal Structure in Achromatopsia Patients With Long-Term Follow-up. Invest Ophthalmol Vis Sci. 2018 03;59(15):5735–44.

26. Aboshiha J, Dubis AM, Cowing J, Fahy RTA, Sundaram V, Bainbridge JW, et al. A prospective longitudinal study of retinal structure and function in achromatopsia. Invest Ophthalmol Vis Sci. 2014 Aug 7;55(9):5733–43.

27. Fischer MD, Michalakis S, Wilhelm B, Zobor D, Muehlfriedel R, Kohl S, et al. Safety and Vision Outcomes of Subretinal Gene Therapy Targeting Cone Photoreceptors in Achromatopsia: A Nonrandomized Controlled Trial. JAMA Ophthalmol. 2020 Jun 1;138(6):643–51.

28. Kay ER. Incorporation of deoxyribonucleic acid by mammalian cells in vitro. Nature. 1961 Jul 22;191:387–8.

29. Sambrook J, Westphal H, Srinivasan PR, Dulbecco R. The integrated state of viral DNA in SV40-transformed cells. Proc Natl Acad Sci U S A. 1968 Aug;60(4):1288–95.

30. zur Hausen H. Condylomata acuminata and human genital cancer. Cancer Res. 1976 Feb;36(2 pt 2):794.

31. Rogers S, Pfuderer P. Use of viruses as carriers of added genetic information. Nature. 1968 Aug 17;219(5155):749–51.

32. Friedmann T, Roblin R. Gene therapy for human genetic disease? Science. 1972 Mar 3;175(4025):949–55.

33. Wilson JM. Lessons learned from the gene therapy trial for ornithine transcarbamylase deficiency. Mol Genet Metab. 2009 Apr;96(4):151–7.

34. Yarborough M, Sharp RR. Public trust and research a decade later: what have we learned since Jesse Gelsinger's death? Mol Genet Metab. 2009 May;97(1):4–5.

35. Hacein-Bey-Abina S, Hauer J, Lim A, Picard C, Wang GP, Berry CC, et al. Efficacy of Gene Therapy for X-Linked Severe Combined Immunodeficiency. N Engl J Med. 2010 Jul 22;363(4):355–64.

36. Cavazzana-Calvo M, Hacein-Bey S, Basile G de S, Gross F, Yvon E, Nusbaum P, et al. Gene Therapy of Human Severe Combined Immunodeficiency (SCID)-X1 Disease. Science. 2000 Apr 28;288(5466):669–72.

37. Hacein-Bey-Abina S, Pai S-Y, Gaspar HB, Armant M, Berry CC, Blanche S, et al. A Modified γ-Retrovirus Vector for X-Linked Severe Combined Immunodeficiency. N Engl J Med. 2014 Oct 9;371(15):1407–17.

38. Audentes Therapeutics. Audentes Therapeutics Provides Update on the ASPIRO Clinical Trial Evaluating AT132 in Patients with X-linked Myotubular Myopathy [Internet]. Audentes Therapeutics. [cited 2020 Sep 10]. Available from:

https://www.audentestx.com/press_release/audentes-therapeutics-provides-update-on-the-aspiro-clinical-trial-evaluating-at132-in-patients-with-x-linked-myotubular-myopathy/

39. Greely HT. CRISPR'd babies: human germline genome editing in the 'He Jiankui affair'*. J Law Biosci. 2019 Aug 13;6(1):111–83.

40. Kozarsky KF, Wilson JM. Gene therapy: adenovirus vectors. Curr Opin Genet Dev. 1993 Jun 1;3(3):499–503.

41. Boucher P, Cui X, Curiel DT. Adenoviral vectors for in vivo delivery of CRISPR-Cas gene editors. J Control Release Off J Control Release Soc. 2020 Sep 3;

42. Waldrop MA, Karingada C, Storey MA, Powers B, Iammarino MA, Miller NF, et al. Gene Therapy for Spinal Muscular Atrophy: Safety and Early Outcomes. Pediatrics. 2020;146(3).

43. Aiuti A, Biasco L, Scaramuzza S, Ferrua F, Cicalese MP, Baricordi C, et al. Lentivirus-based Gene Therapy of Hematopoietic Stem Cells in Wiskott-Aldrich Syndrome. Science. 2013 Aug 23;341(6148):1233151.

44. Marquez Loza LI, Yuen EC, McCray PB. Lentiviral Vectors for the Treatment and Prevention of Cystic Fibrosis Lung Disease. Genes [Internet]. 2019 Mar 14 [cited 2020 Oct 16];10(3). Available from: https://www.ncbi.nlm.nih.gov/pmc/articles/PMC6471883/

45. Rosen S, Tiefenbacher S, Robinson M, Huang M, Srimani J, Mackenzie D, et al. Activity of Transgene-Produced B-Domain Deleted Factor VIII in Human Plasma Following AAV5 Gene Therapy. Blood. 2020 Sep 11;

46. Puranik N, Yadav D, Chauhan PS, Kwak M, Jin J-O. Exploring the role of gene therapy for neurological disorders. Curr Gene Ther. 2020 Sep 17;

47. Pietersz KL, Martier RM, Baatje MS, Liefhebber JM, Brouwers CC, Pouw SM, et al. Transduction patterns in the CNS following various routes of AAV-5-mediated gene delivery. Gene Ther. 2020 Aug 15;

48. Bucher K, Rodríguez-Bocanegra E, Dauletbekov D, Fischer MD. Immune responses to retinal gene therapy using adeno-associated viral vectors - Implications for treatment success and safety. Prog Retin Eye Res. 2020 Oct 15;100915.

49. Raper SE, Chirmule N, Lee FS, Wivel NA, Bagg A, Gao G, et al. Fatal systemic inflammatory response syndrome in a ornithine transcarbamylase deficient patient following adenoviral gene transfer. Mol Genet Metab. 2003 Sep 1;80(1):148–58.

50. Gao GP, Yang Y, Wilson JM. Biology of adenovirus vectors with E1 and E4 deletions for liver-directed gene therapy. J Virol. 1996 Dec;70(12):8934–43.

51. Rollier CS, Spencer AJ, Sogaard KC, Honeycutt J, Furze J, Bregu M, et al. Modification of Adenovirus vaccine vector-induced immune responses by expression of a signalling molecule. Sci Rep. 2020 Mar 31;10(1):5716.

52. Atchison RW, Casto BC, Hammon WM. ADENOVIRUS-ASSOCIATED DEFECTIVE VIRUS PARTICLES. Science. 1965 Aug 13;149(3685):754–6.

53. Rose JA, Maizel JV, Inman JK, Shatkin AJ. Structural Proteins of Adenovirus-Associated Viruses. J Virol. 1971 Nov;8(5):766–70.

54. Balakrishnan B, Jayandharan GR. Basic biology of adeno-associated virus (AAV) vectors used in gene therapy. Curr Gene Ther. 2014;14(2):86–100.

55. Dong-Soo I, Muzyczka N. The AAV origin binding protein Rep68 is an ATP-dependent site-specific endonuclease with DNA helicase activity. Cell. 1990 May 4;61(3):447–57.

56. Chiorini JA, Wiener SM, Yang L, Smith RH, Safer B, Kilcoin NP, et al. The Roles of AAV Rep Proteins in Gene Expression and Targeted Integration. In: Berns KI, Giraud C, editors. Adeno-Associated Virus (AAV) Vectors in Gene Therapy [Internet]. Berlin, Heidelberg: Springer; 1996 [cited 2020 Sep 14]. p. 25–33. (Current Topics in Microbiology and Immunology). Available from: https://doi.org/10.1007/978-3-642-80207-2_2

57. Gao G, Alvira MR, Somanathan S, Lu Y, Vandenberghe LH, Rux JJ, et al. Adeno-associated viruses undergo substantial evolution in primates during natural infections. Proc Natl Acad Sci U S A. 2003 May 13;100(10):6081–6.

58. Gao G, Vandenberghe LH, Alvira MR, Lu Y, Calcedo R, Zhou X, et al. Clades of Adeno-Associated Viruses Are Widely Disseminated in Human Tissues. J Virol. 2004 Jun;78(12):6381–8.

59. Ronzitti G, Gross D-A, Mingozzi F. Human Immune Responses to Adeno-Associated Virus (AAV) Vectors. Front Immunol [Internet]. 2020 [cited 2020 Sep 14];11. Available from: https://www.frontiersin.org/articles/10.3389/fimmu.2020.00670/full#B28

60. Zincarelli C, Soltys S, Rengo G, Rabinowitz JE. Analysis of AAV Serotypes 1–9 Mediated Gene Expression and Tropism in Mice After Systemic Injection. Mol Ther. 2008 Jun 1;16(6):1073–80.

61. Lee E, Cm G, J S. Adeno-Associated Virus (AAV) Vectors: Rational Design Strategies for Capsid Engineering [Internet]. Vol. 7, Current opinion in biomedical engineering. Curr Opin Biomed Eng; 2018 [cited 2020 Oct 14]. Available from: https://pubmed.ncbi.nlm.nih.gov/31106283/

62. Byrne LC, Day TP, Visel M, Strazzeri JA, Fortuny C, Dalkara D, et al. In vivo–directed evolution of adeno-associated virus in the primate retina. JCI Insight [Internet]. [cited 2020 Sep 11];5(10). Available from: https://www.ncbi.nlm.nih.gov/pmc/articles/PMC7259523/

63. Zhong L, Zhao W, Wu J, Li B, Zolotukhin S, Govindasamy L, et al. A dual role of EGFR protein tyrosine kinase signaling in ubiquitination of AAV2 capsids and viral second-strand DNA synthesis. Mol Ther J Am Soc Gene Ther. 2007 Jul;15(7):1323–30.

64. Petrs-Silva H, Dinculescu A, Li Q, Deng W-T, Pang J, Min S-H, et al. Novel Properties of Tyrosine-mutant AAV2 Vectors in the Mouse Retina. Mol Ther. 2011 Feb;19(2):293–301.

65. Maheshri N, Koerber JT, Kaspar BK, Schaffer DV. Directed evolution of adeno-associated virus yields enhanced gene delivery vectors. Nat Biotechnol. 2006 Feb;24(2):198–204.

66. Khabou H, Desrosiers M, Winckler C, Fouquet S, Auregan G, Bemelmans A-P, et al. Insight into the mechanisms of enhanced retinal transduction by the engineered AAV2 capsid variant -7m8. Biotechnol Bioeng. 2016;113(12):2712–24.

67. Lostal W, Kodippili K, Yue Y, Duan D. Full-length dystrophin reconstitution with adeno-associated viral vectors. Hum Gene Ther. 2014 Jun;25(6):552–62.

68. Gil-Farina I, Fronza R, Kaeppel C, Lopez-Franco E, Ferreira V, D'Avola D, et al. Recombinant AAV Integration Is Not Associated With Hepatic Genotoxicity in Nonhuman Primates and Patients. Mol Ther. 2016 Jun;24(6):1100–5.

69. Kruzik A, Fetahagic D, Hartlieb B, Dorn S, Koppensteiner H, Horling FM, et al. Prevalence of Anti-Adeno-Associated Virus Immune Responses in International Cohorts of Healthy Donors. Mol Ther - Methods Clin Dev. 2019 Sep 13;14:126–33.

70. Ertl H, Ka H. Impact of AAV Capsid-Specific T-Cell Responses on Design and Outcome of Clinical Gene Transfer Trials with Recombinant Adeno-Associated Viral Vectors: An Evolving Controversy [Internet]. Vol. 28, Human gene therapy. Hum Gene Ther; 2017 [cited 2020 Oct 14]. Available from: https://pubmed.ncbi.nlm.nih.gov/28042943/

71. Rabinowitz J, Chan YK, Samulski RJ. Adeno-Associated Virus (AAV) Versus Immune Response. Viruses [Internet]. 2019 Feb [cited 2020 Oct 14];11(2). Available from: https://www.ncbi.nlm.nih.gov/pmc/articles/PMC6409805/

72. Vandamme C, Adjali O, Mingozzi F. Unraveling the Complex Story of Immune Responses to AAV Vectors Trial After Trial. Hum Gene Ther. 2017;28(11):1061–74.

73. Reichel FF, Peters T, Wilhelm B, Biel M, Ueffing M, Wissinger B, et al. Humoral Immune Response After Intravitreal But Not After Subretinal AAV8 in Primates and Patients. Invest Ophthalmol Vis Sci. 2018 Apr 1;59(5):1910–5.

74. Farrar GJ, Carrigan M, Dockery A, Millington-Ward S, Palfi A, Chadderton N, et al. Toward an elucidation of the molecular genetics of inherited retinal degenerations. Hum Mol Genet. 2017 Aug 1;26(R1):R2–11.

75. Han IC, Cheng JL, Burnight E, Ralston CL, Fick JL, Thomsen GJ, et al. Retinal Tropism and Transduction of Adeno-Associated Virus (AAV) Varies by Serotype and Route of Delivery (Intravitreal, Subretinal or Suprachoroidal) in Rats. Hum Gene Ther. 2020 Sep 18;

76. Takahashi K, Igarashi T, Miyake K, Kobayashi M, Yaguchi C, Iijima O, et al. Improved Intravitreal AAV-Mediated Inner Retinal Gene Transduction after Surgical Internal Limiting Membrane Peeling in Cynomolgus Monkeys. Mol Ther J Am Soc Gene Ther. 2017 04;25(1):296–302.

77. Talib M, Koetsier LS, MacLaren RE, Boon CJF. Outcome of Full-Thickness Macular Hole Surgery in Choroideremia. Genes [Internet]. 2017 Jul 21 [cited 2020 Oct 16];8(7). Available from: https://www.ncbi.nlm.nih.gov/pmc/articles/PMC5541320/

78. Fischer MD, Dg H, Ms S, Re M. Evaluation of an Optimized Injection System for Retinal Gene Therapy in Human Patients [Internet]. Vol. 27, Human gene therapy methods. Hum Gene Ther Methods; 2016 [cited 2020 Oct 14]. Available from: https://pubmed.ncbi.nlm.nih.gov/27480111/

79. Vasconcelos HM, Lujan BJ, Pennesi ME, Yang P, Lauer AK. Intraoperative optical coherence tomographic findings in patients undergoing subretinal gene therapy surgery. Int J Retina Vitr. 2020;6:13.

80. Lanphier E, Urnov F, Haecker SE, Werner M, Smolenski J. Don't edit the human germ line. Nature. 2015 Mar 26;519(7544):410–1.

81. Watanabe D, Saito Y, Tsuda M, Ohsawa R. Increased awareness and decreased acceptance of genome-editing technology: The impact of the Chinese twin babies. PloS One. 2020;15(9):e0238128.

82. Cwik B. Responsible Translational Pathways for Germline Gene Editing? Curr Stem Cell Rep. 2020 Aug 21;1–8.

83. Zeng Y, Qian H, Wu Z, Marangoni D, Sieving PA, Bush RA. AAVrh-10 transduces outer retinal cells in rodents and rabbits following intravitreal administration. Gene Ther. 2019;26(9):386–98.

84. Grishanin R, Vuillemenot B, Sharma P, Keravala A, Greengard J, Gelfman C, et al. Preclinical Evaluation of ADVM-022, a Novel Gene Therapy Approach to Treating Wet Age-Related Macular Degeneration. Mol Ther J Am Soc Gene Ther. 2019 02;27(1):118–29.

85. Kay CN, Ryals RC, Aslanidi GV, Min SH, Ruan Q, Sun J, et al. Targeting photoreceptors via intravitreal delivery using novel, capsid-mutated AAV vectors. PloS One. 2013;8(4):e62097.

86. Cronin T, Vandenberghe LH, Hantz P, Juttner J, Reimann A, Kacsó A-E, et al. Efficient transduction and optogenetic stimulation of retinal bipolar cells by a

synthetic adeno-associated virus capsid and promoter. EMBO Mol Med. 2014 Sep;6(9):1175–90.

87. Zeng Y, Boyd R, Bartoe J, Wiley HE, Marangoni D, Wei LL, et al. 'Para-retinal' Vector Administration into the Deep Vitreous Enhances Retinal Transgene Expression. Mol Ther Methods Clin Dev. 2020 Sep 11;18:422–7.

88. Duncan JL. Understanding Ocular Inflammation in Eyes Treated With Intravitreal Gene Therapy. JAMA Ophthalmol. 2019 Apr 1;137(4):407–407.

89. Bouquet C, Vignal Clermont C, Galy A, Fitoussi S, Blouin L, Munk MR, et al. Immune Response and Intraocular Inflammation in Patients With Leber Hereditary Optic Neuropathy Treated With Intravitreal Injection of Recombinant Adeno-Associated Virus 2 Carrying the ND4 Gene: A Secondary Analysis of a Phase 1/2 Clinical Trial. JAMA Ophthalmol. 2019 01;137(4):399–406.

90. Hagag AM, Mitsios A, Narayan A, Abbouda A, Webster AR, Dubis AM, et al. Prospective deep phenotyping of choroideremia patients using multimodal structure-function approaches. Eye Lond Engl. 2020 May 28;

91. Foote KG, Roorda A, Duncan JL. Multimodal Imaging in Choroideremia. Adv Exp Med Biol. 2019;1185:139–43.

92. Coussa RG, Kim J, Traboulsi EI. Choroideremia: effect of age on visual acuity in patients and female carriers. Ophthalmic Genet. 2012 Jun;33(2):66–73.

93. Roberts MF, Fishman GA, Roberts DK, Heckenlively JR, Weleber RG, Anderson RJ, et al. Retrospective, longitudinal, and cross sectional study of visual acuity impairment in choroideraemia. Br J Ophthalmol. 2002 Jun;86(6):658–62.

94. Seitz IP, Fischer MD. [The Natural History of Choroideraemia]. Klin Monatsbl Augenheilkd. 2019 Mar;236(3):236–43.

95. Aylward JW, Xue K, Patrício MI, Jolly JK, Wood JC, Brett J, et al. Retinal Degeneration in Choroideremia follows an Exponential Decay Function. Ophthalmology. 2018;125(7):1122–4.

96. Shen LL, Ahluwalia A, Sun M, Young BK, Grossetta Nardini HK, Del Priore LV. Long-term natural history of visual acuity in eyes with choroideremia: a systematic review and meta-analysis of data from 1004 individual eyes. Br J Ophthalmol. 2020 May 29;

97. Jolly JK, Groppe M, Birks J, Downes SM, MacLaren RE. Functional Defects in Color Vision in Patients With Choroideremia. Am J Ophthalmol. 2015 Oct;160(4):822-831.e3.

98. Heon E, Alabduljalil T, McGuigan DB, Cideciyan AV, Li S, Chen S, et al. Visual Function and Central Retinal Structure in Choroideremia. Invest Ophthalmol Vis Sci. 2016 Jul 1;57(9):OCT377–87.

99. Kumaran N, Ripamonti C, Kalitzeos A, Rubin GS, Bainbridge JWB, Michaelides M. Severe Loss of Tritan Color Discrimination in RPE65 Associated Leber Congenital Amaurosis. Invest Ophthalmol Vis Sci. 2018 Jan;59(1):85–93.

100. Chung DC, McCague S, Yu Z-F, Thill S, DiStefano-Pappas J, Bennett J, et al. Novel mobility test to assess functional vision in patients with inherited retinal dystrophies. Clin Experiment Ophthalmol. 2018;46(3):247–59.

101. Fischer MD, Ochakovski GA, Beier B, Seitz IP, Vaheb Y, Kortuem C, et al. Efficacy and Safety of Retinal Gene Therapy Using Adeno-Associated Virus Vector for Patients With Choroideremia: A Randomized Clinical Trial. JAMA Ophthalmol. 2019 Aug 29;

102. MacLaren RE, Groppe M, Barnard AR, Cottriall CL, Tolmachova T, Seymour L, et al. Retinal gene therapy in patients with choroideremia: initial findings from a phase 1/2 clinical trial. Lancet Lond Engl. 2014 Mar 29;383(9923):1129–37.

103. Lam BL, Davis JL, Gregori NZ, MacLaren RE, Girach A, Verriotto JD, et al. Choroideremia Gene Therapy Phase 2 Clinical Trial: 24-Month Results. Am J Ophthalmol. 2019;197:65–73.

104. Rubin GS, Bainbridge JW, Roche H, Robbie SJ, Moore AT, Fujiyama T, et al. Visually-Guided Mobility in Patients Treated With Gene Therapy for Leber's Congenital Amaurosis. Invest Ophthalmol Vis Sci. 2010 Apr 17;51(13):1392–1392.

105. Russell S, Bennett J, Wellman JA, Chung DC, Yu Z-F, Tillman A, et al. Efficacy and safety of voretigene neparvovec (AAV2-hRPE65v2) in patients with RPE65-mediated inherited retinal dystrophy: a randomised, controlled, open-label, phase 3 trial. The Lancet. 2017 Aug 26;390(10097):849–60.

DECLARATION OF CONTRIBUTIONS

Die Arbeit wurde am
Department für Augenheilkunde, Universitäts-Augenklinik Tübingen
unter Betreuung von Prof. Dr. Dr. M. Dominik Fischer durchgeführt.

“Superior Gene Transfer And Biodistribution Profile Of Subretinal Vs. Intravitreal Delivery Of AAV8 In Non-Human Primates.”

Die Konzeption der Studie erfolgte durch die Co-Autoren (RD-Cure Consortium). Die Versuche an non-human primates in Chapter 2.1 wurden durch die Covance Laboratories GmbH in Münster durchgeführt. Die Aufarbeitung der Rohdaten, sowie deren statistische Analyse, einschließlich Hypothesenbildung, wurden eigenständig von mir durchgeführt. Das Manuskript wurde eigenständig von mir konzeptioniert und verfasst, einschließlich aller Darstellungen. M. Dominik Fischer begleitete die Erstellung des Manuskripts als interner Reviewer und Corresponding Author.

“Multimodal Assessment Of Choroideremia Patients Defines Pre-Treatment Characteristics”

Die Konzeption der Studie erfolgte durch M. Dominik Fischer. Die Zusammenstellung der klinischen Daten, sowie deren statistische Analyse, einschließlich Hypothesenbildung, wurden eigenständig von mir durchgeführt. Das Manuskript wurde eigenständig von mir verfasst, einschließlich aller Darstellungen. M. Dominik Fischer begleitete die Erstellung des Manuskripts als interner Reviewer und Corresponding Author.

„Colour Discrimination Ellipses In Choroideremia“

Die Konzeption der Studie erfolgte in gleichen Teilen durch Matthew P. Simunovic, M. Dominik Fischer und mich. Die Versuche an Probanden wurden eigenständig durch mich durchgeführt. Die Bearbeitung der Testergebnisse in Matlab (einschließlich Erstellung notwendiger scripts/functions), sowie die statistische Analyse der Endergebnisse, wurde eigenständig von mir durchgeführt. Das Manuskript, wurde eigenständig von mir konzeptioniert und verfasst, einschließlich aller Darstellungen. Jasleen K Jolly, Matthew P. Simunovic und M. Dominik Fischer begleiteten die Erstellung des Manuskripts als interne Reviewer.

Ich versichere, dieses Manuskript selbstständig verfasst zu haben und keine weiteren als die von mir angegebenen Quellen verwendet zu haben.

Unterschrift: Tübingen, den

ACKNOWLEDGMENTS

I dedicate this work to my grandmother Hanneliese, who was forced by a twist of fate to leave her home and her aspirations in academia behind. Through her selfless determination, to enable her children and grandchildren to achieve what she could not, she created the foundation for my journey. I hope her always curious and inquisitive mind will live on through all those she fostered.

My mother Sabine, an unwavering optimist, whose unconditional support and thoughtful guidance I could always rely on, and my father Stefan, who spurred and enthusiastically curated my interest in science.

My wonderful partner Lena, who unquestioningly supported me, despite all the extra hours, weekends and holidays which I dedicated to my work. She is the joy of my life.

My close friends Jonas, who I shared my life and my troubles with, and who never fails to set me straight or make me laugh, and Felix, who made going to work always fun, and whose opinions and company I value greatly.

My childhood friends Julius, Timothy, Sven, and Gregor, which I am glad to still have in my life, and who I can always escape to.

My uncles Volker, who has been a steady support and inspiration over the years, and Jochen, who taught me to not let life pass by, but to make the most of it.

All of my extended family for enriching my life. I am proud to be one of you.

All my Co-Authors and collaborators, especially Dany, Sophia, Ahmad, Alex, Oksana, Jasleen and Matthew for the pleasant time, and the great work they contributed.

And last, the corresponding author of a significant part of my life, Dominik Fischer, which I am blessed to call a role-model, mentor and friend. Clearly, his relentless enthusiasm and ingenuity are ever-inspiring, and his willingness to create opportunities for others is highly commendable. But most importantly, the trust he placed in me, and the wealth of great memories I owe to him, made me a better man.